POLITEHNICA UNIVERSITY TIMIŞOARA
Civil Engineering Faculty
Department of Steel Structures and Structural Mechanics

ULTIMATE DEFORMATION AND RESISTANCE CAPACITY OF BOLTED T-STUB CONNECTIONS UNDER DIFFERENT LOADING CONDITIONS

Author: Ghazanfar Ali ANWAR, Civ. Eng.

Supervisor: Professor Florea DINU, Ph.D.

Universitatea Politehnica Timişoara, Romania

Study Program: **SUSCOS_M**

Academic year: **2016 / 2017**

Ultimate deformation and resistance capacity of bolted T-Stub connections under different loading conditions

Ghazanfar Ali Anwar

February 2017

European Commission
ERASMUS
MUNDUS

Members of the Jury

President:

Professor Dan Dubina, Ph.D.
C. M. of the Romanian Academy
Politehnica University Timişoara
Str. Ion Curea, Nr. 1
300224, Timisoara – Romania

Thesis Supervisor:

Professor Florea Dinu, Ph.D.
Politehnica University Timişoara
Str. Ion Curea, Nr. 1
300224, Timisoara – Romania

Members:

Professor Adrian Ciutina, Ph.D.
Politehnica University Timişoara
Str. Ion Curea, Nr. 1
300224, Timisoara – Romania

Assoc. Professor Aurel Stratan, Ph.D.
Politehnica University Timişoara
Str. Ion Curea, Nr. 1
300224, Timisoara – Romania

Professor Viorel UNGUREANU, PhD.
Politehnica University Timişoara
Srada Ioan Curea, 1
300224, Timişoara, Timiş, Romania

S.l. Dr. ing. Cristian VULCU
Politehnica University Timişoara
Srada Ioan Curea, 1
300224, Timişoara, Timiş, Romania

Secretary:

Assoc. Professor Adrian DOGARIU, PhD.
Politehnica University Timişoara
Srada Ioan Curea, 1
300224, Timişoara, Timiş, Romania

ACKNOWLEDGMENT

This dissertation work is a partial fulfilment of my master course of SUSCOS (2015-2017) within the department of Steel Structures and Structural Mechanics (www.ct.upt.ro/cmmc) under the Research Center for Mechanics of Materials and Structural Safety, from Politechnica University Timisoara in Romania.

I would like to express deepest gratitude to my supervisor, PhD. Florea Dinu for guidance and help throughout my research activity in Politechnica University Timisoara. Without his help and guidance it would not have been possible to finish this research work. His devotion in helping young researchers is truly appreciable and I wish him all the very best in his future endeavors. Such professors are hard to find and must be truly appreciated.

I would also like to thank Ioan Marginean for his continuous support and guidance in developing Finite element models and being available all the time for clarifying my doubts in numerical modeling. PhD, Ioan Both for his help in experimental testing and PhD. Calin Neagu for his help in understanding high tech equipment used in experimental testing for the development of my thesis.

I am thankful to Professor Dan Dubina for giving me this opportunity to write my thesis with CODEC Research Program (www.ct.upt.ro/centre/cemsig/codec.htm). Furthermore I would like to thank Professor Adrian Ciutina for bearing with us and taking good care of us during our tenure in Romania. I am also thankful to Professor Aurel Stratan for his positive feedbacks.

Moreover I am deeply thankful to my parents for moral support and encouragement in every aspect of my life. I would like to thank my brothers and my sister to support me morally. I feel proud to be a part of such a supporting family. I would also like to thank Monika Mráčková , Jie Xiang, Pierre Darry Versaillot for their help and support.

I am deeply in debt of all the people who helped me in completing my course of SUSCOS (2015-2017) and being part of my life and specially in finalizing this research work.

Finally, I am thankful to GOD Almighty ALLAH for everything I have in my life.

ABSTRACT

Disproportionate or progressive collapse is a phenomenon causing entire structure or large part of it to collapse due to the local failure of a structure. Studies to develop design guidelines to prevent such collapse started after the collapse of Ronan Point apartment in 1968 leading to the development of the concept of robust design of structures. Progressive collapse resistance of steel frames under extreme loading relies primarily on resistance of key structural elements, continuity between elements and ductility of elements and their connections. This dissertation work focuses on the ultimate capacity and ductility of T-Stub macro-components under large deformation demands at different loading rates and temperatures. Extensive experimental testing program on T-stub components is developed to evaluate the ultimate strength and deformation capacity. Based on the experimental data, numerical models are validated and employed in a parametric numerical study aimed at studying strength, stiffness and ductility of T-Stub macro-components on two main parameters i.e. distance between the bolts and end-plate thickness.

This thesis is a part of the project supported by a grant of the Romanian National Authority for Scientific Research, CNDI-UEFISCDI, Project number 55/2012 under a framework of "Structural conception and COllapse control performance based DEsign of multistory structures under aCcidental actions" called CODEC research program.

Table of Contents

List of Tables

List of Figures

1. INTRODUCTION

1.1. Motivation

Disproportionate or progressive collapse is a phenomenon in which entire structure or large part of it collapses because of the local failure of a structure. Studies for the development of design guidelines to prevent such collapse started after the collapse of Ronan Point apartment in West Ham, London in 1968 because of the gas explosion. Furthermore the complete collapse of world trade center identified as progressive collapse calls for the need of proper design guidelines to improve the robustness of a structure.

Following are some notable examples of disproportionate collapse of multistory buildings.

- On November 1, 1966, the 7 story steel frame structure, University of Aberdeen Zoology Department building in Aberdeen, Scotland suffered progressive collapse during its construction [1].
- On May 16, 1968, the 22 story large panel system building, Ronan point apartment in West Ham, London suffered disproportionate collapse of one of its corners because of the gas explosion [2].
- On March 2, 1973, the 26 story steel-reinforced concrete structure, Skyline Towers Building in Fairfax County, Virginia collapsed because of pre removal of wooden shoring [3].
- On March 15, 1986, the 6 story steel-reinforced concrete structure, Hotel New world in Little India, Singapore collapsed progressively because of the structural design error in neglecting buildings self-weight [4].
- On April 19, 1995, the 9 story steel-reinforced concrete structure, Alfred P. Murrah Federal Building in Oklahoma City suffered collapse because of the truck bomb detonated outside the façade [5].
- On June 29, 1995, the 5 story steel-reinforced concrete structure, Sampoong Department Store in Seoul, South Korea suffered progressive collapse because of the removal of several columns on the lower floor to make room for escalators [6].
- On September 11, 2001, World Trade Center buildings in New York City collapsed as a result of terrorist attacks and subsequent fires. The whole structure suffered disproportionate collapse because of the buckling of columns which in turn is due to the sagging of bridge-like floor systems because of fire [7].

1.2. Scope and main objectives

The support for the research has been provided by Politehnica University Timisoara, Laboratory of Steel Structures, within the research grant "Structural conception and collapse control performance based design of multistory structures under accidental actions" CODEC 2012-2016 [8].

The aim of the thesis is to study the behavior of T-Stub components of beam-to-column end plate bolted connections under large deformation demands associated with the loss of a column. For this purpose, an extensive experimental testing program on T-stub components was developed to evaluate the ultimate strength and deformation capacity. Based on the experimental data, numerical models have been validated and employed in a parametric numerical study that aimed at improving the response under large deformation demands.

Following are the main objectives of the thesis

1. Studying post yield behavior of T-Stub macro-component for mode 1 and mode 2.
2. Investigating ultimate capacity and ductility to account for the reserve capacities in T-stub macro-components beyond its yield point.
3. Improving the ductility of a T-stub component by playing with various variables in the T-stub component of bolted extended end plate connection.
4. Improving robustness of connection by studying catenary action of T-stub component and various factors affecting it.

1.3. Research Framework (CODEC Project)

This thesis is a part of CODEC project supported by Romanian National Authority for Scientific Research, 2012-2016 [8].

The main objective of the project was to develop specific design guidelines to improve the overall robustness of multistory buildings and to mitigate progressive collapse under accidental loadings. The research project was divided into seven main phases, see table 1 for detail information

Table 1. CODEC research framework phases

Phase	**Title**
Phase 1	Preliminary investigations
Phase 2	Design of experimental and numerical program
Phase 3	Experimental program on materials, welds details and macro-components
Phase 4	Experimental program on joints
Phase 5	Experimental program on sub-assemblies
Phase 6	Numerical program
Phase 7	Design guidelines and recommendations

Following is the quick summary of different completes phases.

Phase 1: Preliminary investigations

Preliminary investigations involved the study of existing knowledge and analytical tools available in the field of robustness. The study of gaps in knowledge and evaluating effectiveness of the existing design procedures against the collapse control of multistory buildings under accidental loadings

Phase 2: Design of experimental and numerical program

Phase 2 involved the design of experimental and numerical approach based on the case studies of different structures. Experimental program involved testing of material specimens, T-stub components, beam to column joints under different scenarios and Half-scale subassemblies of steel and composite two-bay two span configurations. Numerical program involved revalidating experimental tests by making numerical models using finite element modeling software.

Phase 3: Experimental program on materials, welds details and macro-components

Phase 3 of the project involved determining mechanical properties of materials used in macro-components as structural members. It involved material testing under room temperature (20’C) and elevated temperatures (540’C) under quasi static (0.05 mm/s) and dynamic strain rates (10

mm/s) under monotonic loadings. Experimental testing on T-stub macro components of bolted end plate connections was also part of this phase.

Phase 4: Experimental program on joints

Studying behavior of beam to column joints under large displacements because of the column loss scenario under accidental loadings was part of this phase. Different Joints configurations were testing to study the development of catenary action. Push down tests using hydraulic actuators were carried out which involved pushing the middle column down until failure. Detail study and results can be found in [9]

Phase 5: Experimental program on sub-assemblies

In order to study the response of joints and formation of catenary forces in 3D, sub-assemblies were testing under phase 5. The test specimens are half scaled with two-bay two-span of a typical floor structure with the size of 6.0 x 6.0 x 1.5 meter. Same push down test procedure was applied to study formation of catenary forces in 3D sub-assemblies.

Phase 6: Numerical program

Numerical modeling phase served as a revalidation phase in which experimental results obtained before were used to calibrate the models.

Phase 7: Design guidelines and recommendations

Phase 7 is the last phase presenting the final guidelines and conclusions of the project. Presenting recommendations and general design procedures to avoid progressive collapse scenario in case of accidental loadings.

1.4. Basic terms

Accidental actions:

Accidental actions are hazards having extremely low probability of occurrence that they are ignored in the design of structures directly. Due to its low probability of occurrence it is difficult to incorporate in design because of economic constraints.

Progressive collapse:

Progressive collapse is defined as a disproportionate collapse of a structure in which primary or local failure of a structure triggers the failure of adjoining structural elements which in turn causes the entire structure to collapse.

Robustness:

According to the Eurocode 1991-1-7 [10] , Robustness is defined as an ability of a structure to withstand disproportionate collapse because of accidental loadings like fire, explosions, impacts or consequence of human error.

Structural Integrity:

Structural Integrity is an ability of a structure to withstand accidental loads causing local failure of member hence providing overall ability to withstand the hazard by preventing total collapse of a structure

Catenary action:

Catenary action is a mechanism forms under large displacements in which vertical load in a horizontal member is resisted by means of internal tensile forces. In order for such mechanism to form a rigid horizontal supports at the ends are required to support deflection in the middle as shown in the figure below. The bigger the deflection the smaller is the tension force from equilibrium conditions.

2. REVIEW OF EXISTING STANDARDS AND PROVISIONS FOR PROGRESSIVE COLLAPSE OF MULTI-STOREY FRAME BUILDINGS

Numerous developments have been made in the field of robustness to prevent total collapse of a structure under accidental hazards from nature and man-made. After the collapse of Ronan Point, UK and Canada adopted general rules in the building codes to improve the robustness of a structure and to prevent such collapse in future from happening again. Such provisions include adding redundant members in the structure, tying together building elements to form a more robust load path and to add sufficient strength and ductility to the structure to sustain accidental loads. These general requirements produce more robust structures that are strong and ductile enough to withstand accidental loads by sustaining a feasible load path. U.S. also later added the term structural integrity in there design requirements which serves the purpose of increasing overall robustness of a structure. But these general code requirements do not provide specific provisions which designer can follow in order to achieve more robust structure. These codes do provide some guidance to prevent progressive collapse of a structure by ensuring additional redundant members and by increasing strength and ductility of a structure but no such specific set of rules are available in current codes of practice.

Different government organizations throughout the world are working on this ongoing research on progressive collapse prevention of multistory buildings. In U.S. different organizational units have defined set of general guidelines to improve structural integrity. General Services Administration provide a document “Alternate Path Analysis and Design Guidelines for Progressive Collapse”[11] which surpasses its previous document “GSA progressive Collapse Analysis and Design Guidelines for New Federal Office Buildings and Major Modernization Projects 2003”. Unified Facilities Criteria on “Design of Buildings to Resist Progressive Collapse”[12] gives an alternate path method to improve structural integrity, hence the robustness of a structure. American Society of Civil Engineers ASCE also provide a document which gives general guidelines to improve structural integrity in there document “Seismic Rehabilitation of Existing Buildings”[13] . Steel construction institute in the UK published a document to prevent disproportionate collapse of steel buildings under the title “Structural Robustness of Steel Framed Buildings”[14] .

2.1. Design guidelines based on ASCE Standard 7-05 [15]

ASCE Standard 7-05 [15] presents following three methods to prevent progressive collapse of a structure

- Indirect Method
- Specific Local Resistance Method
- Alternate Load Path Method

American society of civil engineers code 7-05 [15] gives extensive discussion on structural integrity and it gives measure how to improve by presenting general as well as specific set of rules. It presents direct and indirect approaches and three methods to achieve structural integrity and resistance against progressive collapse.

NISTIR 7396 [16] Document provide detailed discussion of these direct and indirect (Specific Local Resistance Method and Alternate Load Path Method) methods to prevent progressive of a structure. It provides general basic set of rules to improve the structural integrity by incorporating redundancy, ties, ductility, adequate shear strength and capacities for resisting load reversals. Connections also play a very important role in improving overall structural integrity of a structure against progressive collapse prevention. This document also gives practical design approaches to prevent progressive collapse. Two main approaches (direct and indirect) are used to differentiate the methods which can be used to make structure more robust under these threats.

Indirect method gives general prescriptive approach to improve progressive collapse resistance by incorporating general set of rules of increasing redundancy, Tie requirements, detailing requirements etc.

Direct methods involve improving the performance of a structure against progressive collapse by improving resistance of key structural elements prone to robustness issues. This therefore involves detailed analysis to identify problematic key structural elements which are weak links in overall structural integrity requirements.

2.1. Robustness of steel frame buildings based on SCI P391 Publication

SCI publication [14] on structural requirements for robustness strategies gives additional requirements other than mentioned in Eurocode standard. It gives additional structural provisions on providing minimum level of horizontal tying within the frame. It allows catenary

action to develop because of the tying effect and provisions such as holding the columns in place. This design guide also gives practical application of design rules which provide general guidelines to make structure more robust under accidental loadings.

2.2. British Standards

After the Ronan Point collapse, British standards incorporated provisions such as tying of various structural elements of a building to make more robustness structural system arrangements. Special provisions for the ties were incorporated to prevent wall panels from out of plane failure. Additional accidental loads were also applied to the structures for its design to improve the overall resistance. The first standard was approved in 1970 and later further provisions were added in 1974. Building regulations, HMSO was released in 1976 containing design provisions to prevent disproportionate collapse. These provisions improved the performance of structures subjected to accidental loadings including explosions, impact etc. for example in april 1992, a bomb explosion took place in the vicinity of a Exchequer Court, St mary's Axe, London, a building consisting steel frame, composite concrete floors designed to resist lateral wind loads through the system of braced steel bays. The explosion caused damage to numerous buildings and incur considerable damage to both its structural and non-structural components but overall the building remained intact (Figure 1) showing the effectiveness of these provisions. Although the St. Mary's explosion was different in nature to the internal gas explosion of Ronan building point causing the disproportionate collapse of that building, continuous research has led to the improvement of design provisions resulting in new version of the guidelines released in 1991, followed by 2004 and 2010 editions. The requirements of these standards are expected to produce more robust structures against impacts as well as gas explosions. Latest version of approved documents released in 2010, has fourteen technical parts

Figure 1. Exchequer Court bombing, St Mary's Axe, London 1992: damage to composite floors; b) ground floor steel columns [17]

Apart from UK, Sweden (Granstrom, S., 1970) was also involved in early studies about progressive collapse and Denmark (Hanson and Olesen, 1969), and also Germany, Netherlands and France. The cooperative effort across Europe and the provisions from various national standards led to the development of the Eurocodes.

2.3. Eurocodes

Eurocode which is adopted code for design of structures in many European countries gives general design recommendations such as good structural layout, tying of structural elements together. Four classes of building importance are also defined considering the importance of building and two high levels required special considerations to ovoid progressive failure of a structure.

Eurocode EN 1991-1-7 [10] gives general design guidelines on accidental loadings on a structure. This publication gives guidance on structural robustness based on Eurocode rules to prevent disproportionate collapse of steel-framed buildings.

Four building classes are defined according to Eurocodes and they gives general recommendations on structural robustness. This document is useful because it gives detailed descriptions on robustness strategies for different classes of steel-frame building when Eurocodes do not give requirements or when they are not specific and open to interpretation.

Currently there are 10 Eurocode documents which altogether gives extensive detailed design requirements in all aspects of structural design. Following is the list of these Eurocode standards

- EN 1990 Eurocode: Basis of structural design
- EN 1991 Eurocode 1: Actions on structures
- EN 1992 Eurocode 2: Design of concrete structures
- EN 1993 Eurocode 3: Design of steel structures
- EN 1994 Eurocode 4: Design of composite steel and concrete structures
- EN 1995 Eurocode 5: Design of timber structures
- EN 1996 Eurocode 6: Design of masonry structures
- EN 1997 Eurocode 7: Geotechnical design
- EN 1998 Eurocode 8: Design of structures for earthquake resistance
- EN 1999 Eurocode 9: Design of Aluminum Structures

2.3.1. Eurocode Robustness Requirements

Eurocode EN 1990 [18] gives principles and requirements for general safety, serviceability and durability concerning structural design. This part of Eurocode highlights several basic requirements for the design of structures under accidental actions stating "sustain all actions and influences likely to occur during execution and use". Furthermore the general clause in the same document stating the engineer is responsible for designing a structure such that it should "have adequate structural resistance, serviceability and durability". According to this document its structural engineers responsibility to make a structure more robust although no specific rules are set out in this standard.

Eurocode standard EN 1991-1-7 gives general requirements that buildings have to be robust to avoid disproportionate collapse during construction and service life of the structure. Some details are specified in this standard to how to meet general requirements concerning robustness but it does not specifically deal with accidental actions caused by explosions or terrorist attacks.

Two general types of strategies against accidental loadings are specified in EN 1991-1-7 which are as follows

- Strategies based on identified accidental actions
- Strategies based on limiting extent of localized failure

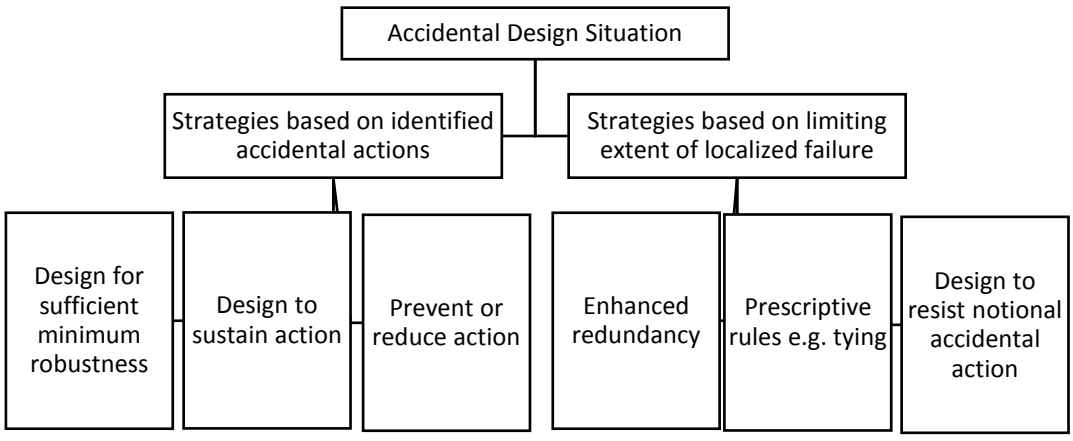

Figure 2. Accidental design situations based on Eurocodes

Strategies which are based on identified accidental actions can be determined on the exact scale and structures can be designed to be robust against such known accidental actions while strategies which are based on unidentified accidental actions covers wide range of possibilities

and can be tackled using enhanced redundancy, prescriptive tying rules and using notional accidental actions on the structure to be designed.

For the consideration of the accidental design situations Eurocode EN 1991-1-7 classifies the building in following three consequences class depending on the importance of the building. Consequence class three involves high consequence for loss of human life therefore for these structures progressive collapse studies are important and structural integrity is to be insured to make structure more robust.

Table 2. Consequences classes based on Eurocodes

Consequences Class	**Description**
CC3	High consequence for loss of human life, or economic, social or environmental consequences very great
CC2	Medium consequence for loss of human life, economic, social or environmental consequences considerable
CC1	Low consequence for loss of human life, and economic, social or environmental consequences small or negligible

The structural requirements are more stringent from consequence class one (CC1) to consequence class three (CC3). Adopting the required recommendations of this Eurocode standard should make structures robust and should prevent from disproportionate collapse.

2.4. Swedish Design Regulations

BKR Swedish design regulations gives three classes of structural safety called safety classes. Only safety class 3 includes the provisions for structural integrity and how to make a structure resistant to progressive collapse. The requirements are presented in following separate handbooks

- Checking the stability of a damaged building under dead and live loads
- Checking the falling debris do not cause the failure of successive floors by insuring enough strength of floors to prevent the collapse

This Design regulations BKR standard contains mandatory provisions and general recommendations on technical requirements for construction works. This standard contains general regulations for structures to check stability and structural integrity.

2.5. ACI 318

This standard “Building Code Requirements for Structural Concrete” from American Concrete Institute covers the materials, design, and construction of structural concrete used in buildings. This standard also covers the strength evaluation of existing concrete structures.

ACI 318 design code follows indirect design approach of ASCE 7-05 in achieving structural integrity including detailing provisions such as ensuring continuity of reinforcements and use of proper ties etc.

3. LITERATURE REVIEW

Performance of multistory steel-frame building under extreme loading conditions may depend on beam to column connections as under large displacements during a column loss scenario, robustness of a structure depends on the ability of a structure to transfer loads using alternate path method (AP). This alternate path method requires the development of catenary forces in the beams which imparts strong tying forces onto the connections forming a mechanism to transfer the load into the foundations through surrounding columns. Hence the deformation capacity of the connections forming the catenary mechanism is vital in structural integrity of a whole structural system. T-stub component which ensures the ductility of the connection is therefore of vital importance in the prevention of disproportionate collapse and the study of robustness. T-stub component is the most important component of connection in a steel-frame structure because it plays a major role in determining the overall strength, stiffness and ductility of a connection [19]. Therefore it is imperative to study behavior of T-Stub components under large axial forces to understand the behavior of structure under accidental loadings and to ensure structural integrity and to make a structure more robust.

3.1. T-Stub model according to Eurocode EN 1993-1-8

According to Eurocode EN 1993-1-8 [20] T-Stub model is used to determine design resistance of the following components in bolted connections

- Column flange in bending
- End plate in bending
- Flange cleat in bending
- Base plate in bending under tension

Eurocode EN 1993-1-8 includes values to be used for different dimensions of T-Stub to calculate overall resistance. Following are the different dimensions used in this standard.

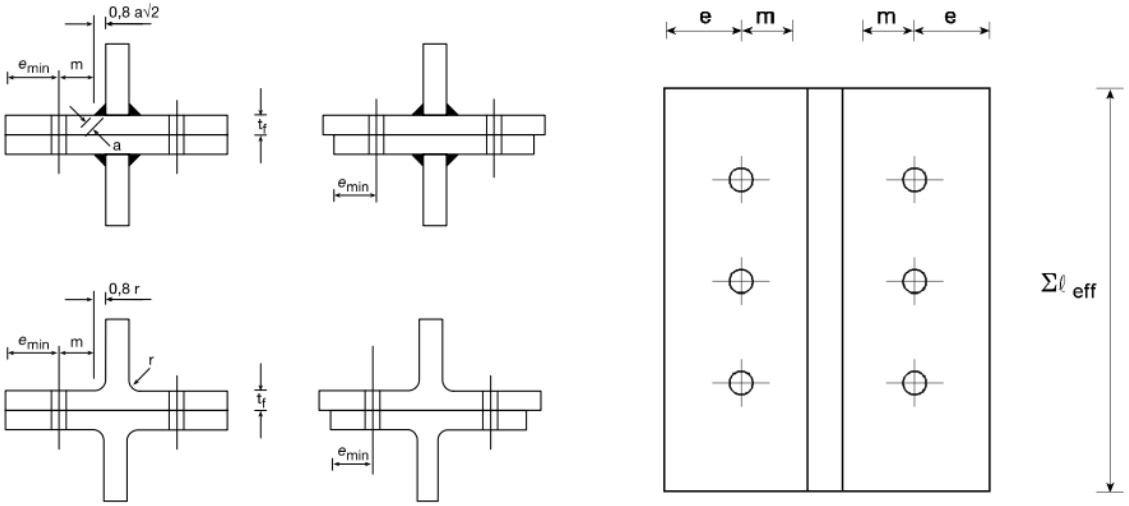

Figure 3. Standard variables used in Eurocodes to determine different failure modes of T-stub

T-stub component model basically consists of tension loaded web causing bending in the end plate and tension forces in the joint according to the EN 1993-1-8 model. Furthermore this standard defines following three failure modes

- Failure mode 1: complete yielding of flanges
- Failure mode 2: Yielding of flanges accompanied by failure of the bolts
- Failure mode 3: Failure of the bolts

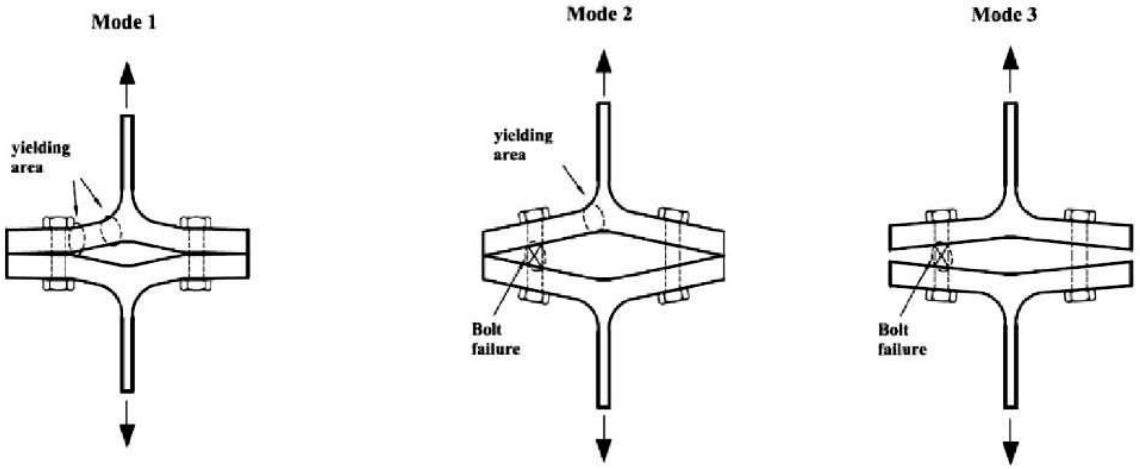

Figure 4. Failure modes of T-stub macro-component

Eurocode defines set of formulas to determine capacities for all the failure modes and the mode with lowest resist is generally the governing failure mode particular T-Stub component.

Table 3. Eurocode method to calculate failure modes of T-stub macro-component

	Prying forces may develop, i.e. $L_b \le L_b^*$		No prying forces
Mode 1	Method 1	Method 2 (alternative method)	$F_{T,1\text{-}2,Rd} = \frac{2M_{pl,1,Rd}}{m}$
without backing plates	$F_{T,1,Rd} = \frac{4M_{pl,1,Rd}}{m}$	$F_{T,1,Rd} = \frac{(8n-2e_w)M_{pl,1,Rd}}{2mn-e_w(m+n)}$	
with backing plates	$F_{T,1,Rd} = \frac{4M_{pl,1,Rd}+2M_{bp,Rd}}{m}$	$F_{T,1,Rd} = \frac{(8n-2e_w)M_{pl,1,Rd}+4nM_{bp,Rd}}{2mn-e_w(m+n)}$	
Mode 2	$F_{T,2,Rd} = \frac{2M_{pl,2,Rd}+n\Sigma F_{t,Rd}}{m+n}$		
Mode 3	$F_{T,3,Rd} = \Sigma F_{t,Rd}$		

3.2. Design guidelines for progressive collapse resistance

Past research includes development of design strategies under gravity loads which give rise to strength design method. Later with the development of dynamics and earthquake forces performance based designs became more relevant in the design of structures. Under localized failures, especially under a column loss scenario special consideration has to be taken for the development of catenary action. Assessment of the progressive collapse of steel-frame building was carried out by [21] using recommended GSA [11] and DoD [12] rules. Authors in [21] suggested the importance of joints to activate full catenary mechanism in the girders they were using in steel-frame building. They assumed a rigid panel assumption but quoted that incase of non-rigid panel condition which is true in semi-rigid connections in steel-frame buildings the effect of column loss would result in higher deflections and hence increasing the potential of progressive collapse of a building.

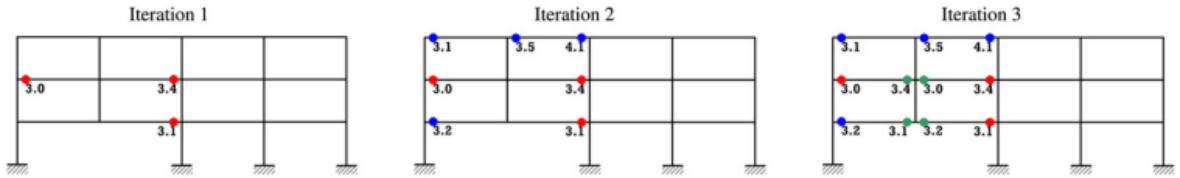

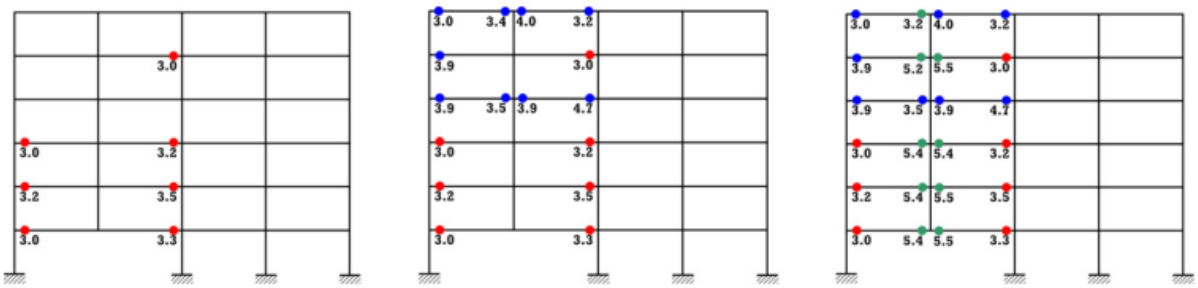

Figure 5. Hinge formation of a frame structure under column loss scenario

3.3. Review of studies on joints and macro components

Authors in [22] did a very valuable research in analysis of following six type of steel beam to column connections.

- Web cleat connection
- Fin plate connection
- Top and seat with web angles connection (8mm thick angle)
- Flush end plate connection
- Extended end plate connection
- Top and seat with web angles connection (12mm thick angle)

Testing was followed by the finite element modeling and both static and dynamic explicit solvers were used for the analysis and different problems in convergence, contact, large deformations and fracture simulations were discussed in detail. Author's study indicate that static solvers provide better results but it has convergence problems in solving finite element equations while dynamic explicit solver is better in simulating fracture and has less convergence problems in solving finite element equations therefore complete fracture studies can only be conducted in dynamic explicit solver. All the six beam to column connections were studied under catenary action stage to predict the overall response of connection and to determine overall rotation capacities. In Europe since most of the region are non-seismic and therefore aforementioned connections are common. Furthermore bolted beam to column connections are mostly classified as simple or semi-rigid joints which are more vulnerable than rigid joints [21] under extreme loadings especially column loss scenario.

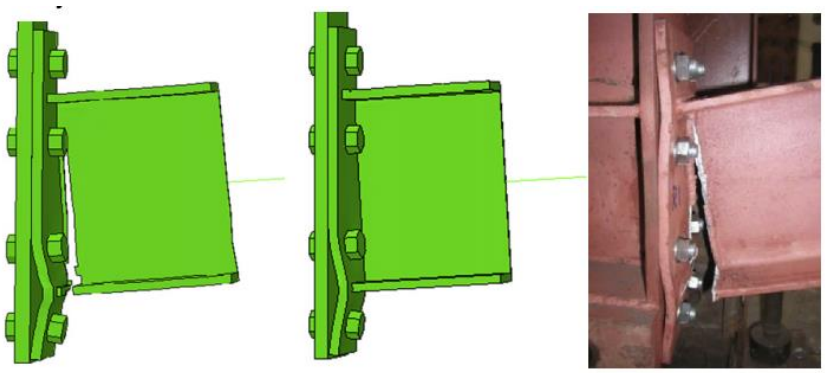

Figure 6.Failure modes of FE simulations and experiment of the extended end plate connection [22]

First figure shows numerical modeling using explicit dynamic solver and following picture shoes numerical finite element modeling in general static solver of Abaqus and the following third picture shows extended end plate connection being tested experimentally.

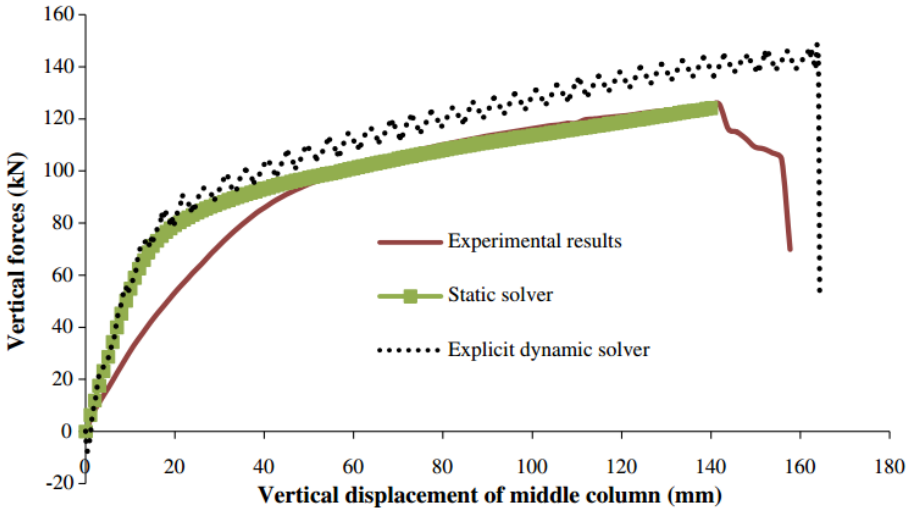

Figure 7. Comparison of the FE simulations to the test data of extended end plate connection [22]

As shown in the picture the experimental results and static solver approximations are quite close to each other and predict the actual behavior of connection but according to author of the paper it has convergence issues and complete fracture simulations can also be not performed in static solver of Abaqus finite element analysis package. Following were the drawn conclusions

- Static solver can usually predict closer simulation results than explicit dynamic solver
- Static solver faces numerical convergence problems specially when modeling fracture simulations. Complete fracture simulations can be performed in dynamic explicit solver but it requires huge computer resources to run the model

- Connection subjected to large catenary forces has significance influence on the connection depth which plays a very important role in determining overall capacities of the connection.
- Large improvements in connection performance under catenary action can be achieved by improving arrangements of the bolts in flush end plate connection configurations.
- Catenary action can increase the load carrying capacity of different bolted joints under column loss scenario [23]
- Experiments shows the tensile capacities (T-stub component) of beam column joints in catenary action stage undergoing large rotations mostly control the failure mode of a connection [23]

3.4. Experimental program on bolted-angle T-Stub component

Similar studies to determine ultimate tensile deformation and strength capacities of bolted angle connections were determined by [24] in which 31 bolted-angle connections were experimentally tested under pure tension. Load deformation curves, ultimate tensile deformation and strength of the bolted-angle connections were evaluated for different failure modes including rupture of the angle and rupture of the bolts. Following four different types of failure modes were observed and deformation patterns were recorded for each failure mode.

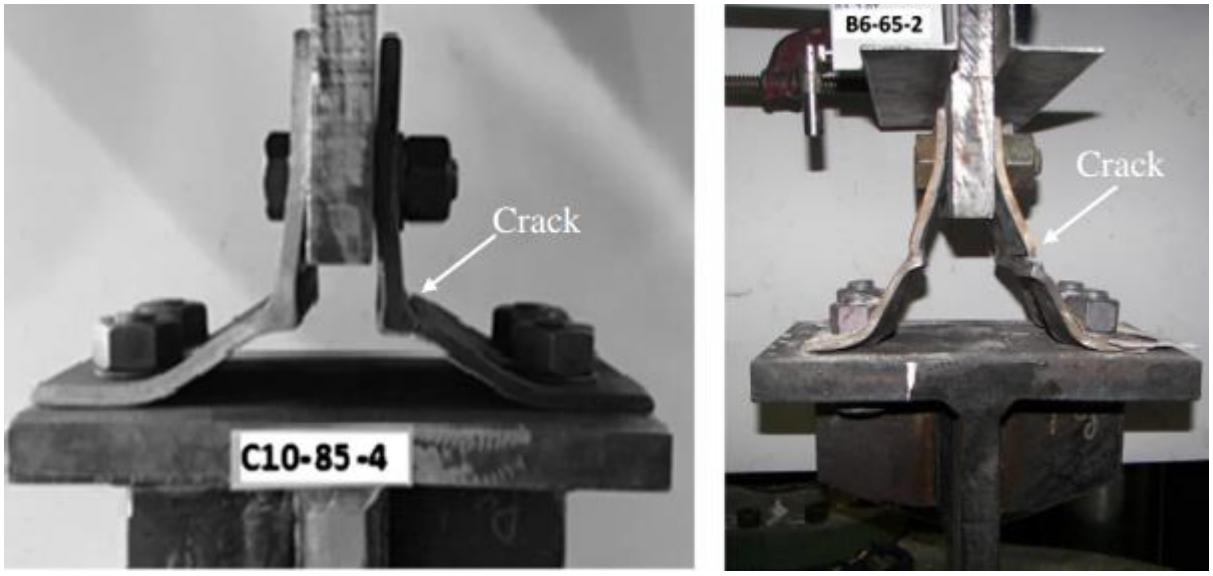

Figure 8. Angle rupture with and without straightened legs

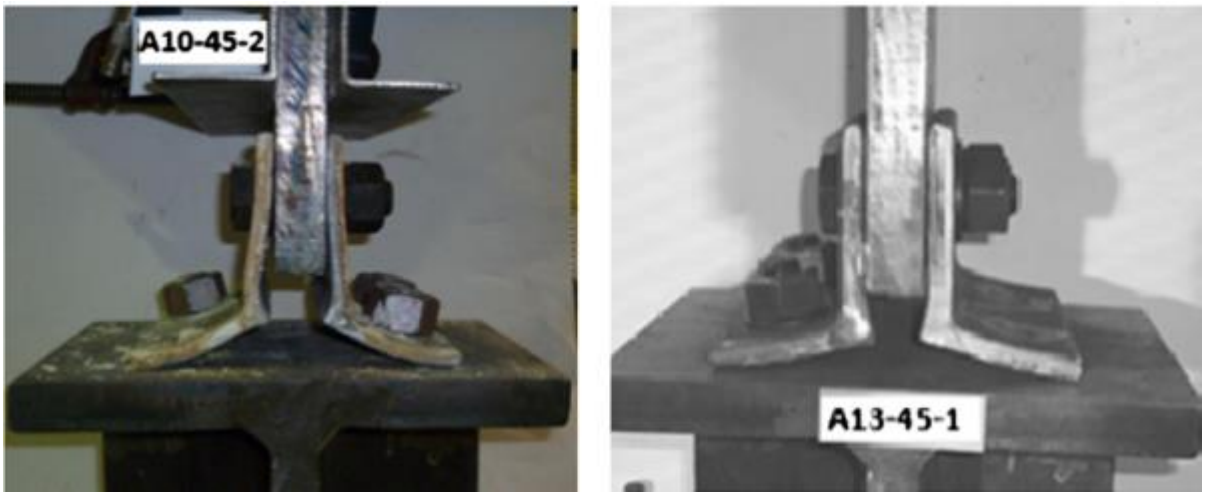

Figure 9. a) Tension bolt rupture with plastic hinges on both legs b) Tension bolt rupture with plastic hinge on framing leg

New equations for predicting axial deformation capacity and prying were proposed for the design of the bolts to ensure ductile failure of the bolted-angle connections. Following main conclusions were made.

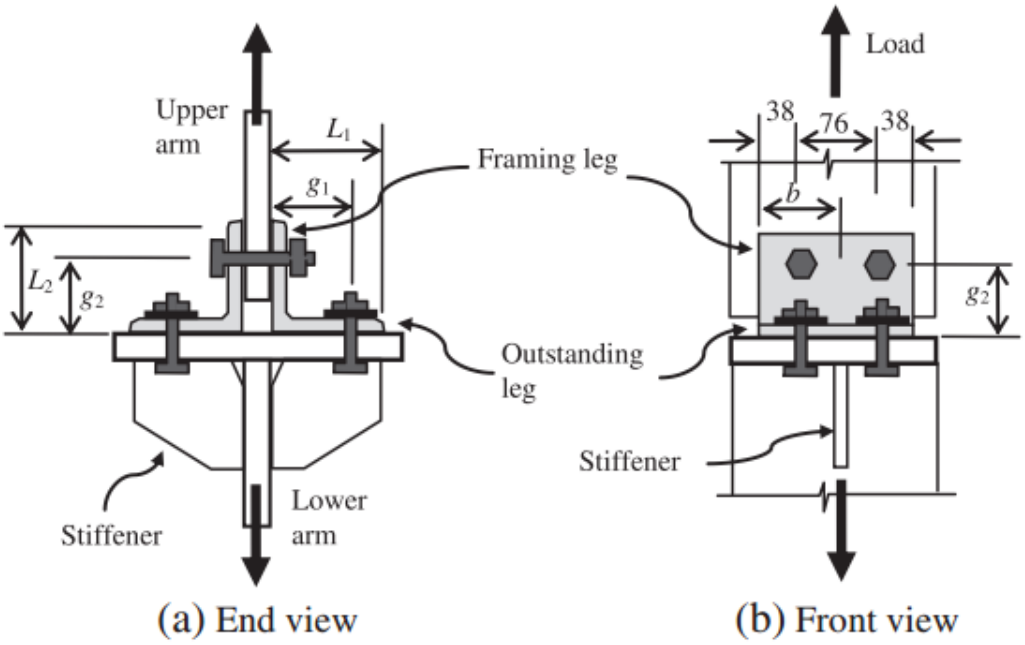

Figure 10. Front and end views of the bolted angle T-stub connection

- In bolted-angles connections to ensure sufficient ductility the rupture of the bolts should be avoided

- The design philosophy presented in [25] should be followed for the robust design of structures.
- This study revealed the minimum tensile capacity of the bolts which should be at least two times the tensile capacity of the angles used.
- Combined shear and tension effects were also incorporated for the prying action of the bolts and new equations were proposed.
- The test program showed that the ultimate deformation capacity of the bolted-angle connections were not proportional to the ratio of distance between the bolts and thickness of the angle.
- The study also revealed that behavior of the bolted-angle connections at ultimate limit states is rather complex, therefore a pure analytical model is hard to come by.

Another study on bolted angle connections was done by [26] to develop a new mechanical model to predict the deformation capacity if each component of the connection. Fourteen specimens were tested with the following parameters under study

- Bolt hole positions
- Angle thickness
- Bolt size
- Material properties

Five different types of failure modes were observed during the experimental procedure. The test results revealed that the ultimate load at large deformations was much higher than that for the yield strength which shows large reserve deformation and load capacity.

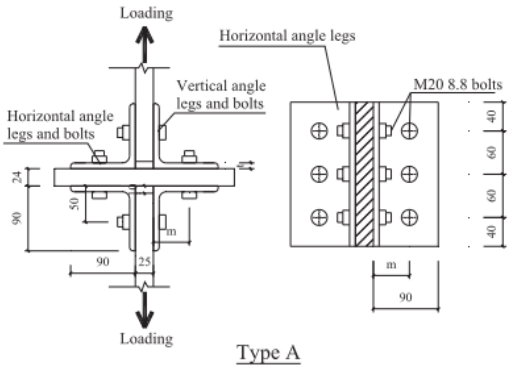

Figure 11. Specimen configuration of a typical connection used for testing

The specimens were subjected to a monotonic force with the strain rate of 0.025mm/s until the complete failure of the bolted-angle connection.

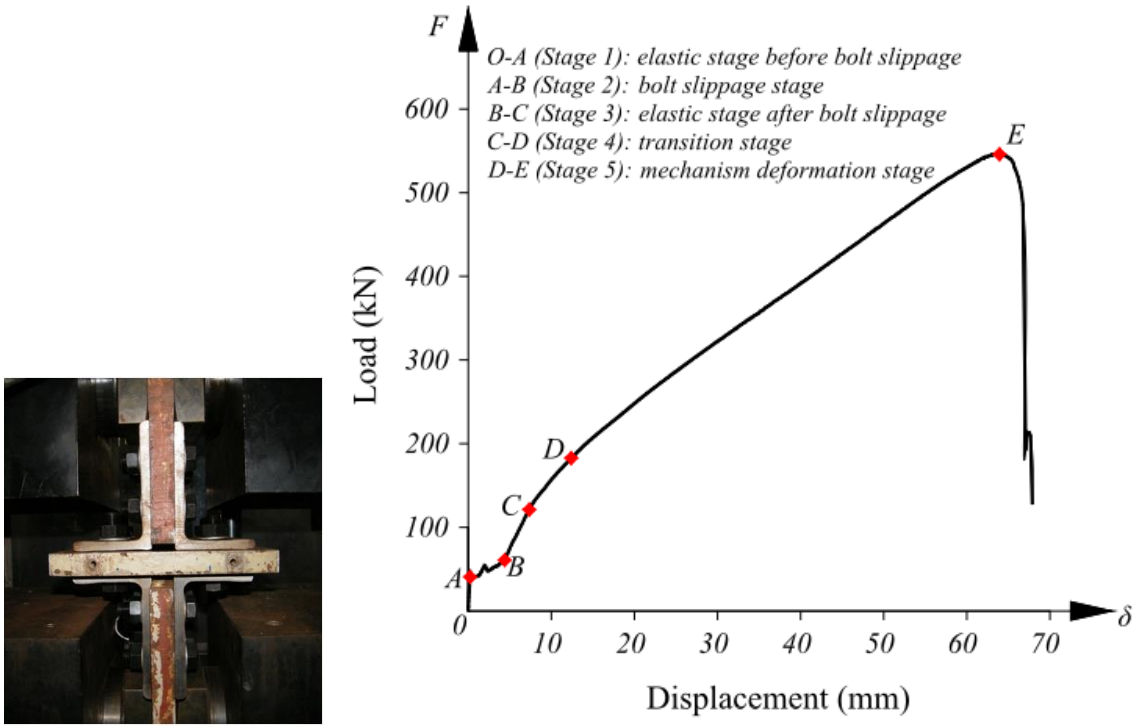

Figure 12. Test setup and load displacement curve of specimen A90-8-50-I

Following were the five different types of failure modes observed

Figure 13. Angle fracture at bolt holes (A90-8-50-I)

Figure 14. Angle fracture close to heel (A90-9-60-III).

Figure 15. Angle fracture at bolt holes with yielded bolts (A90-8-40-I).

Figure 16. Angle fracture close to heel with yielded bolts (A90-10-60-IV).

Figure 17. Bolt fracture with yielded angles (A90-10-50-IV).

Mechanical model for bolted-angle connections was proposed and validated using the experimental test results. Large deformation response taking into account nonlinear geometric and material properties was determined using these proposed numerical models. The test results by the authors revealed that ultimate strength of the bolted-angle connection is much greater than yield strengths and the load-displacement response of the bolted-angle connection depends on large deformation response rather than the small deformation response. Different equations have been proposed by the authors to predict plastic hinge formation and the deformation capacities under tension. The overall proposed mechanical model by the authors gives good prediction of the behavior of the bolted-angle T-stub component of the connection.

3.5. Experimental Program on T-Stub component under different strain rates

Authors in [27] determine influence of strain rate on the response of T-stub component of the connection. The authors conducted an experimental study of T-stub components of flush end-plate beam-to-column bolted connection. The rotation capacity which is the ductility of a connection depends on the deformation capacity of a weaker component of the connection which can be modeled as a T-stub component of the connection. Under this program a total 20 tensile tests on T-stubs were performed with different strain rates to determine the behavior of the T-stubs under different loading configurations. In order to determine the effect of strain rate three different loading conditions were carried out on the same type of specimens.

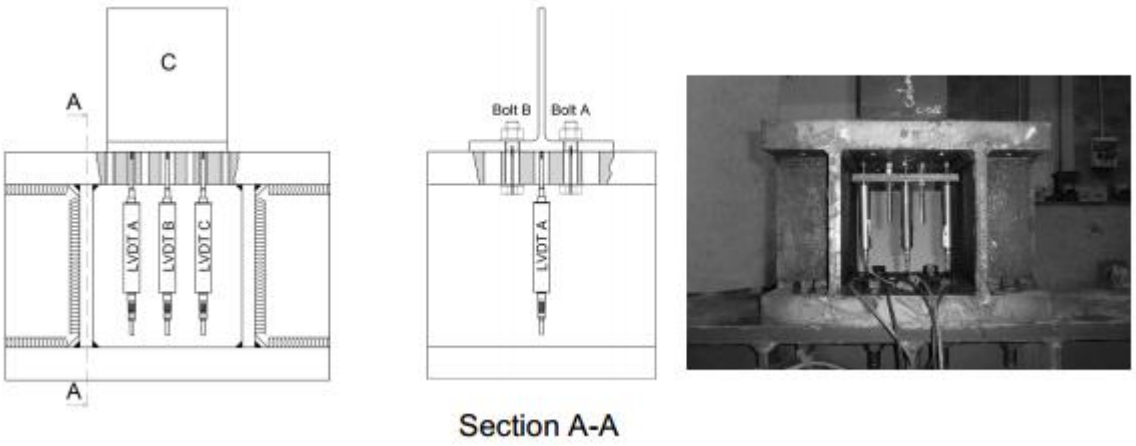

Figure 18. Instrument setup for bolted T-stub

Transducers were used in different locations of the T-stub to measure the deformation in the T-stub and the bolts. Three different deformation rates were applied i.e. 0.07 mm/s , 160 mm/s and 326.90 mm/s.

Load deformation curve for the flange displacement and bolt force was determined. Following are the test results comparing flange displacements for different loading configurations.

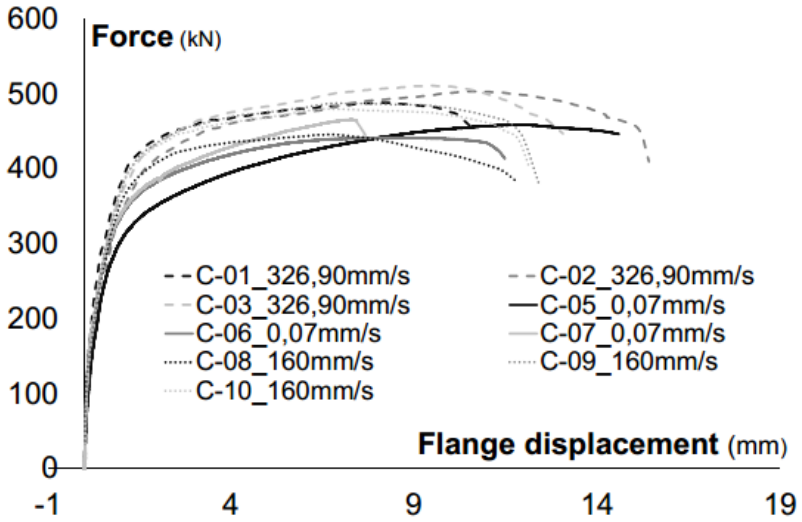

Figure 19. Comparison between test results on column flange T-stub

According to these test results the development of the flange mechanism is independent of the strain rate. Although with the increase of strain rates a slight increase in the axial capacity and a slight reduction in the ductility of the T-stub component of the connection is observed, but these observations has negligible effect. Overall conclusion made is that strain rates have no significant influence on the behavior of the T-stub component of the connection hence the

overall strength, stiffness and ductility of the connection remains unaffected with the increase in strain rates.

3.6. Study of bending of the bolts in T-stub component

T-stub component of the bolted moment connections usually represent the tension component of the connection and the bolts used in the T-stub component usually are considered to be loaded only in tension which might not be the case in reality. The paper [28] investigates the behavior of the bending of the bolts on T-stubs. Different numerical models were used to study the behavior of bolts under bending. The study conducted further investigates the interaction of the axial forces with bending moments to determine the resistance of the bolts and to evaluate the accuracy of the analytical interaction formulas presented in the literature and in different design codes. The resistance of the T-stubs is mainly dependent upon the bending resistance of the end plate and the tensile resistance of the bolts. However it has been reported in the research that the bending of the bolts were observed at failure which shows the bolts undergoes bending hence the overall resistance of the bolts is reduced because of the axial force and bending interaction. Following figure shows the increase in the overall stresses in the bolt M12 because of the bending stresses in addition to the axial stresses.

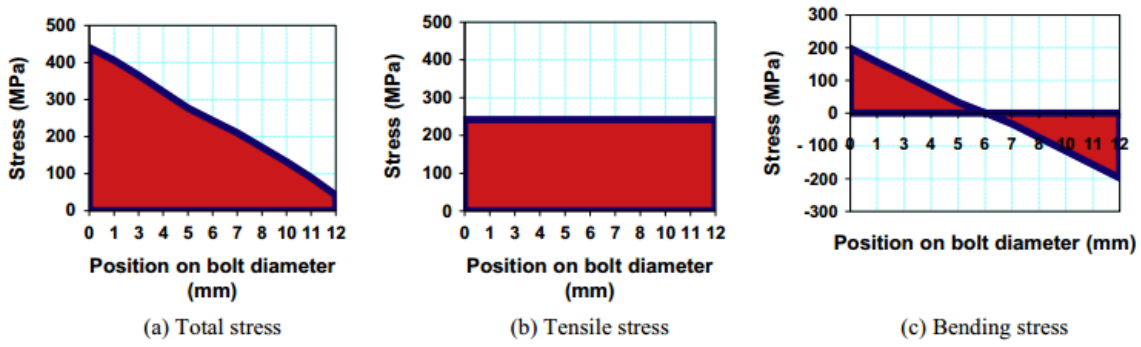

Figure 20. Distribution of bending and tensile stresses in Tb_M12 bolt from [28]

The authors concluded that ignoring bending moments in the bolts results in bolt capacity to reach only 70% of its ultimate capacity and the increase in the thickness of the flange end plate would result in the decrease of the bending moment in the bolt hence overall increasing the bolt capacity to reach closer to its ultimate capacity.

3.7. Study of elevated temperatures on T-stub component

Different authors also studies T-stub behavior under ambient and high temperatures to study the effect of high temperatures on the behavior of T-stub components. One of the study conducted by [29] on T-stub joint component at ambient and elevated temperatures. Results of the experiments on T-stub at ambient temperature showed that strength and stiffness of the T-stub component is directly dependent on the geometrical characteristics, material properties of the end plate and the bolts. Ductility depends on the plastic deformation capacity of the flanges of the T-stub which in turn depends on the geometrical characteristics, mechanical properties of the flange and the bolts along with the weld resistance.

At elevated temperatures, experimental and numerical results showed reduction in strength and stiffness. According to authors ductility showed a different tendency. Increasing temperatures results in the increase in the ductility. The increase in ductility at higher temperatures is a favorable contribution which results in the increase of the joint rotation hence providing more survival time for the structure. A less ductile failure mode was also observed because of the difference in degradation properties of the bolts and carbon steel. The authors in [30] tested simple beam end framing connections at elevated connections. Experiments on connection sub-assemblies were carried out at elevated temperatures under this research to characterize strength, stiffness, deformation capacity as well as different failure modes of the connection. Following figures shows the failure of a same connection at different temperatures. The experiment revealed that increasing the temperature shifts the failure mode from failure of bearing of the plates to the failure of the bolts which shows high strength loss of bolts under elevated temperatures.

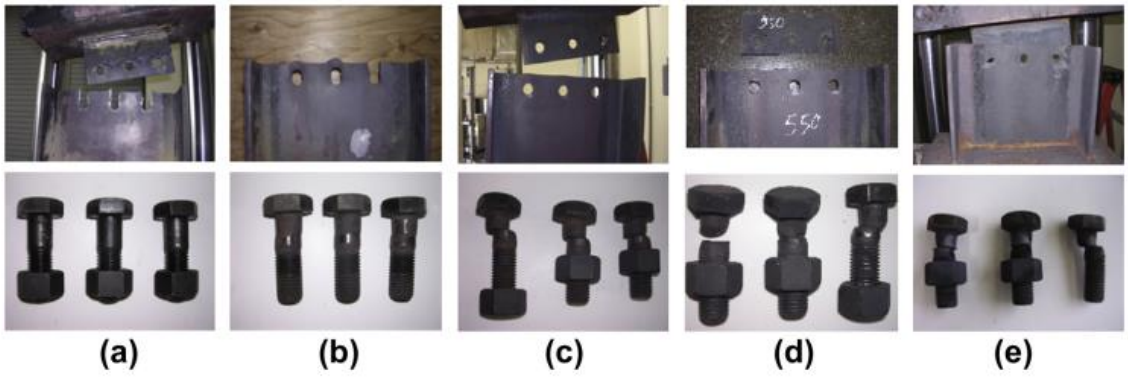

Figure 21. Connection failures after axial tension tests at (a) 20 ‘C, (b) 400 ‘C, (c) 500 ‘C, (d) 550 ‘C, and (e) 700 ‘C – W12 x 26 – 3/4 in. (19.1 mm) A325 bolts.

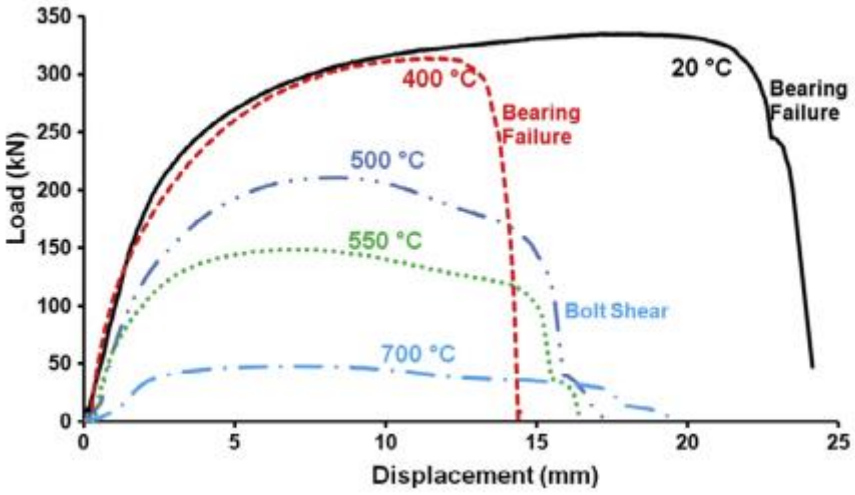

Figure 22. Load displacement response of connections with W12 x 26 beams and 3/4 in. (19.1 mm) A325 bolts under axial tension

As observed from the experimental results the shift from bearing failure to bolt shear failure with increase in temperatures suggests bolts are potentially more vulnerable than any other component in the connection. The authors suggest that bolts lose more strength than structural steel at elevated temperatures.

3.8. Concluding remarks, needs for new development

Capacity of the multi-story steel frame buildings to resist accidental loadings may depend on the performance of the beam-to-column joints which helps in providing continuity across the damaged region. Robustness of beam-to-column joints allow the development of alternate load paths preventing collapse of the structure to a larger extent. The continuity and ductility of the joints are important aspects to prevent disproportionate collapse. End plate bolted connections are widely used connections in the steel frame construction which ranges from simple connections which are flexible to rigid connections which are stiff and strong. Much of the developments to study different aspects of beam-to-column joints for bolted angle connections are presented in the literature review. For bolted angle beam-to-column connections the web in the T-stub macro-component is usually welded with the end plate of the T-stub and that is bolted with another T-stub component of the column with its web welded with end plate in a same fashion. Development of the catenary forces to provide alternate load paths for a robust design requires specific problems to be considered when localized failure e.g. column loss occurs. It is therefore of great interest to study the ultimate capacity of actual design procedures in order to provide enough robustness for connections to prevent disproportionate collapse under extreme loadings. T-stub components play important role in providing strength, stiffness

and ductility and the behavior of these properties in combination to each other is critical and needs to be studied for robust design of a steel frame building. T-stubs designed to fail in mode 1 and mode 2 depicts a rather complex phenomenon when it comes to ultimate capacities. Not much research is available to study the T-stubs with welded end plates with the web which are commonly used T-stub macro-components of the beam-to-column bolted connections widely used in the construction industry. There is a need to study the post yield behavior of T-stub macro-components failing in mode 1 and mode 2 to determine the reserve ultimate capacities and ductility in order to study and improve the robustness of beam-to-column connections ultimately improving steel frame buildings against progressive collapse under extreme loadings.

4. PRELIMINARY NUMERICAL MODELING

Numerical simulations were performed in finite element analysis software Abaqus version 6.14-4. Explicit dynamic solver was used in all finite element modeling because of its convergence efficiencies over general static solver. Nonlinear analysis was used in all the FEM modeling because of the need to study catenary action in post yield behavior of a structure.

4.1. Implicit and Explicit procedures

Abaqus/Standard and Abaqus/Explicit procedures are used to solve wide variety of problems. Following table extracted from [31] formulates key differences in Implicit and Explicit procedures. Understanding the characteristics of these standard and explicit procedures are important to use them for specific problems.

Table 4. Comparison between Abaqus/Standar and Abaqus/Explicit procedure

Quantity	**Abaqus/Standard**	**Abaqus/Explicit**
Element library	It offers extensive element library	It also offers extensive library of elements but only suited for explicit analyses. The elements available are subset of those available in Abaqus/Standard
Analysis procedures	It provides general and linear perturbation procedures	It provides only general procedures
Material models	It provides a wide range of material models	It also provides a wide range of material models and failure models are allowed
Contact formulation	It has robust capability for solving contact problems	It also has robust contact functionality that can readily solves the most complex contact simulations
Solution technique	It uses stiffness-based solution technique which is unconditionally stable	It uses explicit integration solution technique which is conditionally stable
Disk space and memory	Because of the large number of iterations possible in an increment, the disk space and memory usage can be usually large	Disk space and memory usage in Abaqus/Explicit is usually much smaller than that for Abaqus/Standard

In choosing between Abaqus/standard and Abaqus/explicit number of factors have to be taken in account. Since in this thesis fracture simulations would be performed and because of the contact and material complexities Abaqus/explicit is the best choice in resolving convergence problems and large number of interactions can be saved using explicit solver because in complex situations like in this thesis Abaqus/standard may face convergence problems, fracture simulations can't be fully modeled and because of the contact and material complexities it can take lot of iterations in Abaqus/standard taking long modeling analysis time. Since increasing number of degrees of freedom increase the computer cost as shown in figure below. Hence for modeling Abaqus/Explicit was used.

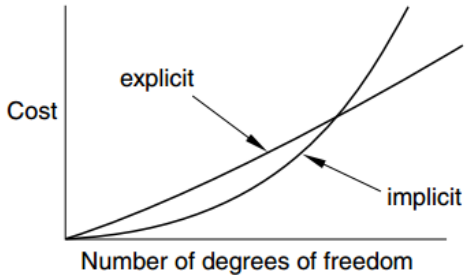

Figure 23. Cost vs degrees of freedom relation in Abaqus FEM

4.2. Finite Elements

Finite elements and rigid bodies are basic components in Abaqus. Rigid bodies are usually un-deformable while finite elements are deformable components. Abaqus contains wide range of elements for different modeling analysis. Generally elements are characterized as following

- Family
- Degrees of freedom
- Number of nodes
- Formulation
- Integration

Each element has a unique name in Abaqus which identifies different characteristics of the elements. A complete list of element types is available in Abaqus documentation [31]. Following figure shows general name convention of solid elements in Abaqus.

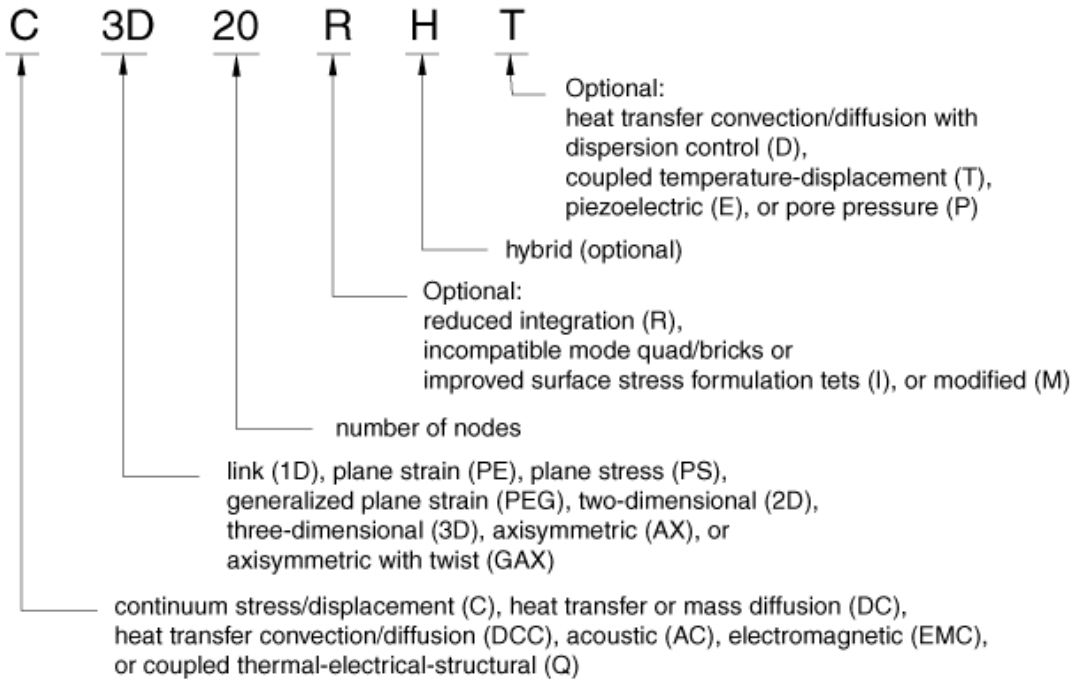

Figure 24. Naming convention of solid elements in Abaqus

4.2.1. Family

Following are the common element families that are used in Abaqus

- Continuum (solid) elements
- Shell elements
- Beam elements
- Rigid elements
- Membrane elements
- Infinite elements
- Springs and dashpots
- Truss elemets

4.2.2. Degrees of freedom

Degrees of freedom are the basic fundamental variables which are calculated during finite element analysis in Abaqus. Following are the six degrees of freedem conventions used in Abaqus for a 3D analysis for a stress/displacement simulations which would be the case in this thesis.

- Translation in direction 1,2 and 3
- Rotation about the 1-axis, 2-axis and 3-axis

4.2.3. Number of nodes

Degrees of freedem such as displacements, rotations, temperatures etc are calculated only at the nodes of an element. At any other points such entities are calculated by interpolations between the nodes.

4.2.4. Integration

Abaqus uses numerical integration to determine various quantities over the volume of elements. Abaqus provide full and reduced integration for various analysis problems in Abaqus standard while Abaqus/explicit only provides reduced integration elements.

4.3. Solid Elements

The solid (or continuum) elements will be used in this thesis. Abaqus using solid elements will be used for complex nonlinear analyses involving contact, plasticity, and large deformations.

4.3.1. Choosing between quadrilateral and tetrahedral mesh element shapes

With tetrahedral mesh elements it is easy to mesh large complex shapes and it has large automatic meshing algorithims which makes it easy to mesh very complicated geometry. Tetrahedral mesh elements are therefore more suited to mesh very complicated parts or instances but quadrilateral mesh element type provides solutions of equal accurancy and at less computer cost. Quadrilateral mesh elements are efficent in convergence than tetrahedral mesh element shapes. Quadrilateral mesh elements perform better if there shapes is approximately rectangular however tetrahedral mesh elements doesn't depend on initial element geometry.

4.3.2. Choosing between first-order and second-order elements

Second-order elements have higher accuracy in Abaqus/Standard than first-order elements for problems that do not involve complex contact conditions, impact, or severe element distortions. Second order elements capture stress concentrations more efficiently and are better for modeling geometric features.

First-order triangular and tetrahedral elements should be avoided in stress analysis problems because of the overly stiff nature of elements. These elements also exhibit slow convergence with mesh refinement, which is problem with first-order tetrahedral elements.

4.4. Calibration of material in FE models

4.4.1. Material calibration

The material model used is based on experimental tests performed on the coupons which were extracted from the same steel plates and steel profiles used to manufacture the T-stub specimen. The tensile test summary on steel plates used in T-stub component are described in the following table

Table 5.Coupon specimen details extracted from T-Stub macro-component

Coupon	Element	Dimension	Material	Thickness	fy
				(mm)	N/mm2
P-19	T-stub web	Pb55x10	S355	10	390
P-20	T-stub flange	Pb55x10	S235	10	310
P-21	T-stub flange	Pb55x12	S235	12	305
P-22	T-stub flange	Pb55x15	S235	15	275
P-23	T-stub flange	Pb55x18	S235	18	420

Tests on coupons were performed and since the engineering stress-strain curves for the same batch of coupons were almost similar therefore only one curve was used for the material modeling. For the material calibration in Abaqus the Engineering Stress-Strain curves were transformed to True Stress-Strain curves using the equations (3.1) and (3.2) from EN 1993-1-5 . Since Abaqus will incorporate the reduction in area itself. The formulas presented in EN 1993-1-5 are valid up to the necking point, after which the materials seems to soften but it actually hardens because of the fact that after necking significant reduction in cross-sectional area takes place which results in reduction in material resistance hence the stress values goes down but actually material continues hardening till fracture.

$$\sigma_{true} = \sigma (1+ \varepsilon) \quad (3.1)$$

$$\varepsilon_{true} = \ln (1+ \varepsilon) \quad (3.2)$$

Aforementioned formulas were used up to the maximum load. After the maximum load of engineering stress, the curve was considered ascending till fracture.

Finite element model of the tensile test coupons were modeled in Abaqus with the actual dimensions of the specimen. The experimental conditions were replicated using two reference points and linking them with kinematic restraints. One reference point was fixed in all degrees

of freedom while another reference point was displaced longitudinally using displacement boundary condition in dynamic explicit step. The quasi-static analysis was performed in dynamic explicit step using mass scaling option to get reasonable computational time. The procedure was quasi static since the ratio of kinematic energy and external work was maintained less than 1%.

For the calibration of the steel material to be used in T-stub component, a tension coupon tests were extracted from the T-stub macro-components. For the same class of the coupon three different tests were performed and the results were found to be almost the same.

For detailed discussion of numerical calibration, coupon with the dimensions shown in (Figure 25) with the thickness dimension of 10mm used for the numerical validation of web part of T-stub component is presented.

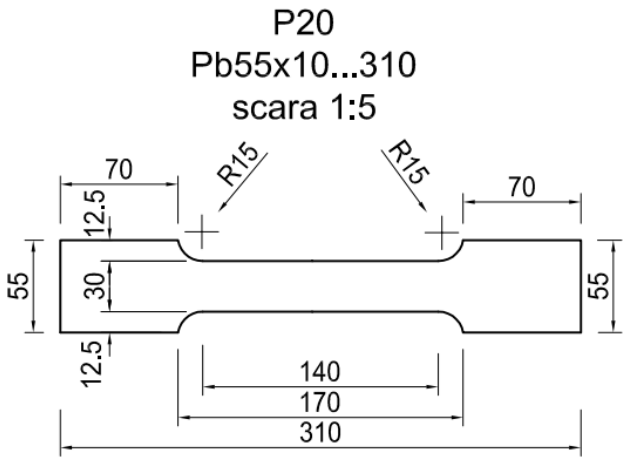

Figure 25. Dimensions of the coupon

3D deformable part was used with the following elastic material properties and density.

Table 6. Elastic properties of coupon P20 material

Elastic Property	**Value**	**Unit**
Young's Modulus	210000	N/mm^2
Poisson's Ratio	0.3	-
Density	$7.85x10^{-9}$	$Tons/mm^3$

For the plastic material property engineering stress-strain shown in (Figure 26) was converted to True stress-strain see (Figure 27) using the formulas presented in equations (3.1) and (3.2).

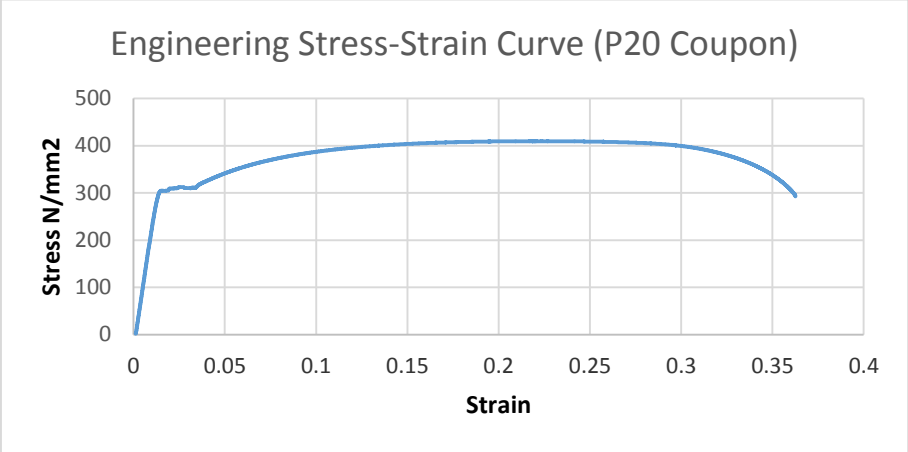

Figure 26. Engineering stress-strain curve of P20 coupon from test data

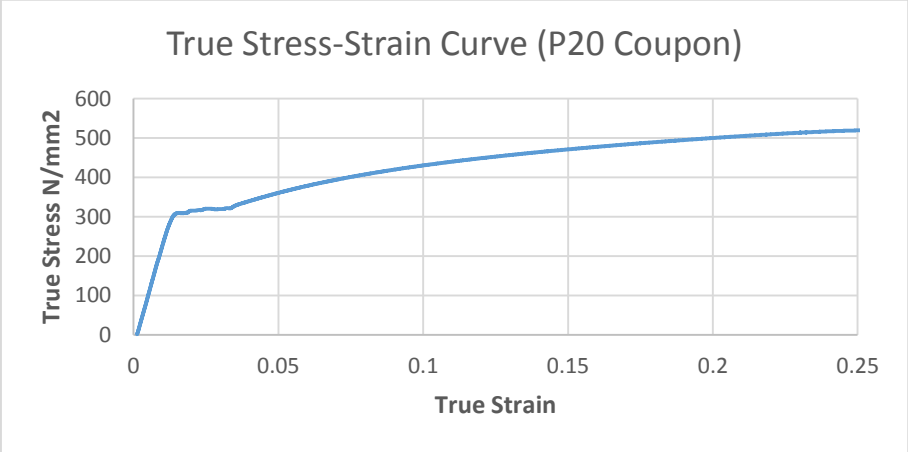

Figure 27. True stress-strain curve of P20 coupon up to the necking point

The formulas presented in EN 1993-1-5 are only valid till the necking point, after the necking point significant reduction in cross-sectional area takes place. True stresses were extrapolated in increasing fashion considering the fact that strain hardening continues even after the necking till fracture. (Figure 28) shows the plastic material property that was used in the calibration of coupon P20 in Abaqus software.

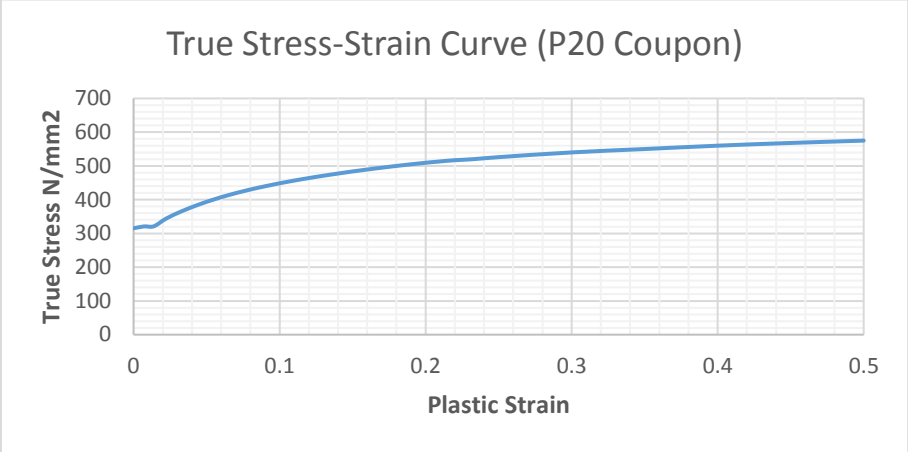

Figure 28. Plastic material properties of P20 Coupon used in Abaqus model

Ductile damage criteria was used in damage for ductile metals with following properties. It is important to note the coefficients for the ductile damage criteria depends on the mesh size and shape as well.

Table 7. Coefficients used for determining damage of ductile material for P20 coupon

Coefficients	**Value**
Fracture Strain	0.4
Stress Triaxiality	0.8
Strain Rate	0.5
Displacement at Failure	0.4

Sub option for damage evolution was used with the displacement type with linear softening and maximum degradation. Displacement at failure was 0.4 see (Table 7).

Dynamic Explicit step was used including the geometric nonlinearity of large displacements. Mass scaling was used to replicate the quasi-static response of the coupon. There are two mass scaling option in Abaqus: fixed mass scaling and variable mass scaling. Semi-automatic mass scaling was used in whole model at the beginning of the step with scale to target time increment of $5x10^{-06}$ as shown in (Table 8)

Table 8. Mass scaling details used in Abaqus modeling of P20 coupon

Region	Type	Frequency/ Interval	Factor	Target Time Increment
Whole Model	Target Time Inc.	Beginning of Step	None	5e-06

Two reference points were selected on ends of the coupon with the kinematic coupling constraint with all degrees of freedom fixed with the surface of the coupon.

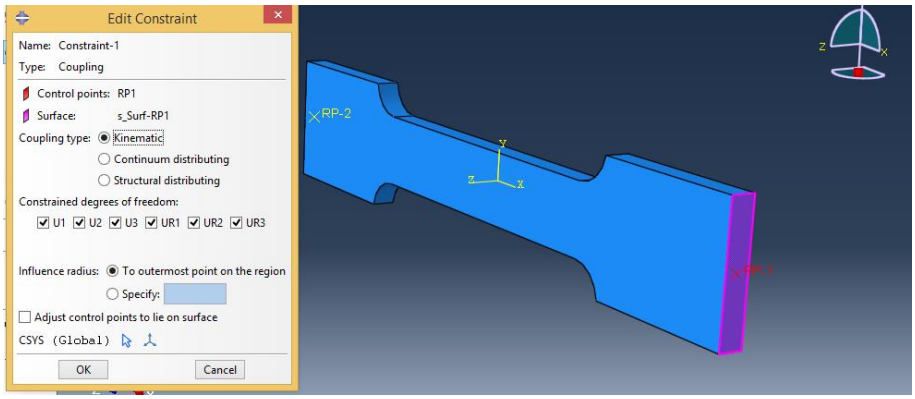

Figure 29. Reference points kinematic coupling of P20 coupon

Reference point 2 was fixed and reference point 1 was applied with displacements to replicate the test conditions.

Linear hexahedral elements were used for meshing with approximate global size of 10mm.

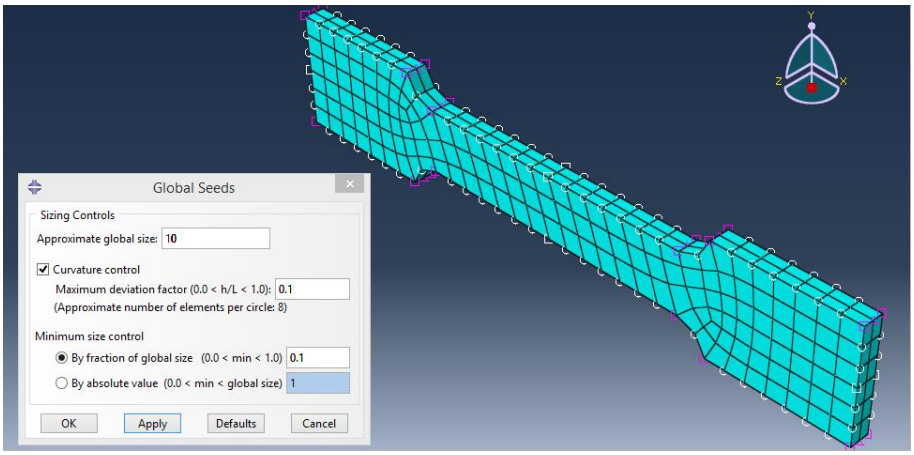

Figure 30. Meshing of P20 coupon in Abaqus

Experimental force displacement behavior was validated numerically and different Abaqus material parameters and mesh size were established to be used in T-Stub numerical modeling. Following results show good approximation of the real behavior of coupons.

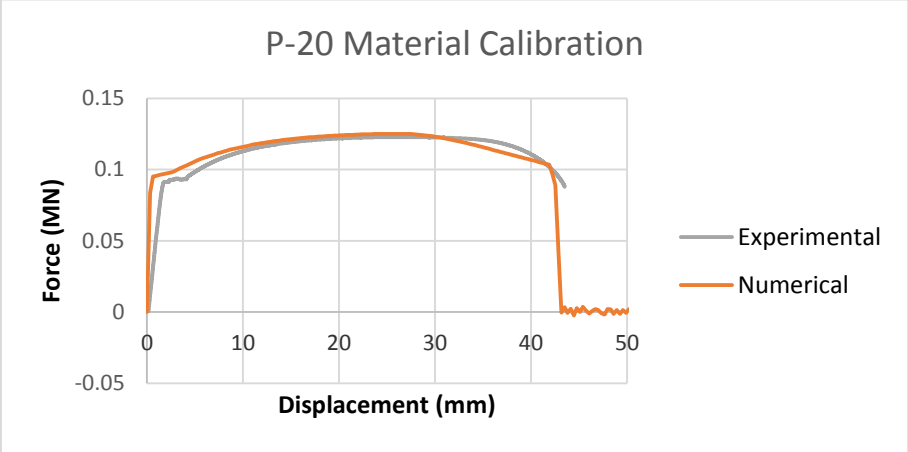

Figure 31. Numerical and Experimental comparison of P20 coupon

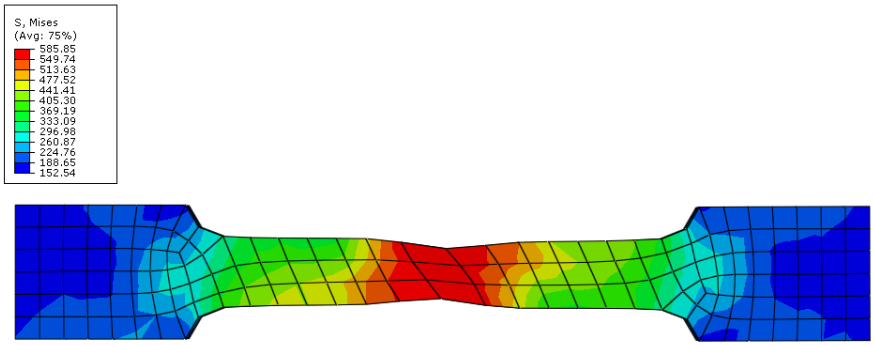

Figure 32. Stress before failure in an extracted coupon

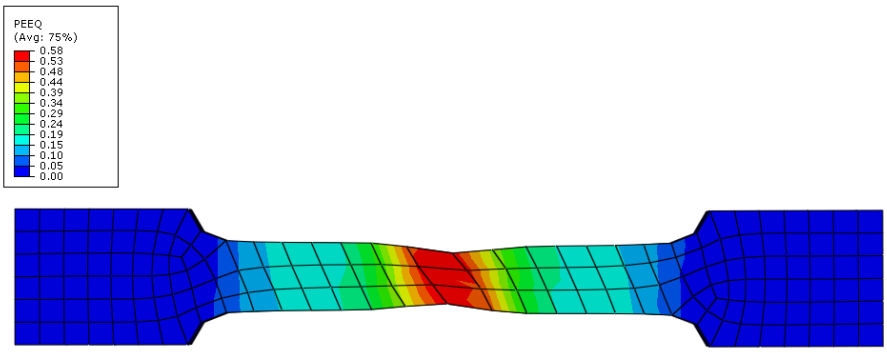

Figure 33. PEEQ before failure in an extracted coupon

Material calibration results for different coupons used in T-stub validation are presented below

For detailed description of material calibration of rest of the coupons, see Annex I

5. EXPERIMENTAL PROGRAM

5.1. Description of experimental framework

This chapter provides description about the experimental program for bolted T-stub components with following typologies. See (Table 9)

Table 9. T-stub macro-components typologies used for experimental program

T-Stub	Thickness of the End Plate	Diameter of the bolt	Distance between the bolts
	mm	mm	mm
T-10-16-100 C	10	16	100
T-10-16-120 C	10	16	120
T-10-16-140 C	10	16	140
T-12-16-100 C	12	16	100
T-12-16-120 C	12	16	120
T-12-16-140 C	12	16	140
T-15-16-100 C	15	16	100
T-15-16-120 C	15	16	120
T-15-16-140 C	15	16	140
T-18-16-100 C	18	16	100
T-18-16-120 C	18	16	120
T-18-16-140 C	18	16	140

First letter T designates as a T-Stub followed by the term indicating the thickness of the end plate. Second term represents the diameter of the bolt and last term represents the distance between the bolts. All the units are in millimeters. The suffix C stands for cold meaning the specimens were testing in room temperature conditions with the strain rate of 0.5mm/seconds replicating the quasi static conditions. The suffix Cs is used for cold with high strain rate of 10mm/second. The suffix T is used for high temperature with low strain rate and similarly suffix Ts is used with high temperature with high stain rates. The steel grade S355 is used for the web of the T-stub and S235 is used for the flange of the T-stub. Class 10.9 bolts with diameter of 16mm were used. Flange and web parts of the T-stub were welded using 7mm throat thickness.

(Table 10) shows the steel grades and bolt class with average properties used for the T-Stub specimen.

Table 10. Details of material properties of components of T-stubs

Element	Part	Thickness	Material	Coupon	Yield strength
		mm			N/mm^2
T-Stub	Web	10	S355	P-19	390
T-Stub	Flange	10	S235	P-20	310
T-Stub	Flange	12	S235	P-21	305
T-Stub	Flange	15	S235	P-22	275
T-Stub	Flange	18	S235	P-23	420
Bolt	M16	16	10.9		965

Mechanical properties of materials were already tested and experimental data was available for different coupon materials see (Table 10). Tensile tests of the coupons taken from the T-stub macro-components were carried out at room temperatures i.e. 20'C and elevated temperatures i.e. 540'C under quasi-static i.e 0.05mm/s and dynamic loading conditions i.e. 10mm/sec. The weld details were also subjected to monotonic loadings in "Research Center for Mechanics of Materials and Structural Safety" under the project "Structural conception and collapse control performance based design of multistory structures under accidental actions".

Since the most important macro-component of bolted end plate beam to column connections are T-stub components and from the literature review we know that the behavior of such T-stub components depends on the material properties, bolt arrangements, thickness of the end-plate and loading conditions. The design of the T-stubs to achieve ductile failure mode is based on static loading conditions according to Eurocode EN-1993-1-8 [20]. The ductile failure mode can be altered under different loading conditions and temperatures [29]. Additionally under large displacements the behavior of the specimen is not the same and the connections need to resist additional catenary forces from the beams which are necessary for the catenary mechanism to from and for the structure to resist large displacement actions.

In order to evaluate all such factors and to study the exact behavior of T-stub macro-components under different loading conditions and different temperatures, an experimental program under the CODEC [8] was established in which T-stubs are tested at room (20'C) and elevated (540'C) temperatures under two types of loading conditions i.e. quasi-static (0.05mm/s) and dynamic (10mm/s) loading condition. Following figure shows the testing scheme for T-stubs. Details can be seen in Annex-II.

Table 11. Detailed experimental testing scheme of T-stubs undertaken in CODEC program

Varianta S235		2	3	4	5	7	8	9	10	12	13	14	15	17	18	19	20	22	23	24	25	27	28	29	30	34	35	39	40
t	10	X	X	X	X	X	X	X	X																				
	12									X	X	X	X	X	X	X	X												
	15																	X	X	X	X	X	X	X	X				
	18																									X	X	X	X
c	70																												
	90	X				X				X				X				X				X							
	100		X				X				X				X				X				X						
	120			X				X				X				X				X				X		X		X	
	140				X				X				X				X				X				X		X		X
M.16	8.8	X	X	X	X					X	X	X	X					X	X	X	X					X	X		
	10.9					X	X	X	X					X	X	X	X					X	X	X	X			X	X
M20	8.8																												
	10.9																												
Mode 1		101	87	67	55	101	87	67	55	144	123	95	77	144	123	95	77	202	173	134	109	202	173	134	109	294	240	294	240
Mode 2		87	81	71	63	102	95	83	73	106	98	85	76	121	112	98	87	131	122	106	94	147	136	118	105	192	170	204	181
Mode 3		181	181	181	181	244	244	244	244	181	181	181	181	244	244	244	244	181	181	181	181	244	244	244	244	181	181	244	244

According to this scheme of T-stub testing a four different types of T-stubs with end plate thickness of 10mm to 18mm is to be tested with varying distance between the bolts of the T-stub from 90mm to 140mm, bolt diameter of 16mm and 20mm, bolt strength of 8.8 and 10.9 according to the European norms. T-stubs with end plate thickness of 10mm and 12mm were already tested with varying distances between the bolts of 90mm, 100mm, 120mm and 140mm. The strength of the bolts was 10.9 i.e. ultimate strength is 1000 MPa and yield strength of the bolt is 900MPa.

Following table shows the T-stubs which were tested and the test results are presented later in this chapter.

Table 12. T-stubs tested under CODEC Program

Varianta S235		28	29	30	34	35	39	40
t (mm)	10							
	12							
	15	X	X	X				
	18				X	X	X	X
c (mm)	70							
	100	X						
	120		X		X		X	
	140			X		X		X
M.16	8.8				X	X		
	10.9	X	X	X			X	X
Mode 1	kN	173	134	109	294	240	294	240
Mode 2	kN	136	118	105	192	170	204	181
Mode 3	kN	244	244	244	181	181	244	244

(Table 12) explains T-stub configurations e.g. column 28th indicates the T-stub with end plate thickness of 15mm has bolt to bolt distance of 100mm and the bolts used are 16mm with ultimate capacity of 1000MPa. Similarly the second column indicates the similar configurations with the distance between the bolts to be 120mm instead.

The general configuration of the T-stub is as follows

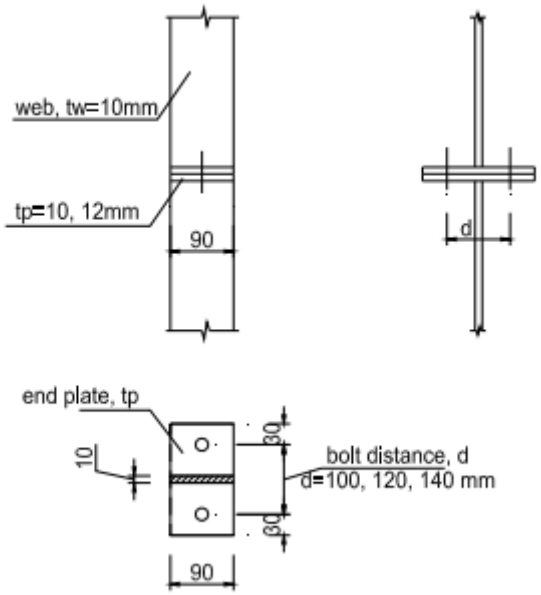

Figure 34.Typical T-stub configuration used for experimental testing

The web of the T-Stub is approximately 685mm of length on average with the end plate thickness varying for different specimens. The width of the web for T-stub specimens is 90mm and the distance from the bolt center to the end of the flange is 30mm with center to center distance of the bolts varying for different specimens. The steel grade of the flanges is S235 and for the web it's S355. The T-stubs are fillet welded with the throat thickness of 7mm.

5.2. Specimens and test set-up for T-stub tests

INstron 8805 a 4 column with a 1000kN static and 1200kN dynamic maximum load capacity, servohydraulic fatigue testing machine was used to test T-stubs. The testing was done in Politehnica University Timisoara laboratory. Different specimens were testing with different loading and temperature actions depending upon the type of specimen tested.

Figure 35. INstron 8805 testing machine [32]

Force and displacements were measured using INstron 8805 together with Rod type position sensors [33] and VIC-3D [34].

Figure 36. Rod type position sensors from novotechnik

These Rod type position sensors called transducers were connected with the computer system by series of cables and were connected to the T-stub speciment using wires which were connected to the rod welded to the T-stub specimen. Rod type position sensers measure the displacements directly from the movement of the end plate as they are connected at the center of the end plate for both of the flanges of the T-stub specimen.

Figure 37. Vic 3D from correlated solutions

Visual image correlation machine used for measuring strains and displacements of different points on a specimen is a high tech and very powerful machine for measuring shape, displacement and strains of specimen surface in a three dimensions. Vic 3D has a capacity to measure arbitrary displacement and strains 50 macrostrains to 2000% strain and more [35]. Vic 3D is connected to a different set of computer system which is connected to the INstron machine system indirectly with connected cables. To measure the strains and displacements the T-stub specimen has to be marked with two types of markings on a white background for a machine to make it readable. First a white spray is done on a typical T-stub specimen and left it for some time to let it dry. Then two different types of markings are done on the T-stub specimen. First is the random small black dot markings over the front part of the T-stub specimen, second a defined and measured dot marking with a bit bigger dots are marked. Small random dot markings are used by the Vic 3D to measure strain variations throughout the T-stub which helps us in determining stresses and strains which can be compared with the analytical models for validation and comparisons. The measured specific dot markings were used to measure the displacements of the T-stub flange. Following sample tested T-stub shows the random and specific markings

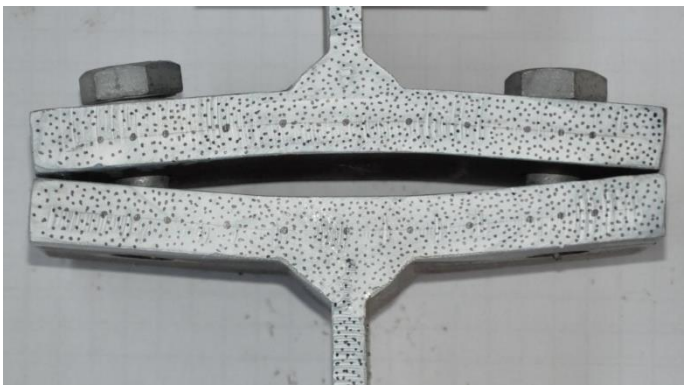

Figure 38. Typical T-stub specimen showing random and specific markings for Vic 3D readings

All the T-stubs and bolts were marked, dimensioned and exact readings were noted down. The bolts were measured accurately using Vernier caliper and were marked according to the T-stub specimen in which they are to be bolted using hand tightening technique. Generally the observed readings for diameter of the bolts were slightly less than the shop drawings and overall no variations among the diameter of the bolts was observed but for the lengths of the shank of the bolt variations were observed. Same dimensions were used for the numerical modeling of the T-stub macro-component with the exception that for the bolts only shank part was modeled and threaded part was ignored owing to the complexity of the numerical modeling and was not the point of concern as well.

Figure 39. Bolt class 10.9 measured and marked

Similarly welded end plates with flanges were also measured and readings were noted down. On average very little variation has been observed in the measured values as compared to the shop drawings. In most of the cases measured values were always 1 mm or less short than the shop drawings which was noted down and similar dimensions were used for numerical modeling to get real behavior of the actual T-Stub macro-component.

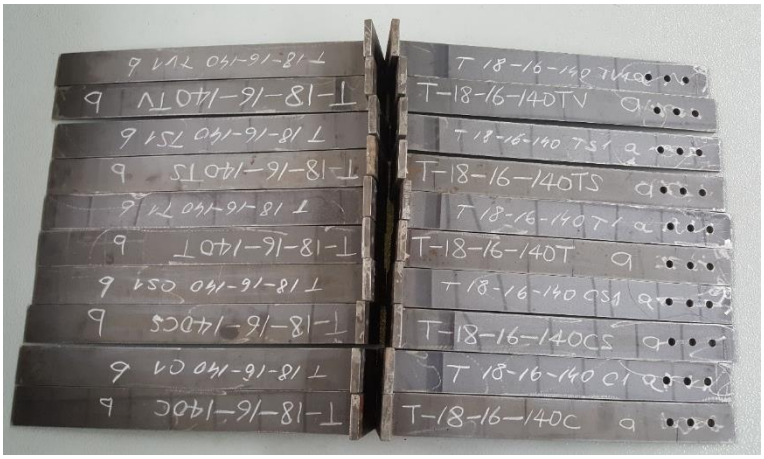

Figure 40. T-Stubs measured and marked

After marking and dimensioning, the T-stub specimens were prepared. The bolts were installed in the right place and were hand tightened. The prepared T-stub specimen was placed in testing machine. The force displacement curves were obtained from machine, rod type position sensors and Vic 3D for comparison. Two types of strain rates were applied as explained in the description of experimental framework.

Environmental chamber was used to simulate high temperature conditions in which specimens were heated at 544'C and were tested at low and high strain rates accordingly.

Figure 41. Instron environmental chamber

To test under non-ambient testing conditions Instron environmental chambers are very useful since they provide wide range of temperature testing capabilities for evaluating material properties of the specimens. These chambers use forced convection mechanism to ensure optimum temperature distribution and a digital controller is used to control values [36]. Environmental chamber is attached to the test system using mounting brackets and lift stands see (Figure 42).

Figure 42. Mounting Brackets and Lift Stands [36]

5.3. Experimental test results

T-15-16-100C T-15-16-100Cs T-15-16-100T T-15-16-100Ts

Figure 43. T-Stubs before experiment for T-15-16-100

Figure 44. T-Stubs after experiment for T-15-16-100

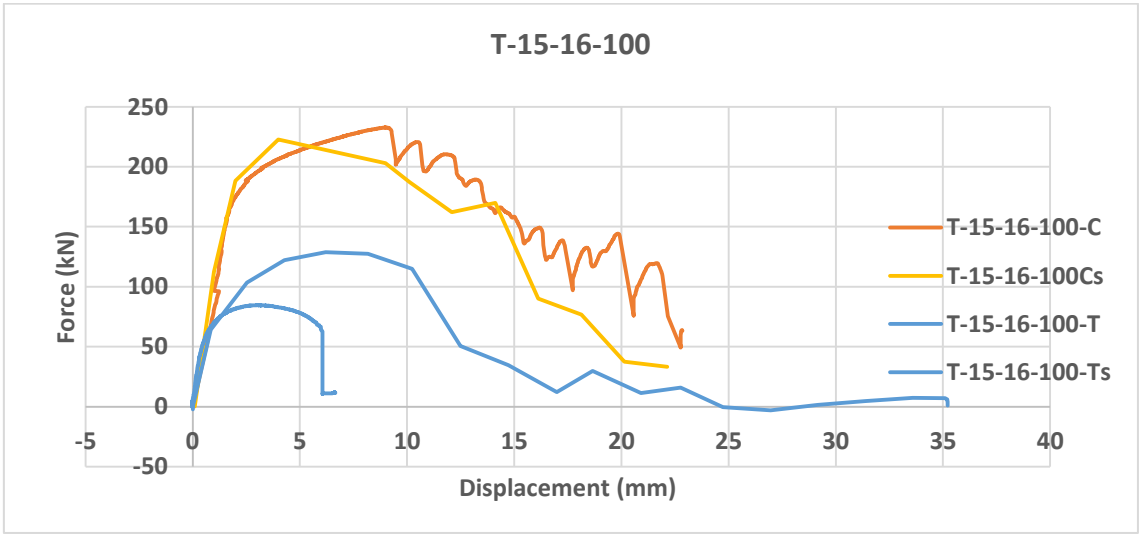

Figure 45. Force-displacement relationship for T-15-16-100

T-15-16-120C T-15-16-120Cs T-15-16-120T T-15-16-120Ts

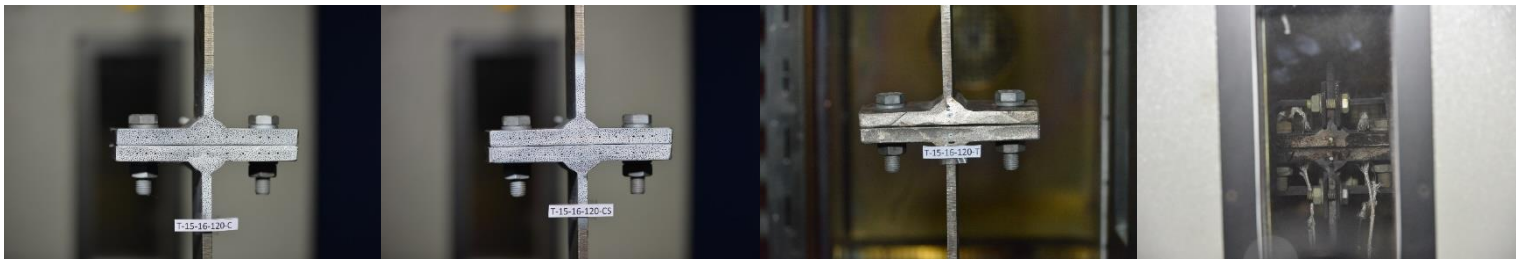

Figure 46. T-Stubs before experiment forT-15-16-120

Figure 47. T-Stubs after experiment for T-15-16-120

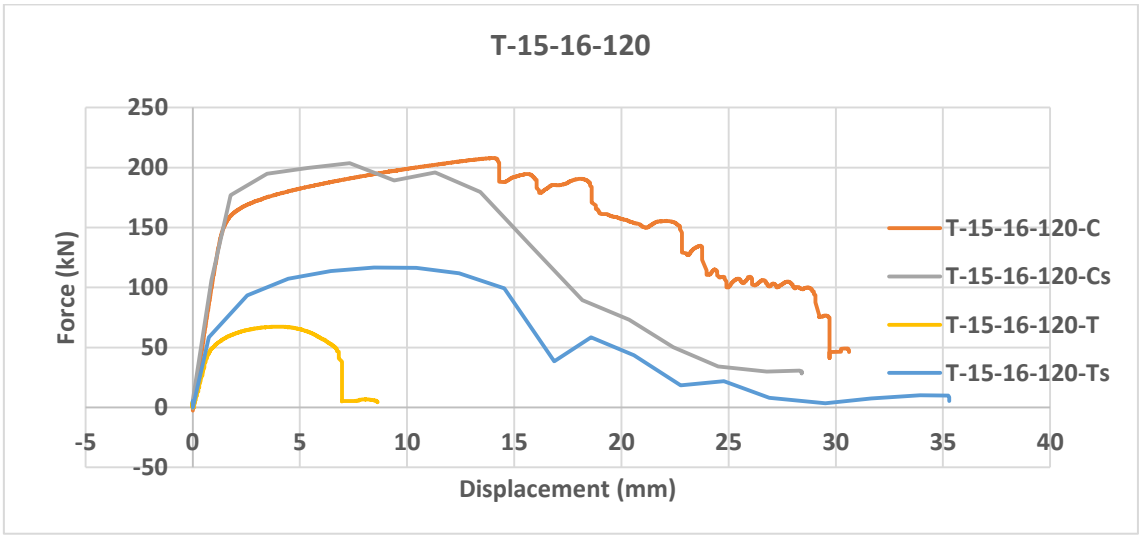

Figure 48. Force-displacement relationship for T-15-16-120

T-15-16-140C T-15-16-140Cs T-15-16-140T T-15-16-140Ts

Figure 49. T-Stubs before experiment for T-15-16-140

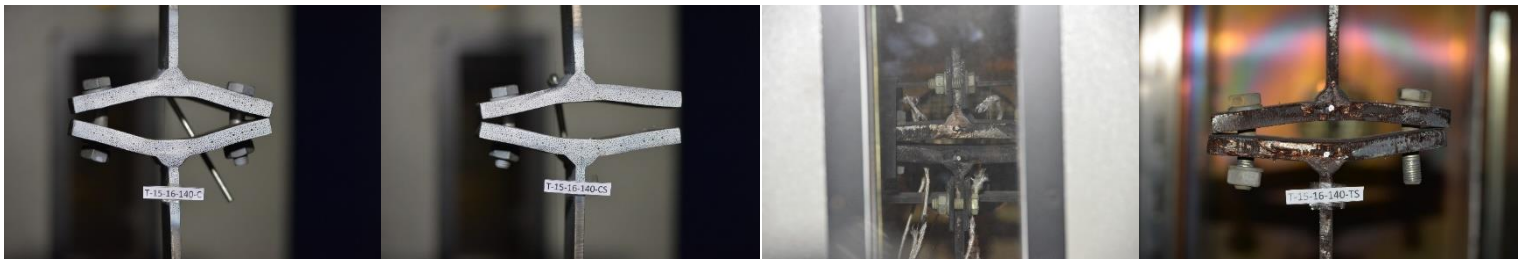

Figure 50. T-Stubs after experiment for T-15-16-140

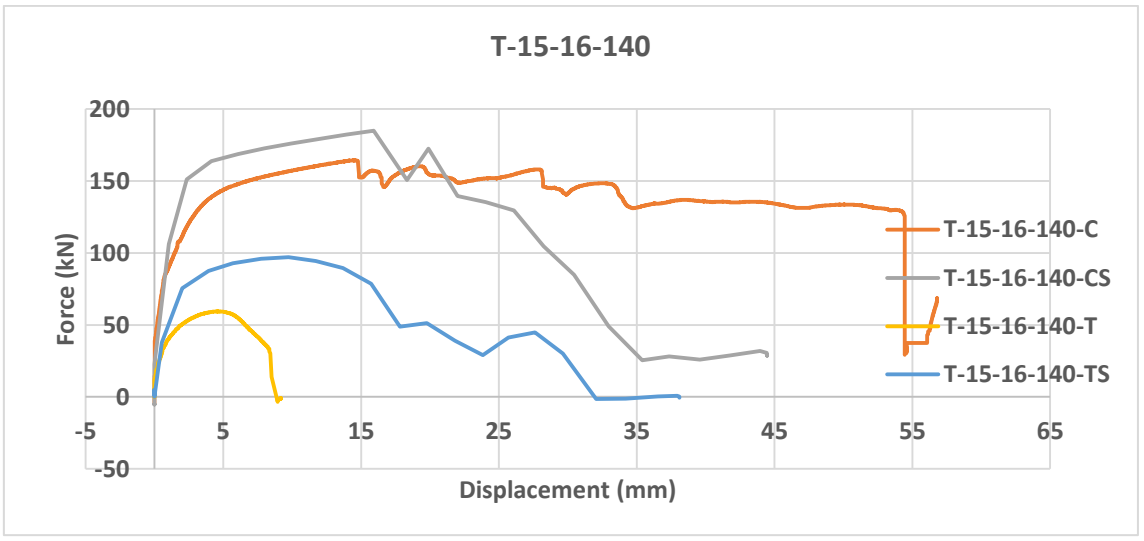

Figure 51. Force-displacement relationship for T-15-16-140

T-18-16-120C T-18-16-120T T-18-16-120Ts

Figure 52. T-Stubs before experiment for T-18-16-120

Figure 53. T-Stubs after experiment for T-18-16-120

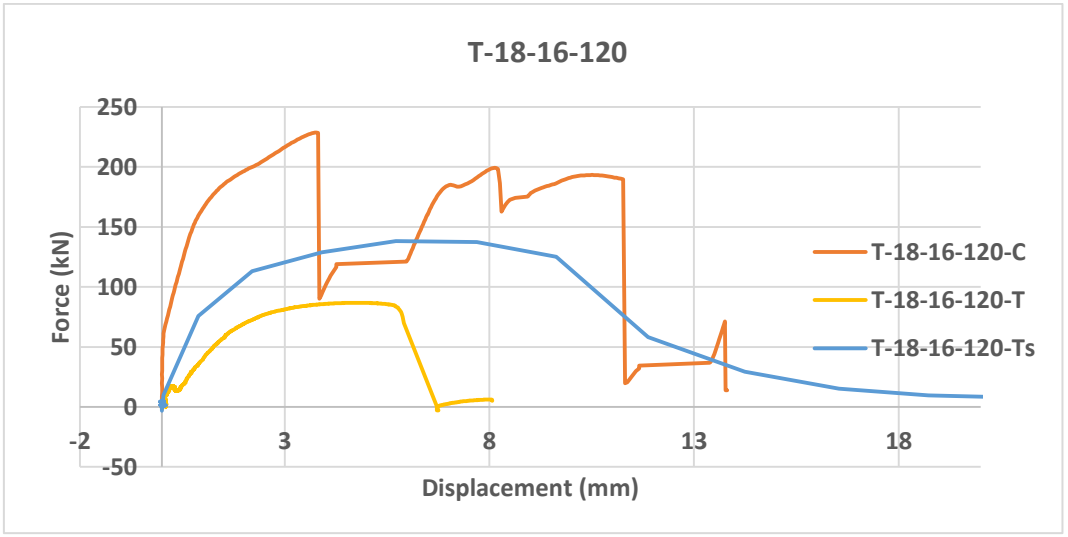

Figure 54. Force-displacement relationship for T-18-16-120

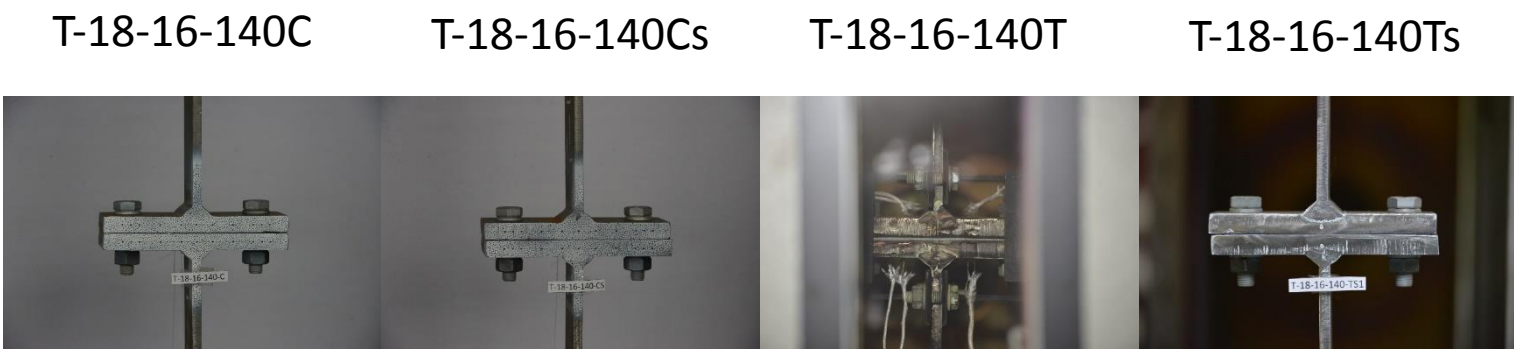

Figure 55. T-Stubs before experiment for T-18-16-140

Figure 56. T-Stubs after experiment for T-18-16-140

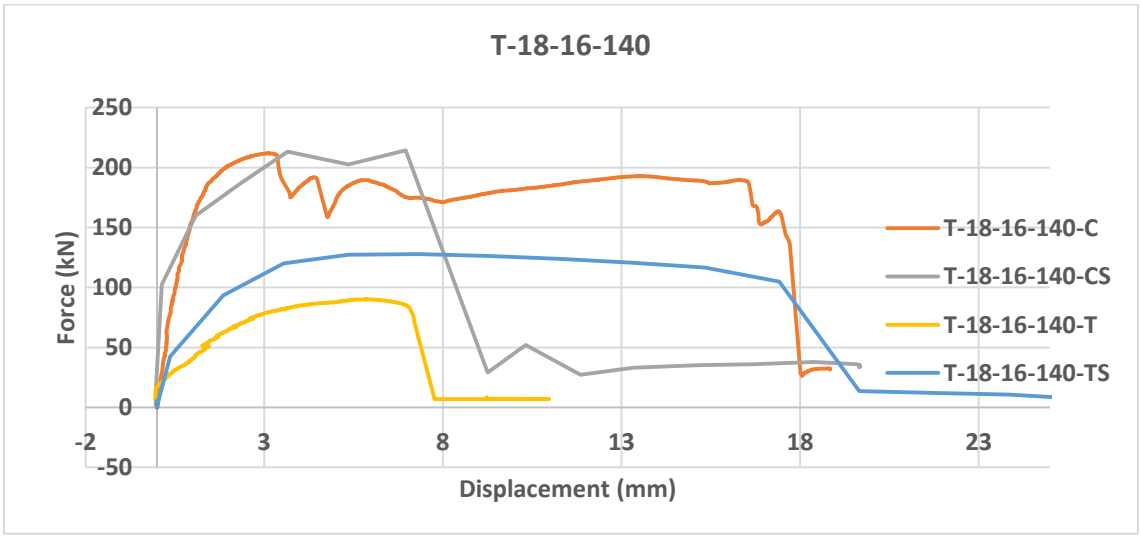

Figure 57. Force-displacement relationship for T-18-16-140

6. NUMERICAL PROGRAM AT AMBIENT TEMPERATURE

Experimental tests were validated using Abaqus finite element analysis software. Numerical models were modeled using precise measurements taken during the experimental tests. Calibrated Material properties see (Chapter 4). In this chapter brief modeling description of T-Stub T-15-16-100C is presented.

6.1. T-stub numerical models, description

T-15-16-100C is a T-Stub specimen with end plate thickness of 15mm, bolt diameter of 16mm and the distance between the bolts 100mm.

6.1.1. Part module:

Two parts of the T-stub component were drawn in the part module using following characteristics

Table 13.Part module modeling description of T-Stub

Modeling Space	3D
Type	Deformable
Shape	Solid
Type	Extrusion

6.1.2. Property module:

In property module following material properties were defined to different parts of the T-Stub

Table 14. Property module modeling description of T-stub

Material Properties	**Part of T-Stub**
10.9	Bolts
S235	End plate
S355	Web

Elastic and plastic material properties were defined in this module, discussed in chapter 4. Ductile damage parameters determined after calibrating material properties were also used in this module.

6.1.3. Assembly module:

Assembly module is used to assemble bolt and T-stub to form a T-stub assembly similar to the one used for experimental testing.

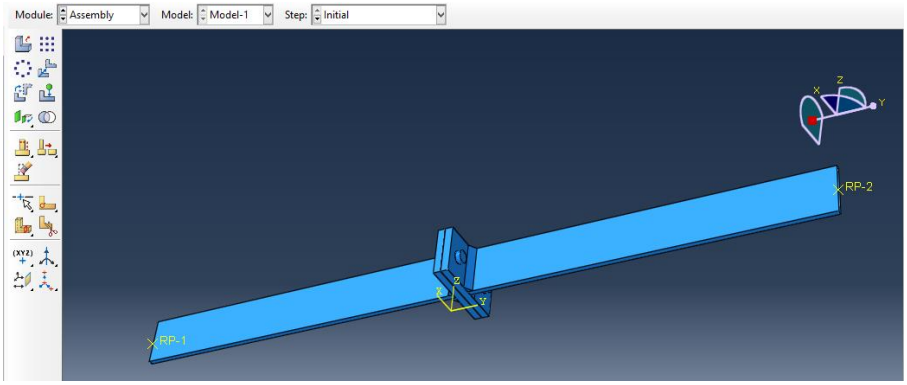

Figure 58. Assembled T-stub in assembly module

6.1.4. Step module:

Dynamic explicit step with mass scaling was used to simulate quasi static response for testing T-stub at room temperature with low strain rate. History output request manager was used to determine force and displacements at a specified points similar to the test conditions.

6.1.5. Interaction module:

General contact was used with friction coefficient of 0.8 in tangential behavior and hard contact was used for specifying normal behavior in contact property options. Separation was allowed after the general contact takes place. Two reference points were selected at the opposite ends of the T-stubs and were coupled using kinematic coupling type with all degree of freedoms constrained with the surface of the T-stub see (Figure 58)

6.1.6. Load module:

Reference point one was fixed using displacement/rotation boundary type with all the displacements and rotations fixed at the reference point. Reference point two was allowed a uniform displacement along the longitudinal axis of the T-stub to replicate the experimental test conditions. Displacements are increased uniformly using amplitude.

6.1.7. Mesh module:

Meshing size was used similar to the one used in calibrating material properties. Approximate global mesh size of 20mm was used for the web and 10mm was used for the end plate of the T-Stub component. Mesh size was further reduced around the bolt holes.

6.1.8. Visualization module:

Visualization module was used for getting results. Following figure shows PEEQ and maximum stresses followed by the force displacement curve.

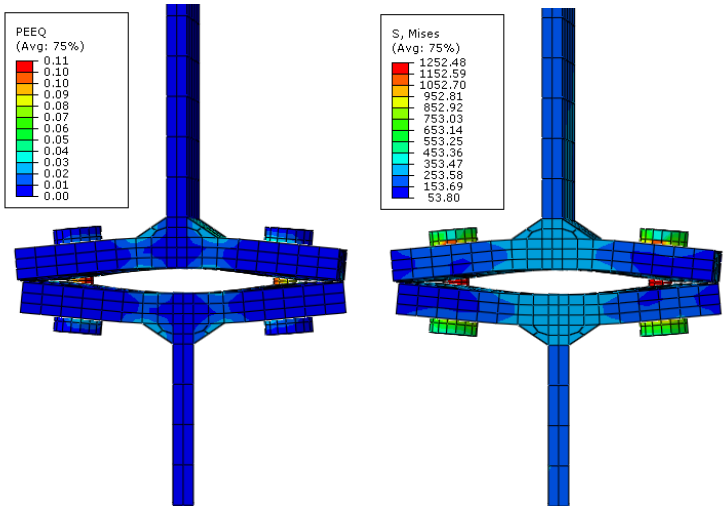

Figure 59. Visualization module showing maximum PEEQ and mises stresses in T-stub

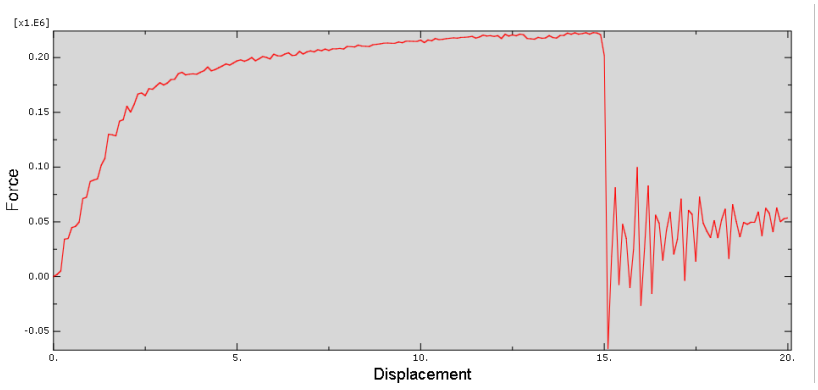

Figure 60. Force displacement curve of a T-stub in visualization module of Abaqus

6.2. Validation against experimental tests, numerical vs experimental

T-10-16-100C

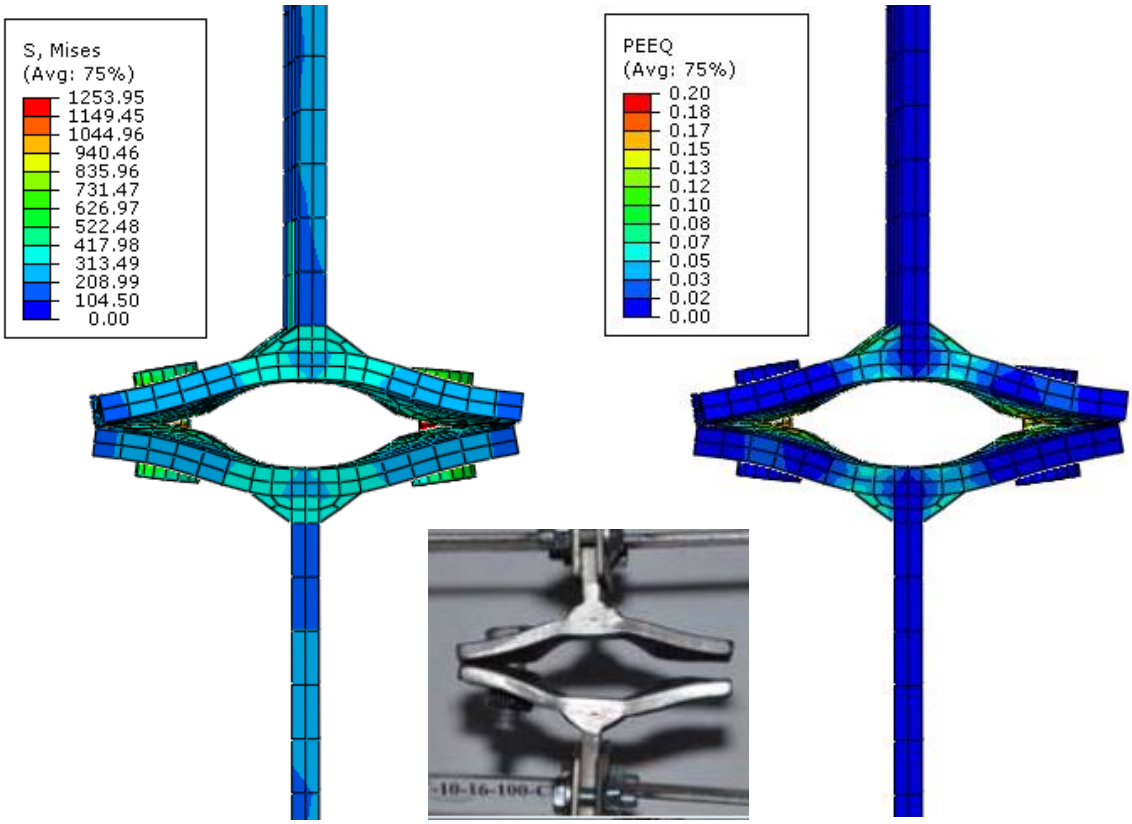

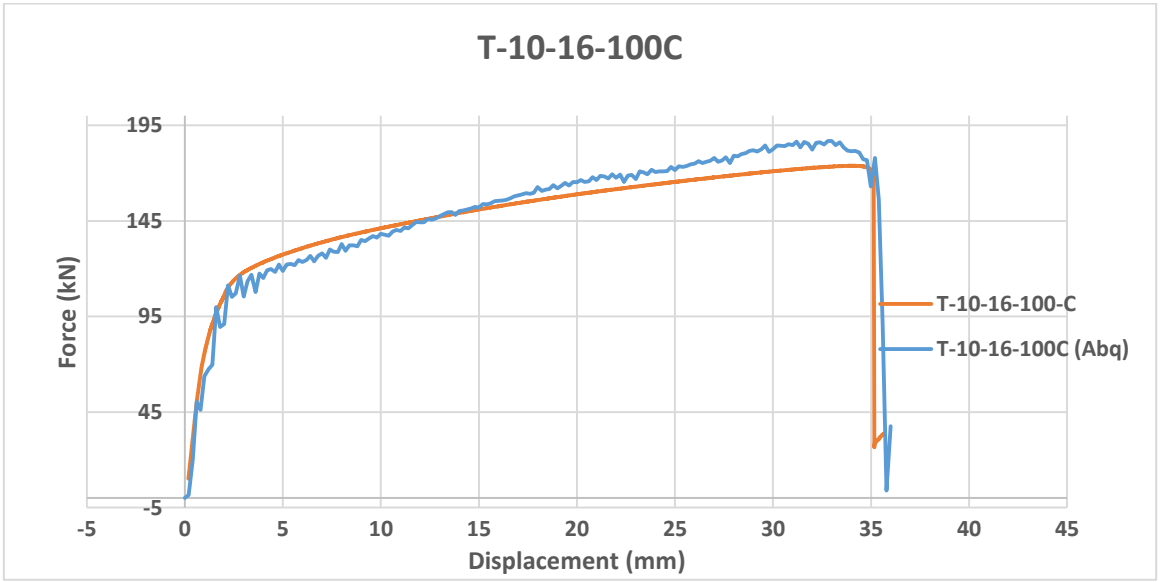

T-10-16-100C

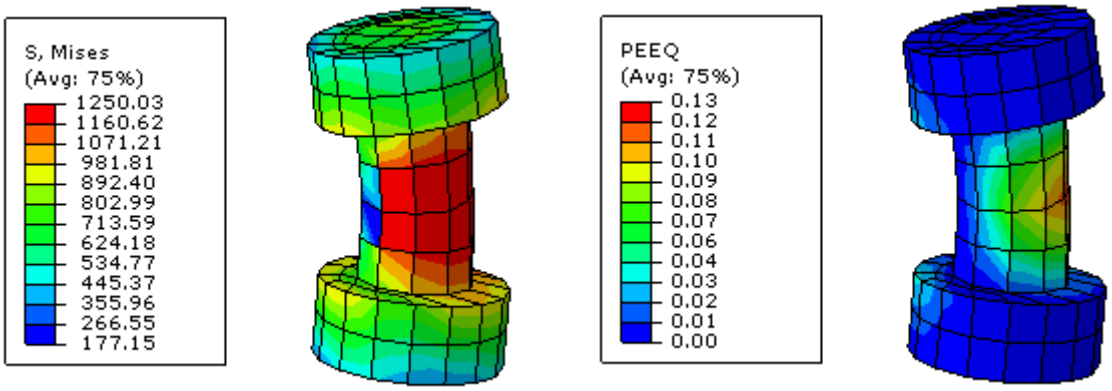
S, Mises
(Avg: 75%)
1250.03
1160.62
1071.21
981.81
892.40
802.99
713.59
624.18
534.77
445.37
355.96
266.55
177.15
PEEQ
(Avg: 75%)
0.13
0.12
0.11
0.10
0.09
0.08
0.07
0.06
0.04
0.03
0.02
0.01
0.00

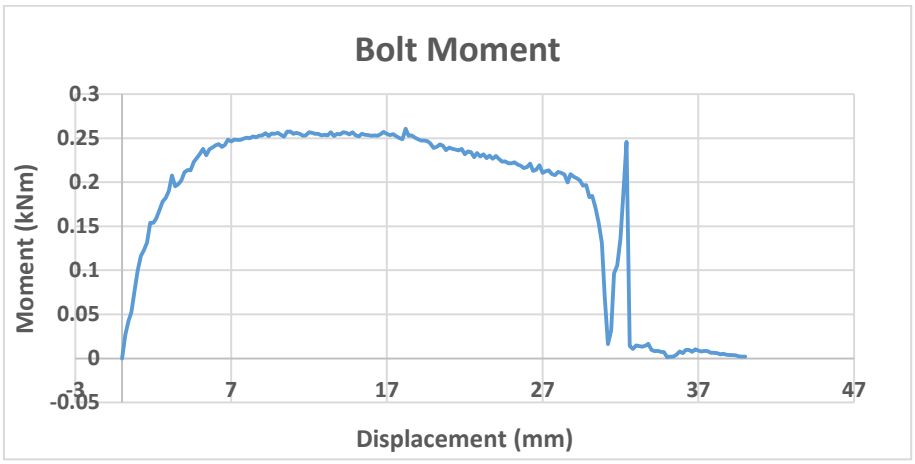
Bolt Moment
Moment (kNm)
0.3
0.25
0.2
0.15
0.1
0.05
0
-0.05
-3
7
17
27
37
47
Displacement (mm)

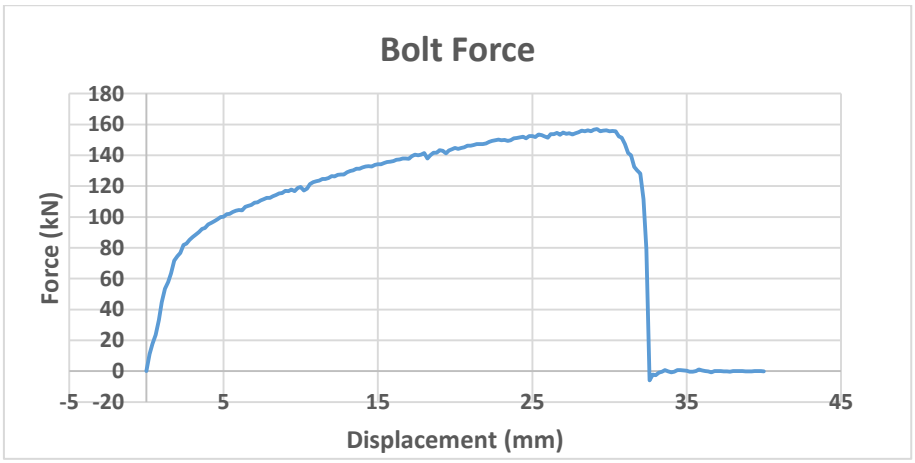
Bolt Force
Force (kN)
180
160
140
120
100
80
60
40
20
0
-5
-20
5
15
25
35
45
Displacement (mm)

T-10-16-120C

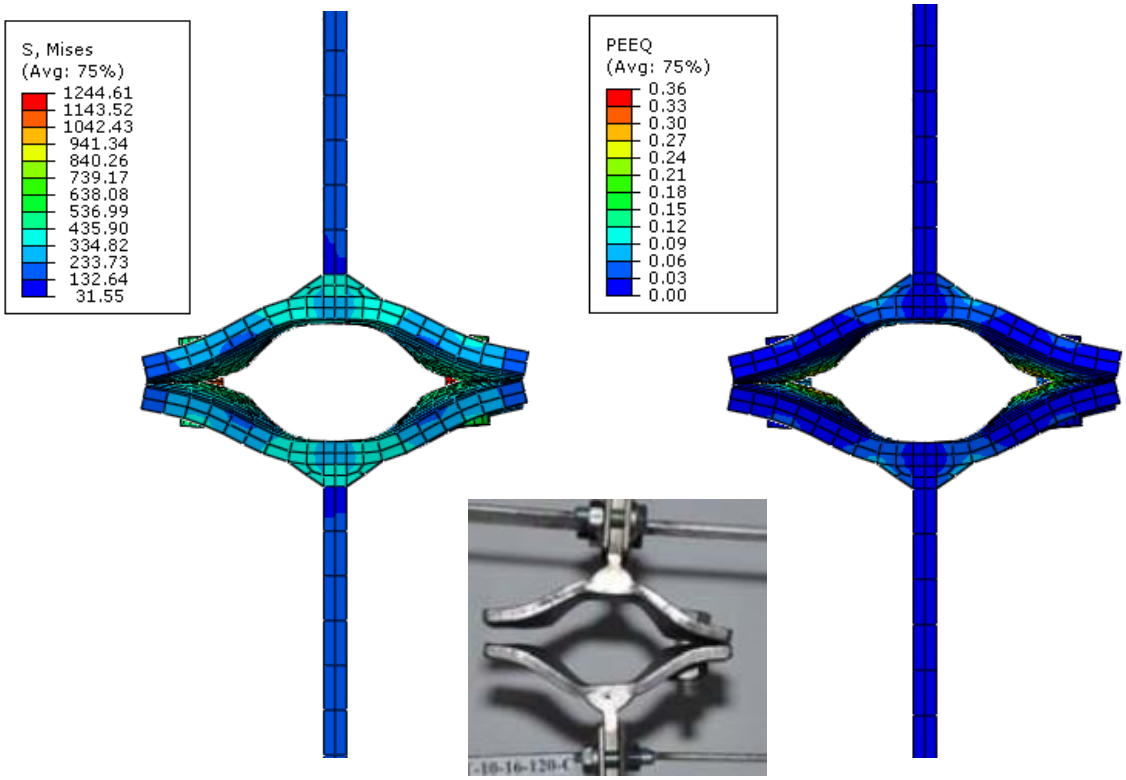
S, Mises
(Avg: 75%)
1244.61
1143.52
1042.43
941.34
840.26
739.17
638.08
536.99
435.90
334.82
233.73
132.64
31.55
PEEQ
(Avg: 75%)
0.36
0.33
0.30
0.27
0.24
0.21
0.18
0.15
0.12
0.09
0.06
0.03
0.00

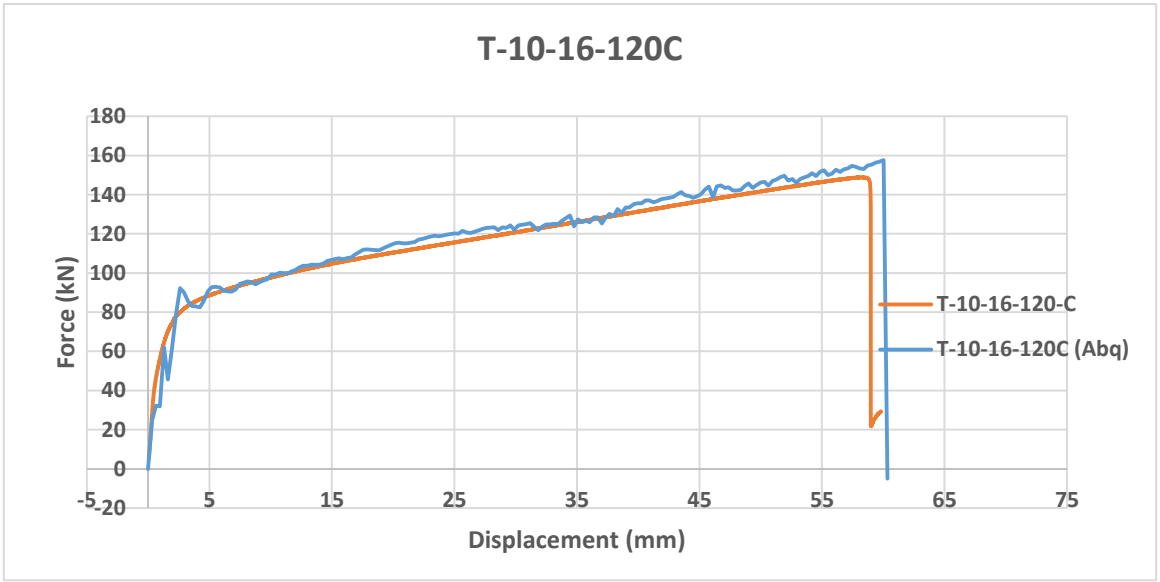
T-10-16-120C
Force (kN)
Displacement (mm)
T-10-16-120-C
T-10-16-120C (Abq)
180
160
140
120
100
80
60
40
20
0
-20
-5
5
15
25
35
45
55
65
75

T-10-16-120C

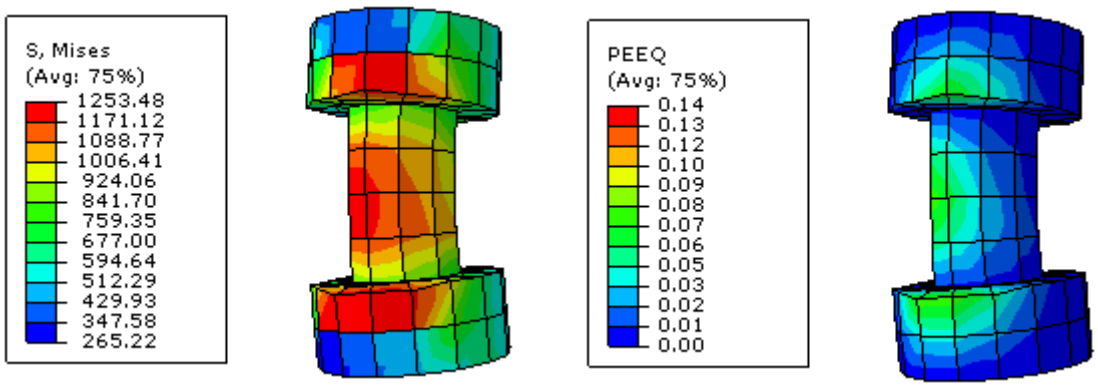
S, Mises
(Avg: 75%)
1253.48
1171.12
1088.77
1006.41
924.06
841.70
759.35
677.00
594.64
512.29
429.93
347.58
265.22
PEEQ
(Avg: 75%)
0.14
0.13
0.12
0.10
0.09
0.08
0.07
0.06
0.05
0.03
0.02
0.01
0.00

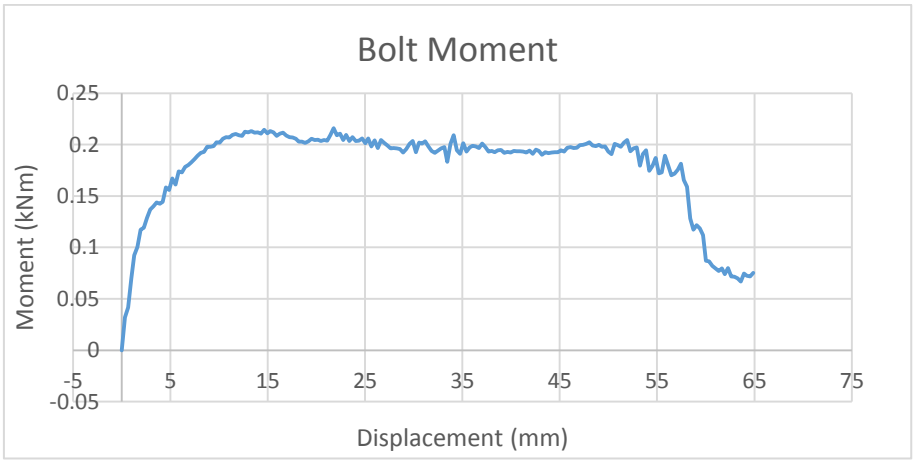
Bolt Moment
Moment (kNm)
0.25
0.2
0.15
0.1
0.05
0
-0.05
-5
5
15
25
35
45
55
65
75
Displacement (mm)

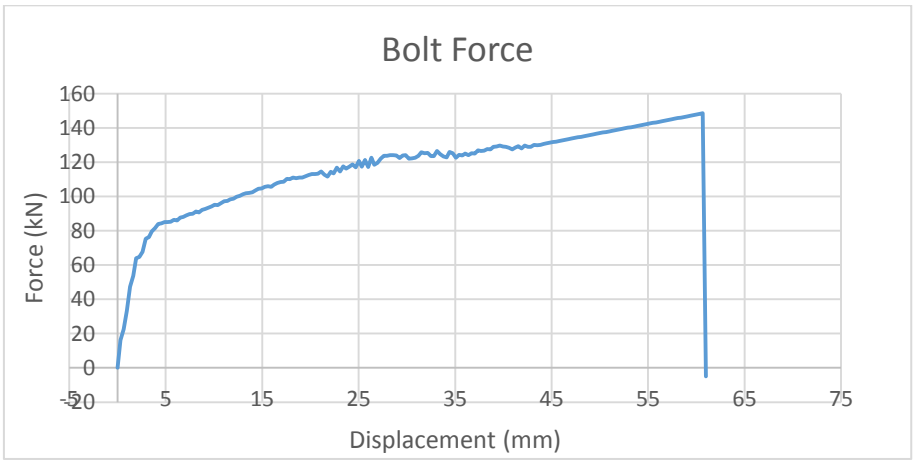
Bolt Force
Force (kN)
160
140
120
100
80
60
40
20
0
-20
-5
5
15
25
35
45
55
65
75
Displacement (mm)

T-10-16-140C

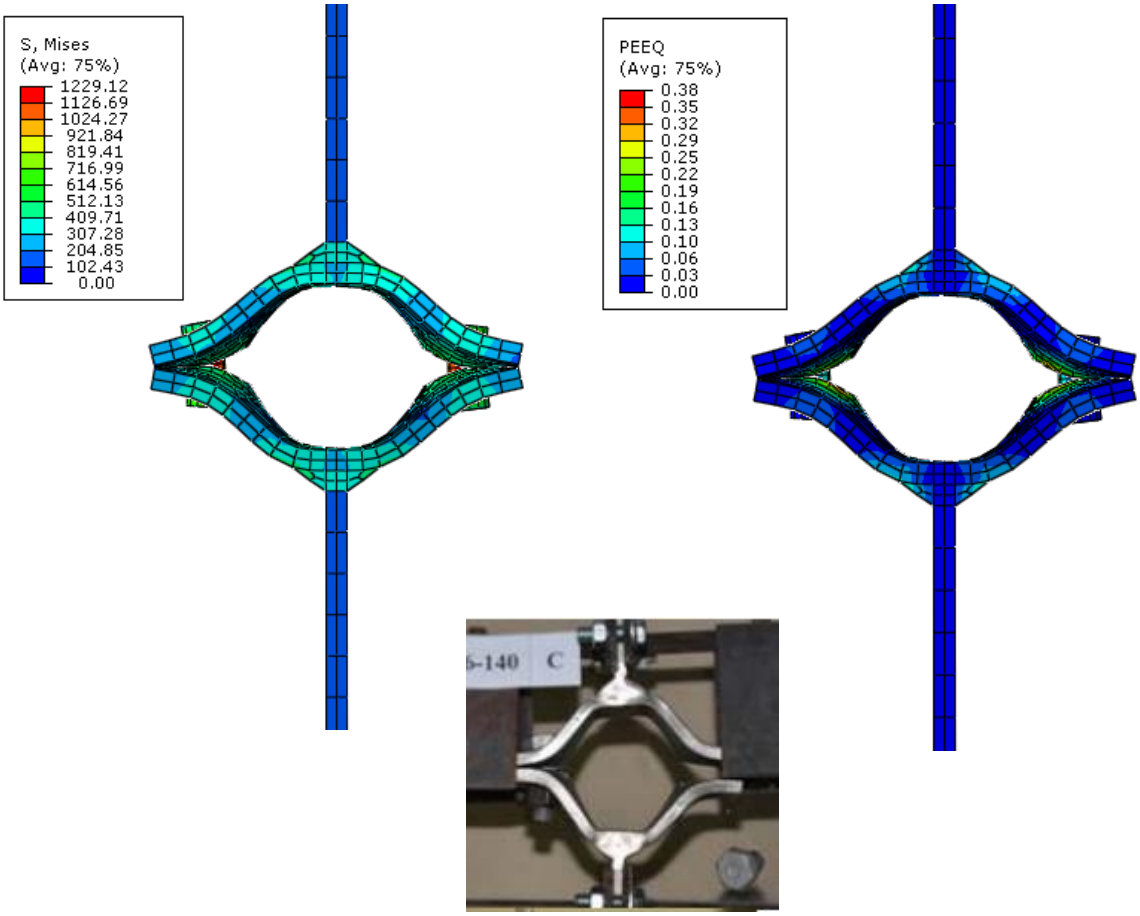
S, Mises
(Avg: 75%)
1229.12
1126.69
1024.27
921.84
819.41
716.99
614.56
512.13
409.71
307.28
204.85
102.43
0.00
PEEQ
(Avg: 75%)
0.38
0.35
0.32
0.29
0.25
0.22
0.19
0.16
0.13
0.10
0.06
0.03
0.00
-140 C

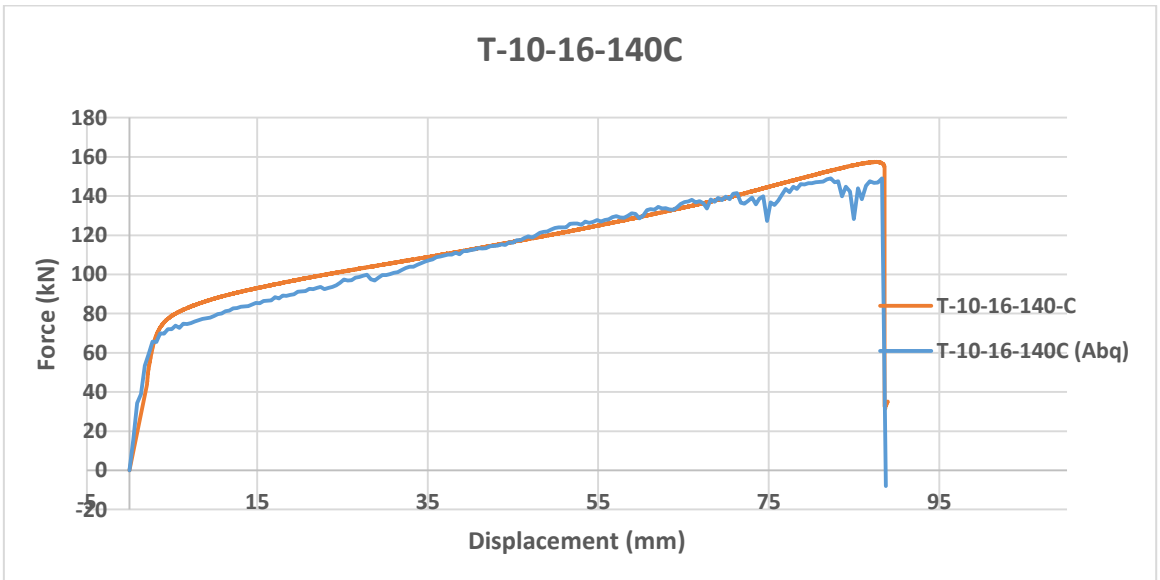
T-10-16-140C
Force (kN)
Displacement (mm)
180
160
140
120
100
80
60
40
20
0
-20
-5
15
35
55
75
95
T-10-16-140-C
T-10-16-140C (Abq)

T-10-16-140C

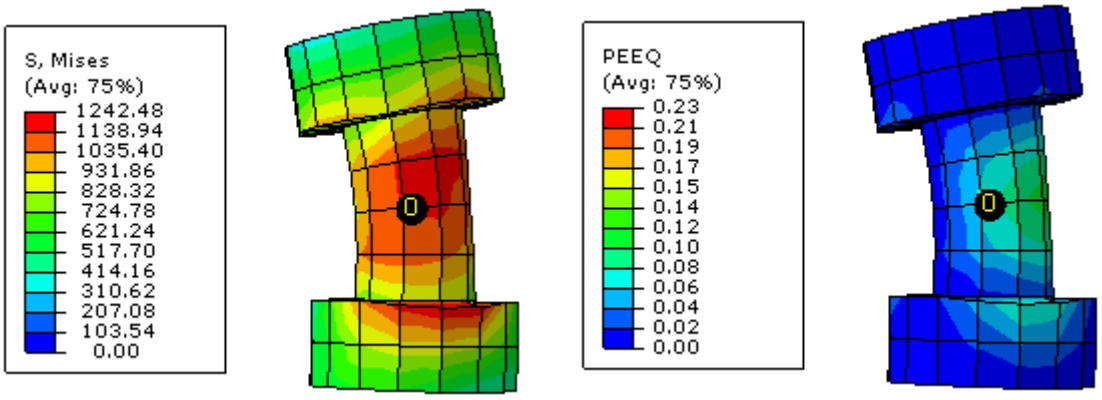
S, Mises
(Avg: 75%)
1242.48
1138.94
1035.40
931.86
828.32
724.78
621.24
517.70
414.16
310.62
207.08
103.54
0.00
PEEQ
(Avg: 75%)
0.23
0.21
0.19
0.17
0.15
0.14
0.12
0.10
0.08
0.06
0.04
0.02
0.00

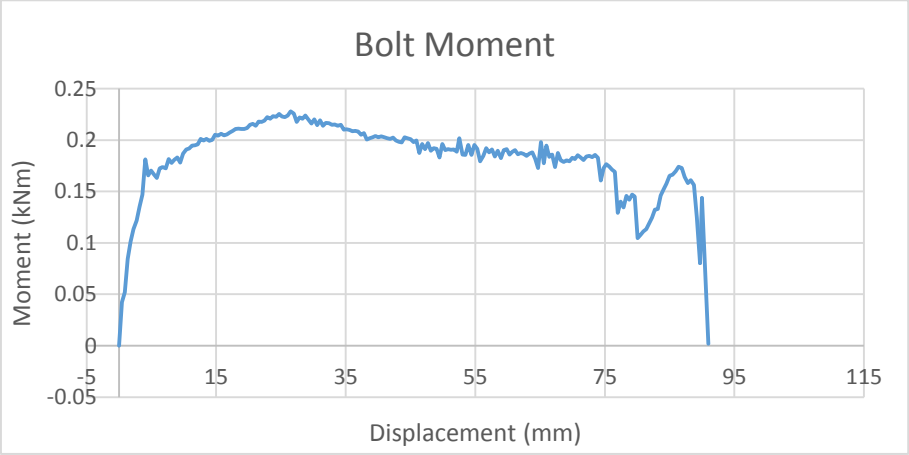
Bolt Moment
Moment (kNm)
0.25
0.2
0.15
0.1
0.05
0
-0.05
-5
15
35
55
75
95
115
Displacement (mm)

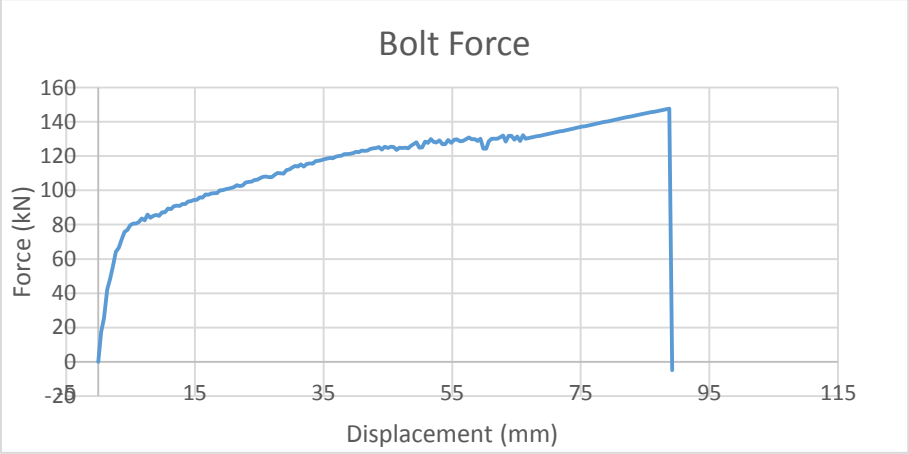
Bolt Force
Force (kN)
160
140
120
100
80
60
40
20
0
-20
-25
15
35
55
75
95
115
Displacement (mm)

T-12-16-100C

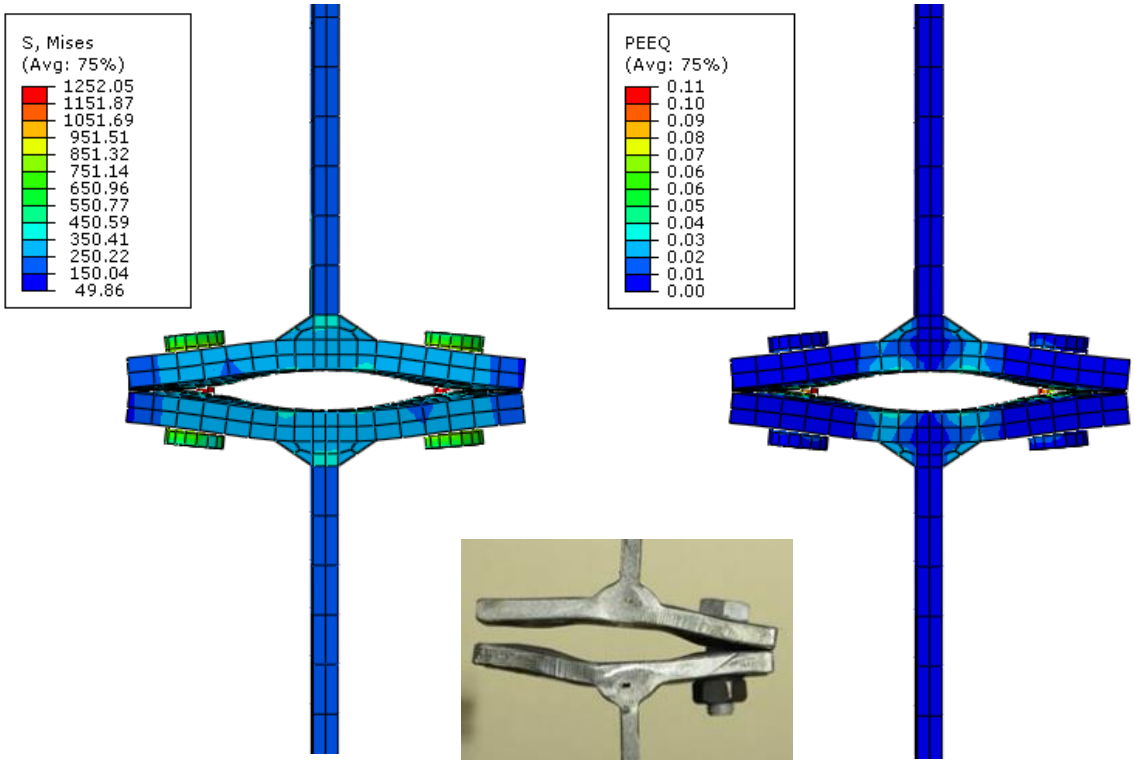
S, Mises
(Avg: 75%)
1252.05
1151.87
1051.69
951.51
851.32
751.14
650.96
550.77
450.59
350.41
250.22
150.04
49.86
PEEQ
(Avg: 75%)
0.11
0.10
0.09
0.08
0.07
0.06
0.06
0.05
0.04
0.03
0.02
0.01
0.00

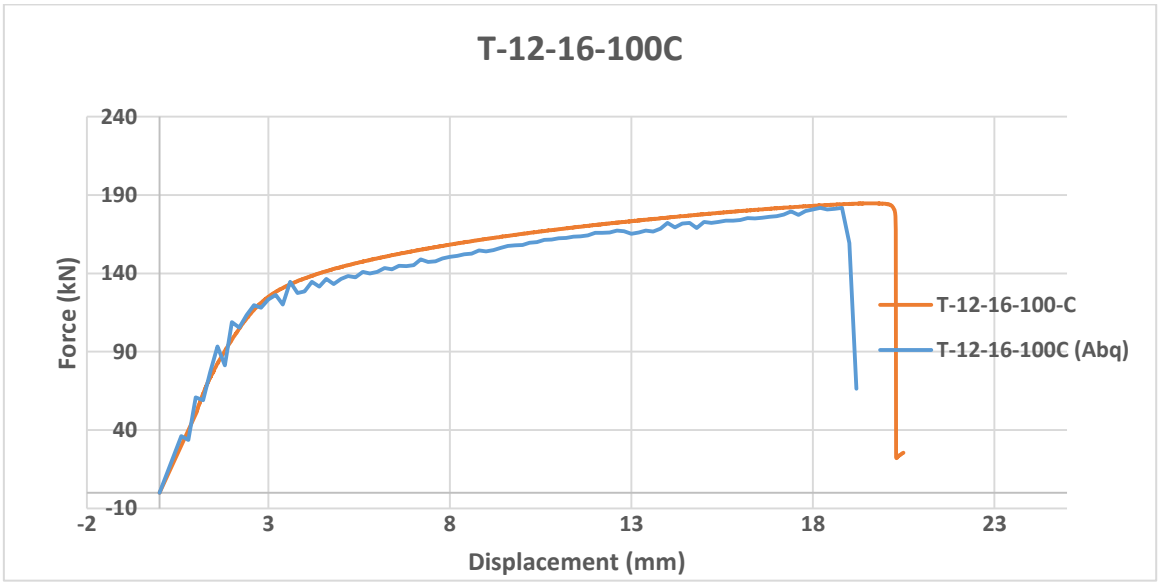
T-12-16-100C
240
190
140
90
40
-10
Force (kN)
-2
3
8
13
18
23
Displacement (mm)
T-12-16-100-C
T-12-16-100C (Abq)

T-12-16-100C

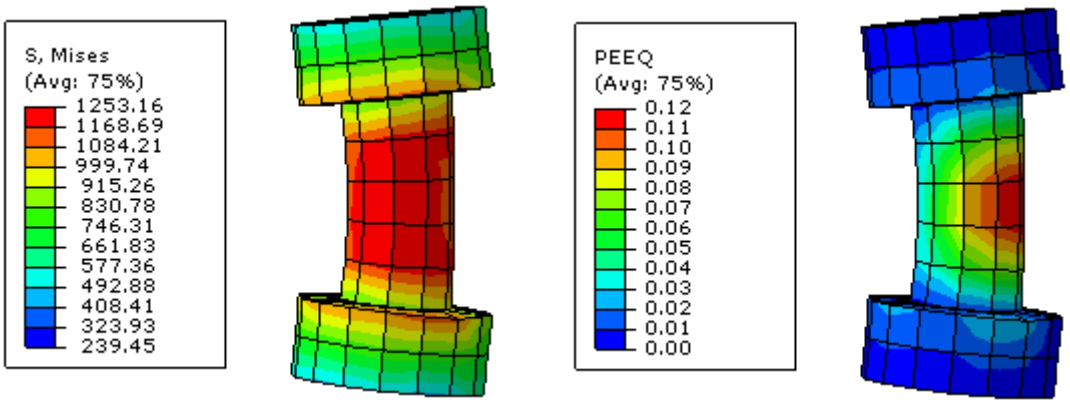
S, Mises
(Avg: 75%)
1253.16
1168.69
1084.21
999.74
915.26
830.78
746.31
661.83
577.36
492.88
408.41
323.93
239.45
PEEQ
(Avg: 75%)
0.12
0.11
0.10
0.09
0.08
0.07
0.06
0.05
0.04
0.03
0.02
0.01
0.00

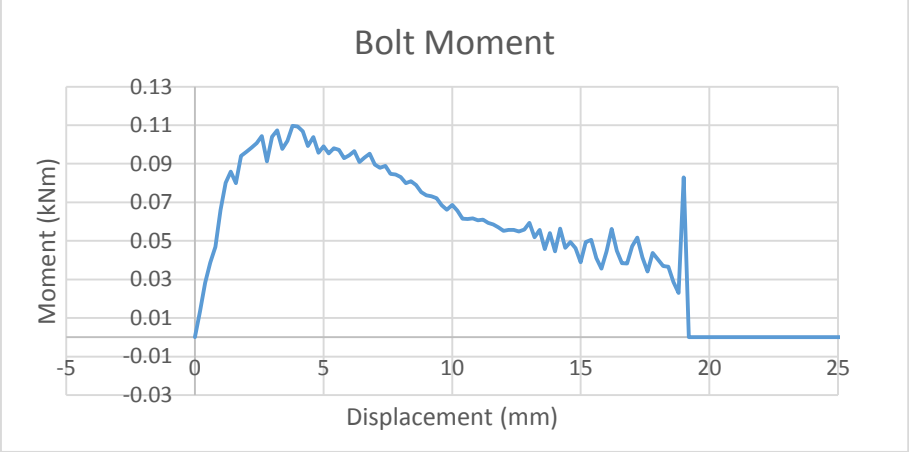
Bolt Moment
Moment (kNm)
0.13
0.11
0.09
0.07
0.05
0.03
0.01
-0.01
-0.03
-5
0
5
10
15
20
25
Displacement (mm)

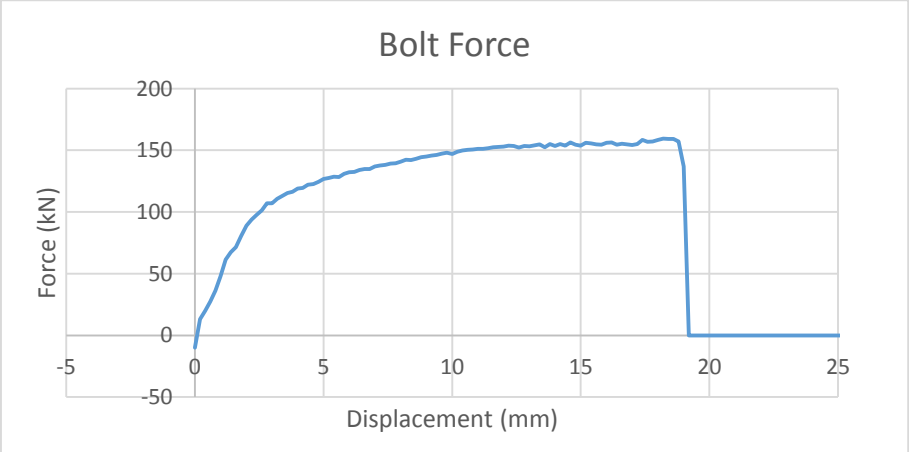
Bolt Force
Force (kN)
200
150
100
50
0
-50
-5
0
5
10
15
20
25
Displacement (mm)

T-12-16-120C

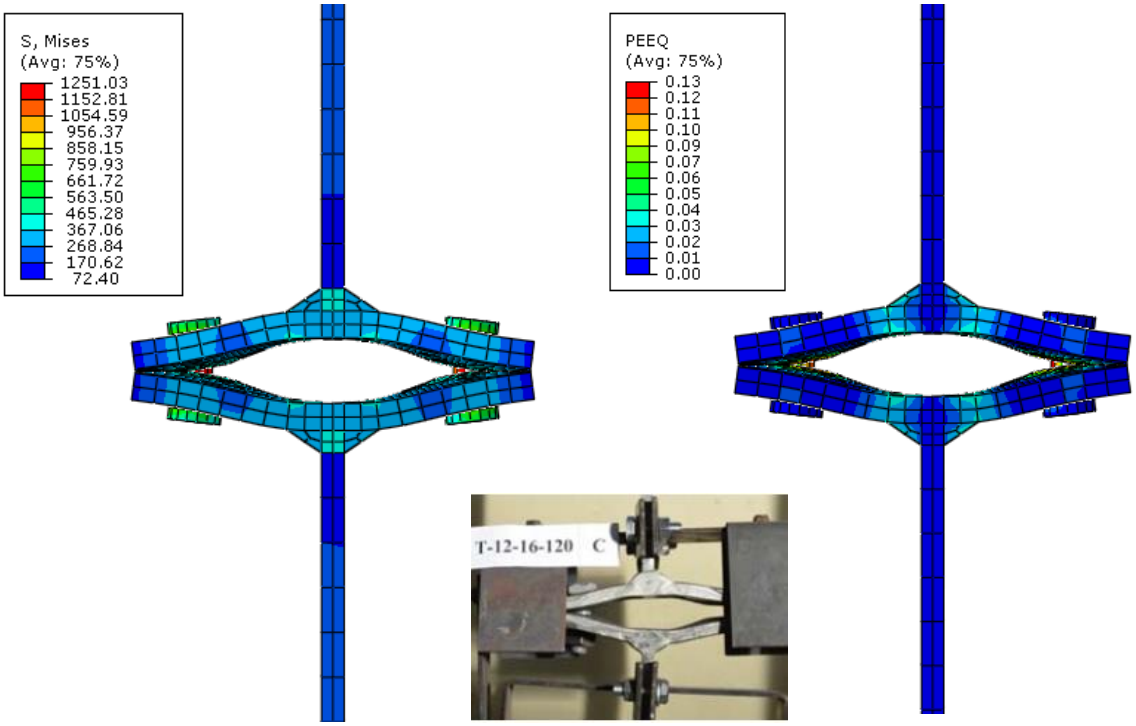
S, Mises
(Avg: 75%)
1251.03
1152.81
1054.59
956.37
858.15
759.93
661.72
563.50
465.28
367.06
268.84
170.62
72.40
PEEQ
(Avg: 75%)
0.13
0.12
0.11
0.10
0.09
0.07
0.06
0.05
0.04
0.03
0.02
0.01
0.00
T-12-16-120 C

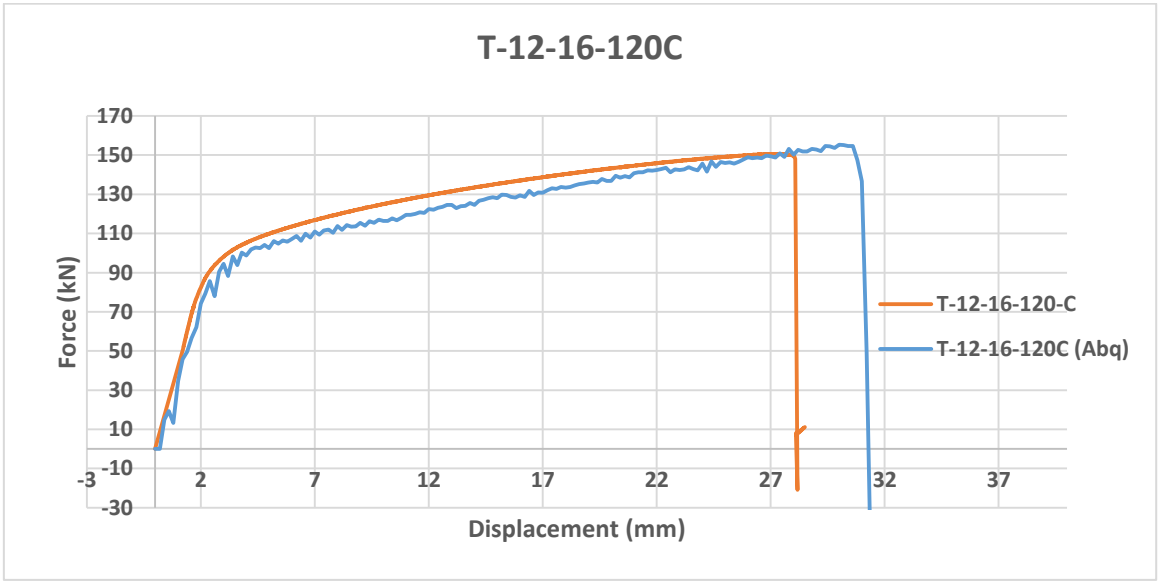
T-12-16-120C
Force (kN)
170
150
130
110
90
70
50
30
10
-10
-30
-3
2
7
12
17
22
27
32
37
Displacement (mm)
T-12-16-120-C
T-12-16-120C (Abq)

T-12-16-120C

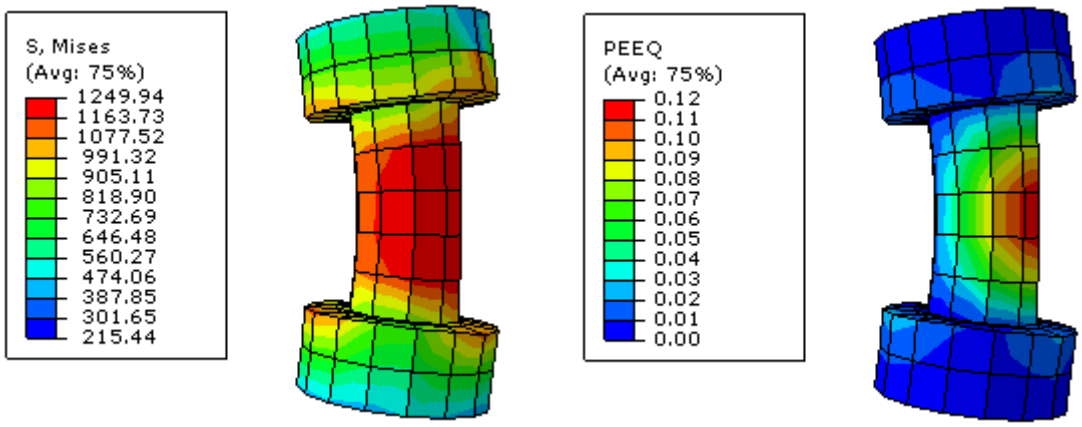
S, Mises
(Avg: 75%)
1249.94
1163.73
1077.52
991.32
905.11
818.90
732.69
646.48
560.27
474.06
387.85
301.65
215.44
PEEQ
(Avg: 75%)
0.12
0.11
0.10
0.09
0.08
0.07
0.06
0.05
0.04
0.03
0.02
0.01
0.00

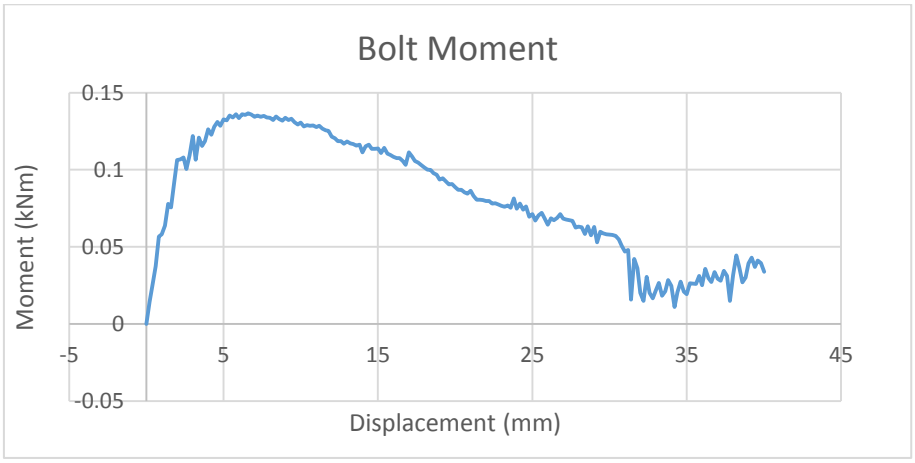
Bolt Moment
Moment (kNm)
0.15
0.1
0.05
0
-0.05
-5
5
15
25
35
45
Displacement (mm)

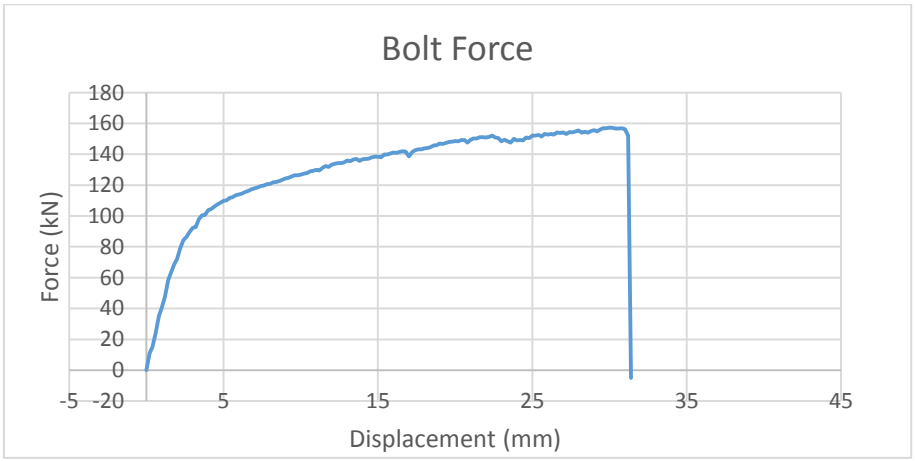
Bolt Force
Force (kN)
180
160
140
120
100
80
60
40
20
0
-20
-5
5
15
25
35
45
Displacement (mm)

T-12-16-140C

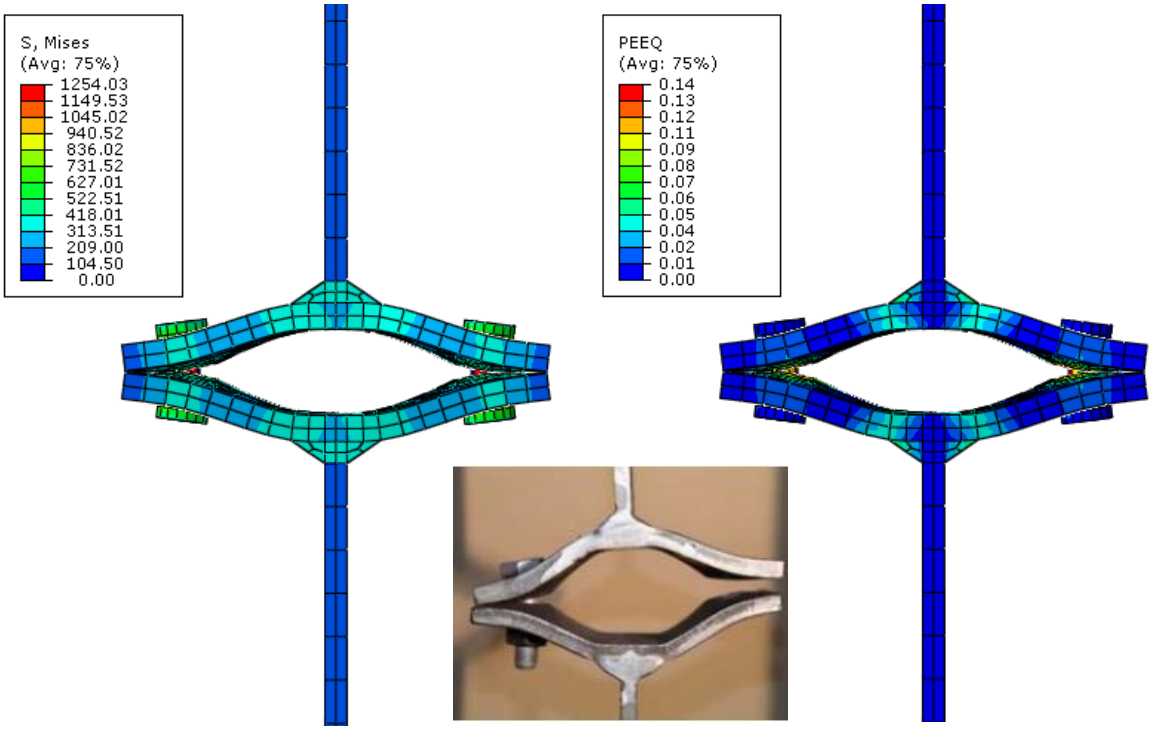
S, Mises
(Avg: 75%)
1254.03
1149.53
1045.02
940.52
836.02
731.52
627.01
522.51
418.01
313.51
209.00
104.50
0.00
PEEQ
(Avg: 75%)
0.14
0.13
0.12
0.11
0.09
0.08
0.07
0.06
0.05
0.04
0.02
0.01
0.00

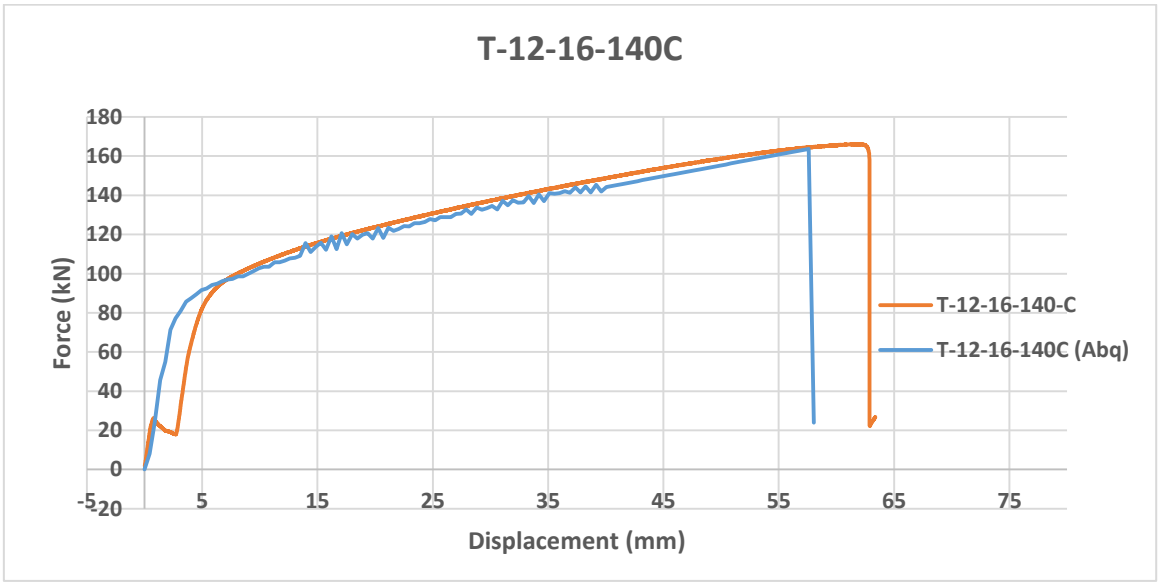
T-12-16-140C
Force (kN)
Displacement (mm)
180
160
140
120
100
80
60
40
20
0
-20
-5
5
15
25
35
45
55
65
75
T-12-16-140-C
T-12-16-140C (Abq)

T-12-16-140C

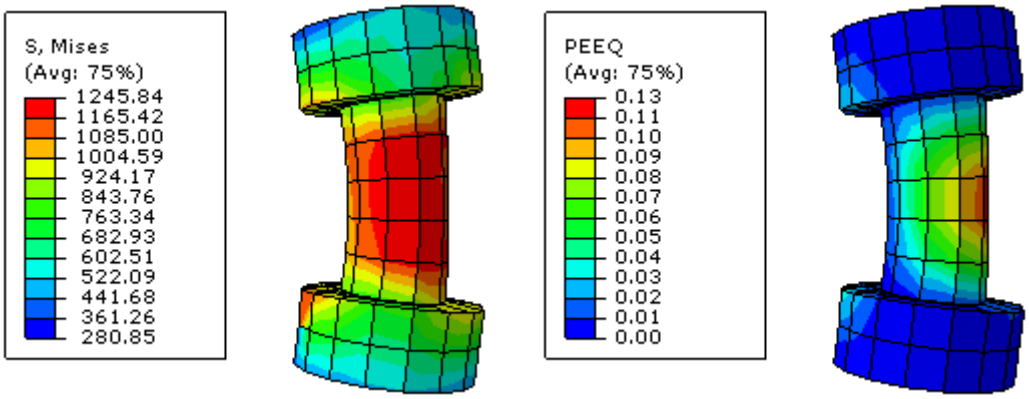
S, Mises
(Avg: 75%)
1245.84
1165.42
1085.00
1004.59
924.17
843.76
763.34
682.93
602.51
522.09
441.68
361.26
280.85
PEEQ
(Avg: 75%)
0.13
0.11
0.10
0.09
0.08
0.07
0.06
0.05
0.04
0.03
0.02
0.01
0.00

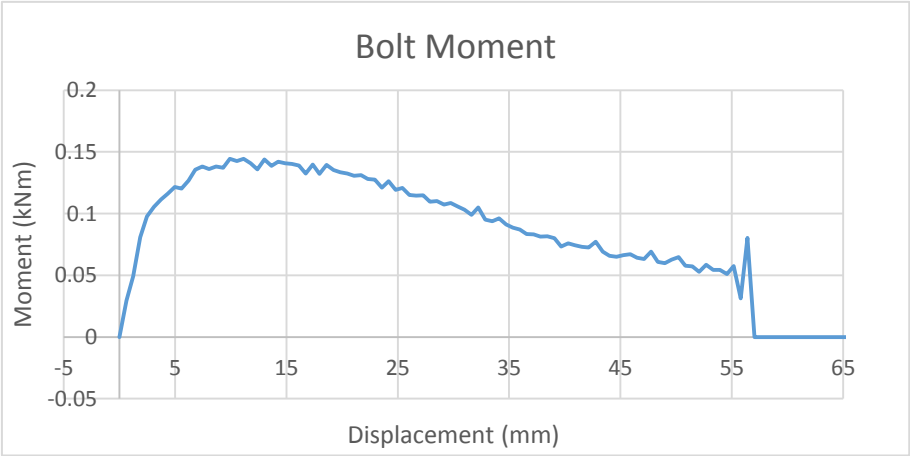
Bolt Moment
Moment (kNm)
0.2
0.15
0.1
0.05
0
-0.05
-5
5
15
25
35
45
55
65
Displacement (mm)

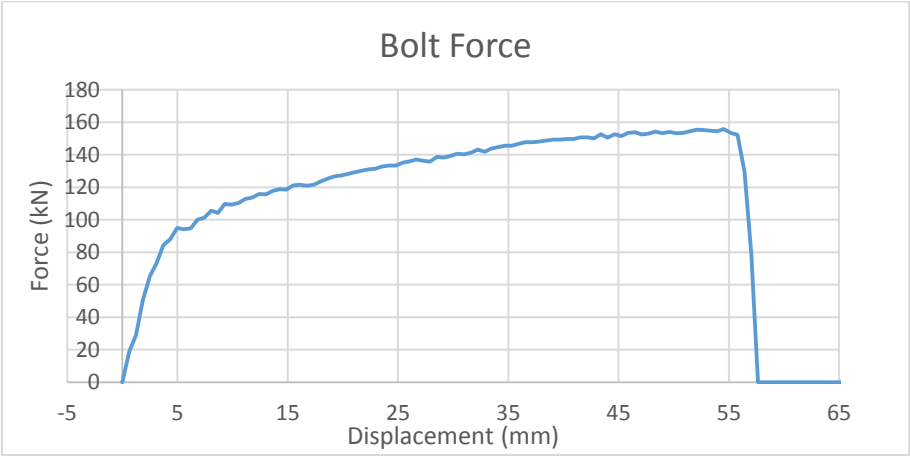
Bolt Force
Force (kN)
180
160
140
120
100
80
60
40
20
0
-5
5
15
25
35
45
55
65
Displacement (mm)

T-15-16-100C

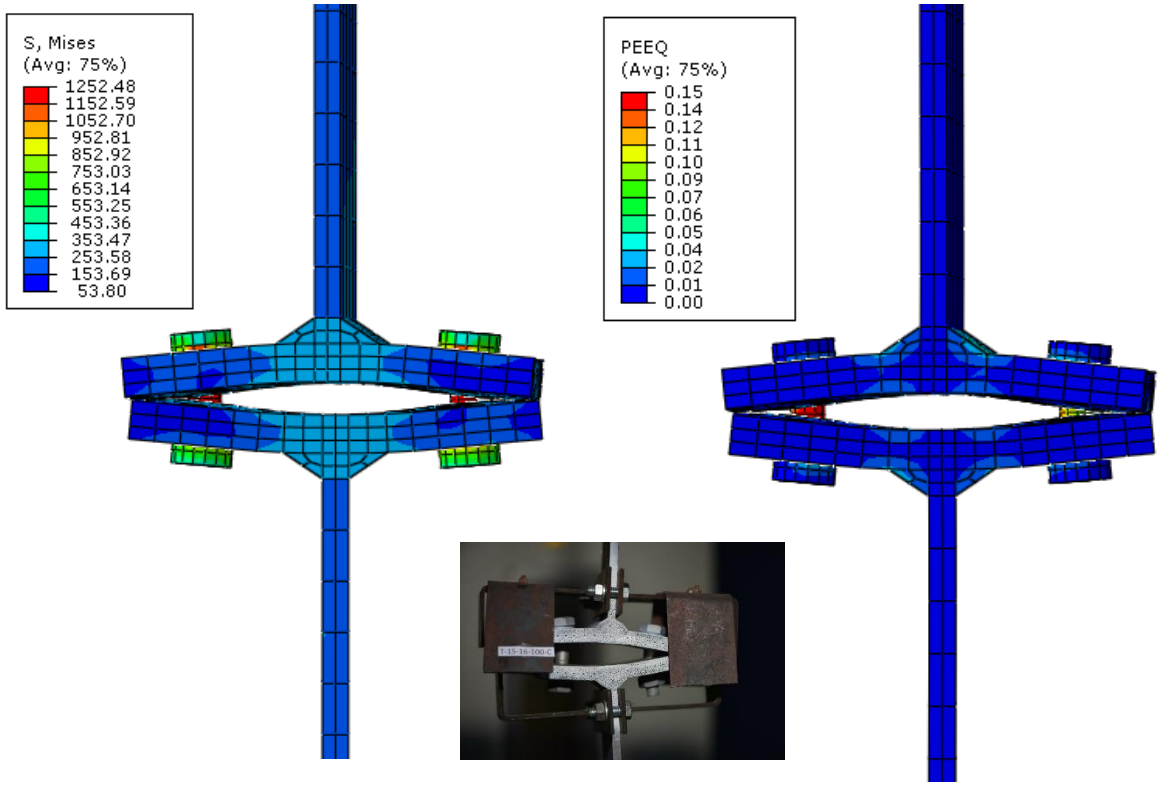
S, Mises
(Avg: 75%)
1252.48
1152.59
1052.70
952.81
852.92
753.03
653.14
553.25
453.36
353.47
253.58
153.69
53.80
PEEQ
(Avg: 75%)
0.15
0.14
0.12
0.11
0.10
0.09
0.07
0.06
0.05
0.04
0.02
0.01
0.00

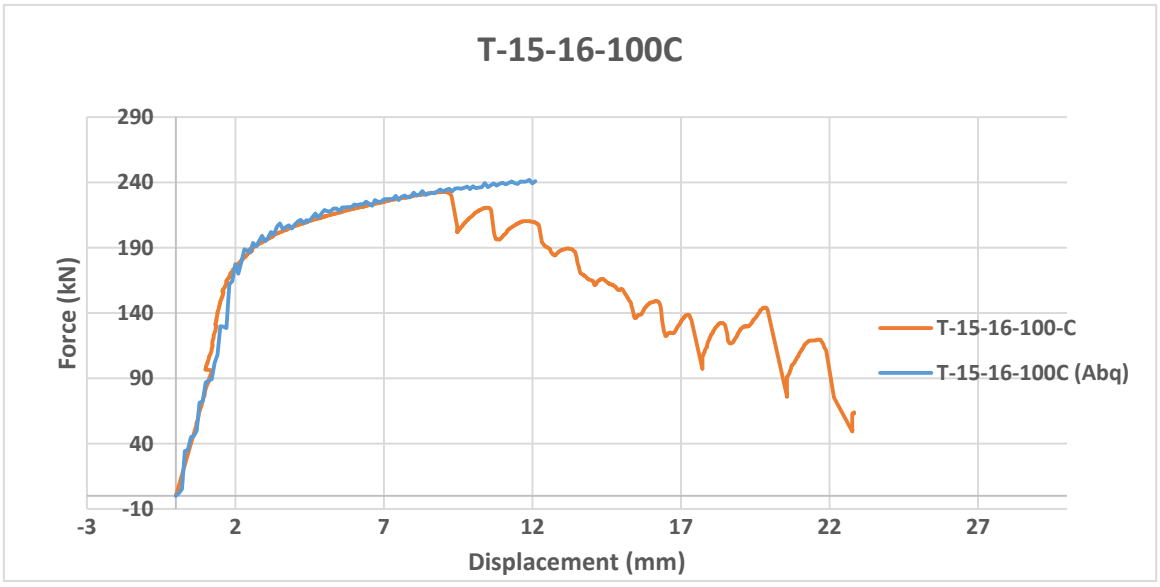
T-15-16-100C
290
240
190
140
90
40
-10
Force (kN)
-3
2
7
12
17
22
27
Displacement (mm)
T-15-16-100-C
T-15-16-100C (Abq)

T-15-16-120C

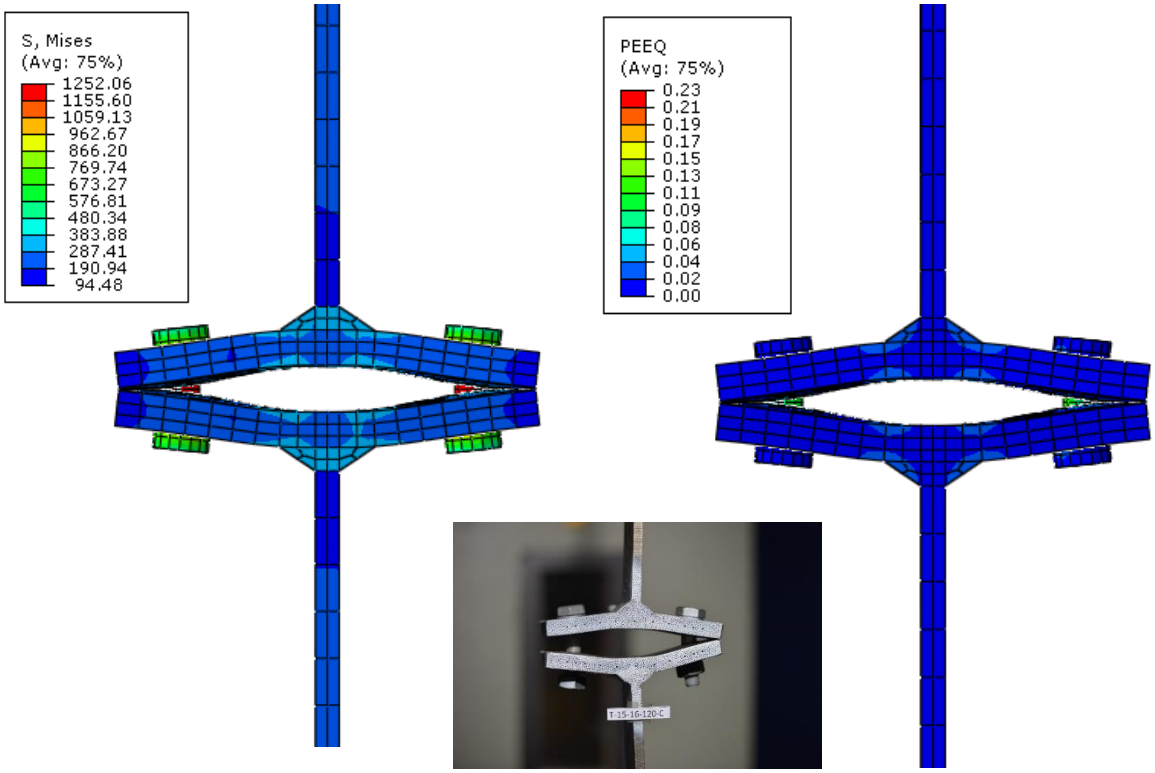
S, Mises
(Avg: 75%)
1252.06
1155.60
1059.13
962.67
866.20
769.74
673.27
576.81
480.34
383.88
287.41
190.94
94.48
PEEQ
(Avg: 75%)
0.23
0.21
0.19
0.17
0.15
0.13
0.11
0.09
0.08
0.06
0.04
0.02
0.00

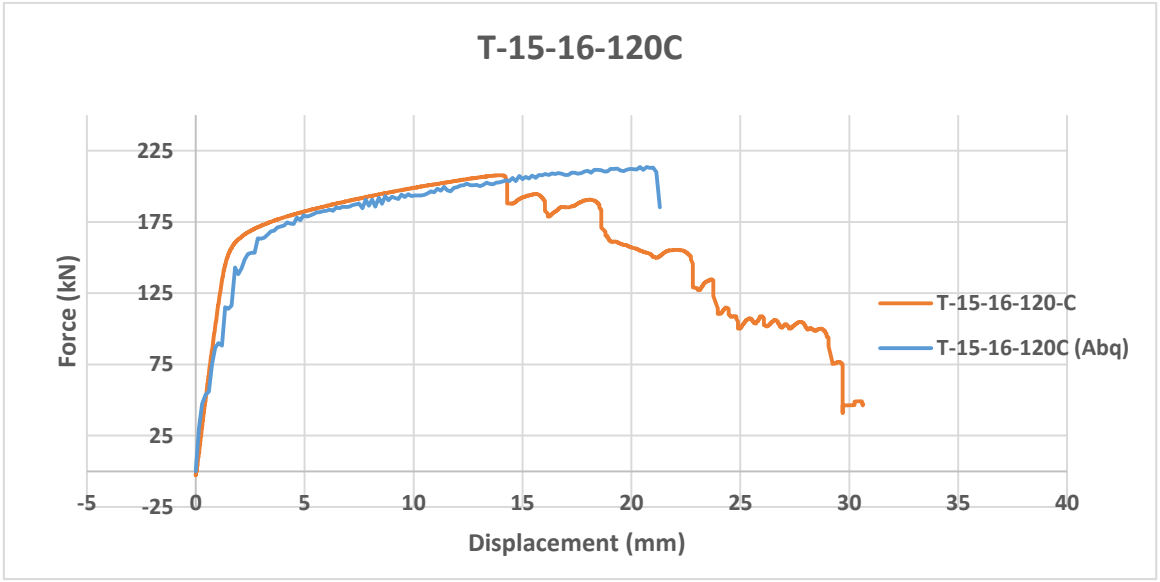
T-15-16-120C
Force (kN)
225
175
125
75
25
-25
-5
0
5
10
15
20
25
30
35
40
Displacement (mm)
T-15-16-120-C
T-15-16-120C (Abq)

T-15-16-140C

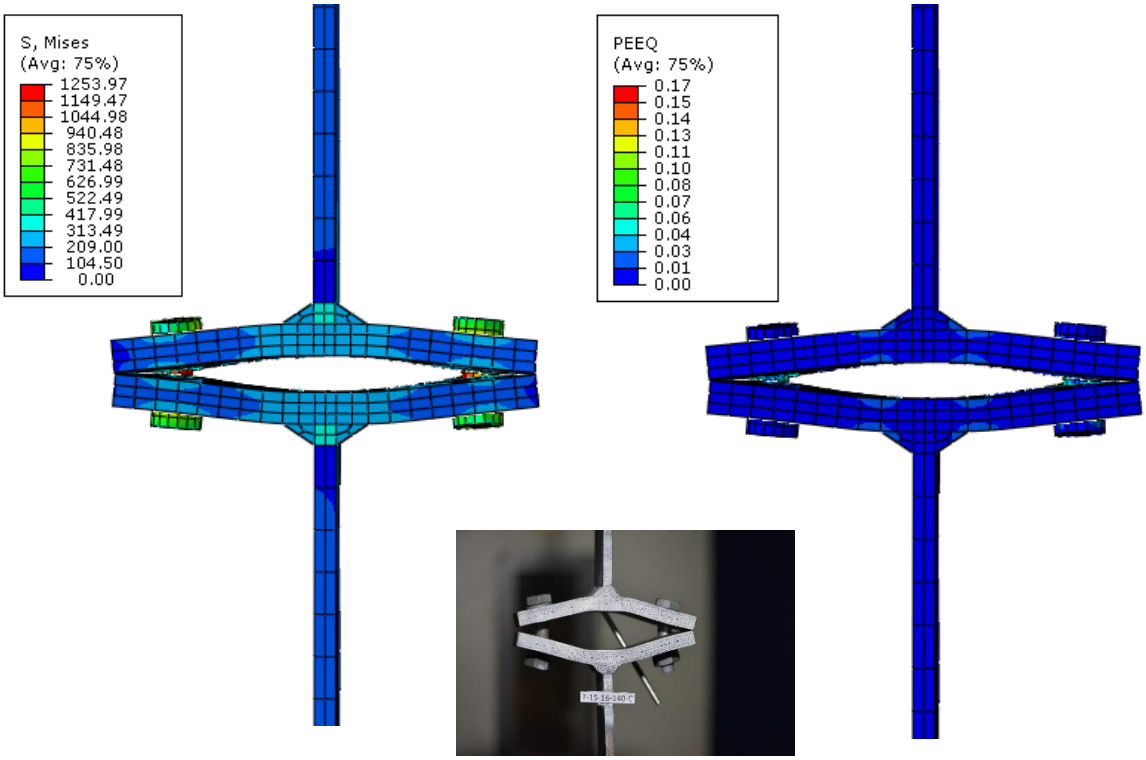
S, Mises
(Avg: 75%)
1253.97
1149.47
1044.98
940.48
835.98
731.48
626.99
522.49
417.99
313.49
209.00
104.50
0.00
PEEQ
(Avg: 75%)
0.17
0.15
0.14
0.13
0.11
0.10
0.08
0.07
0.06
0.04
0.03
0.01
0.00

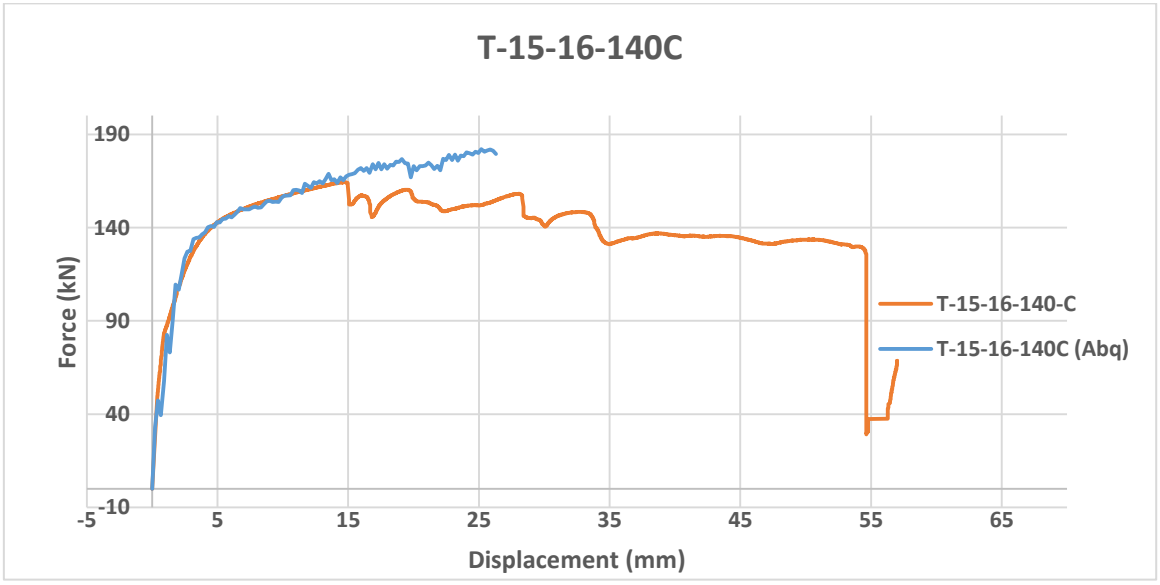
T-15-16-140C
190
140
90
40
-10
-5
5
15
25
35
45
55
65
Force (kN)
Displacement (mm)
T-15-16-140-C
T-15-16-140C (Abq)

T-18-16-120C

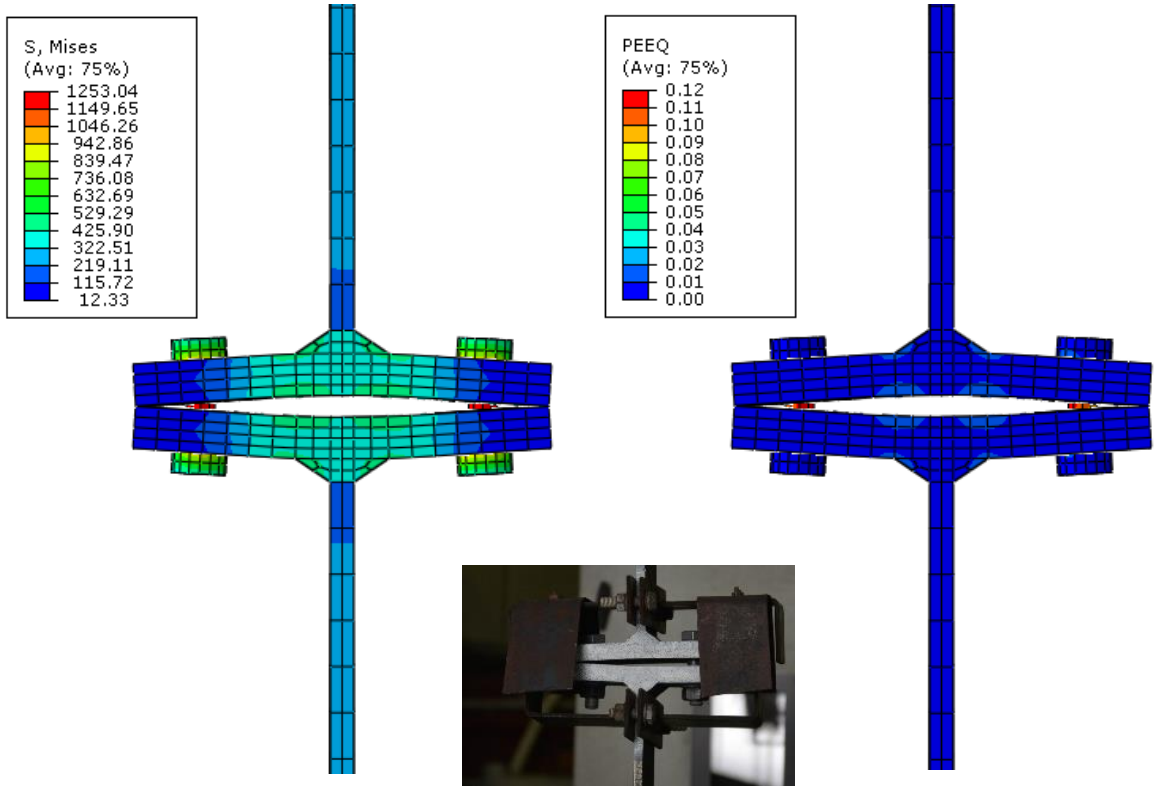
S, Mises
(Avg: 75%)
1253.04
1149.65
1046.26
942.86
839.47
736.08
632.69
529.29
425.90
322.51
219.11
115.72
12.33
PEEQ
(Avg: 75%)
0.12
0.11
0.10
0.09
0.08
0.07
0.06
0.05
0.04
0.03
0.02
0.01
0.00

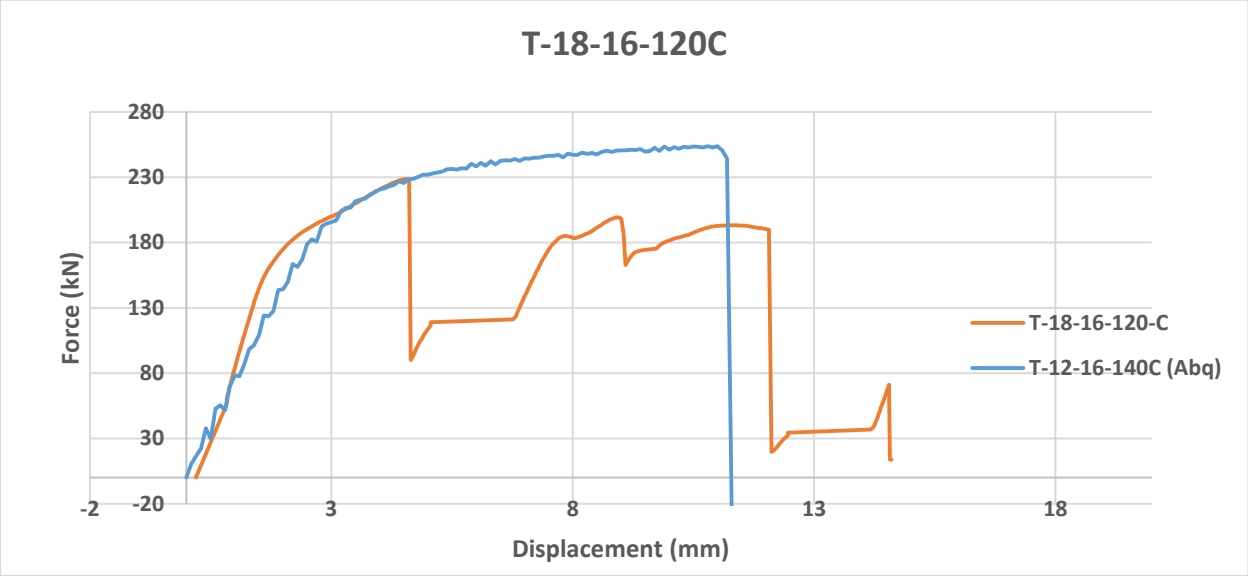
T-18-16-120C
Force (kN)
280
230
180
130
80
30
-20
-2
3
8
13
18
Displacement (mm)
T-18-16-120-C
T-12-16-140C (Abq)

T-18-16-140C

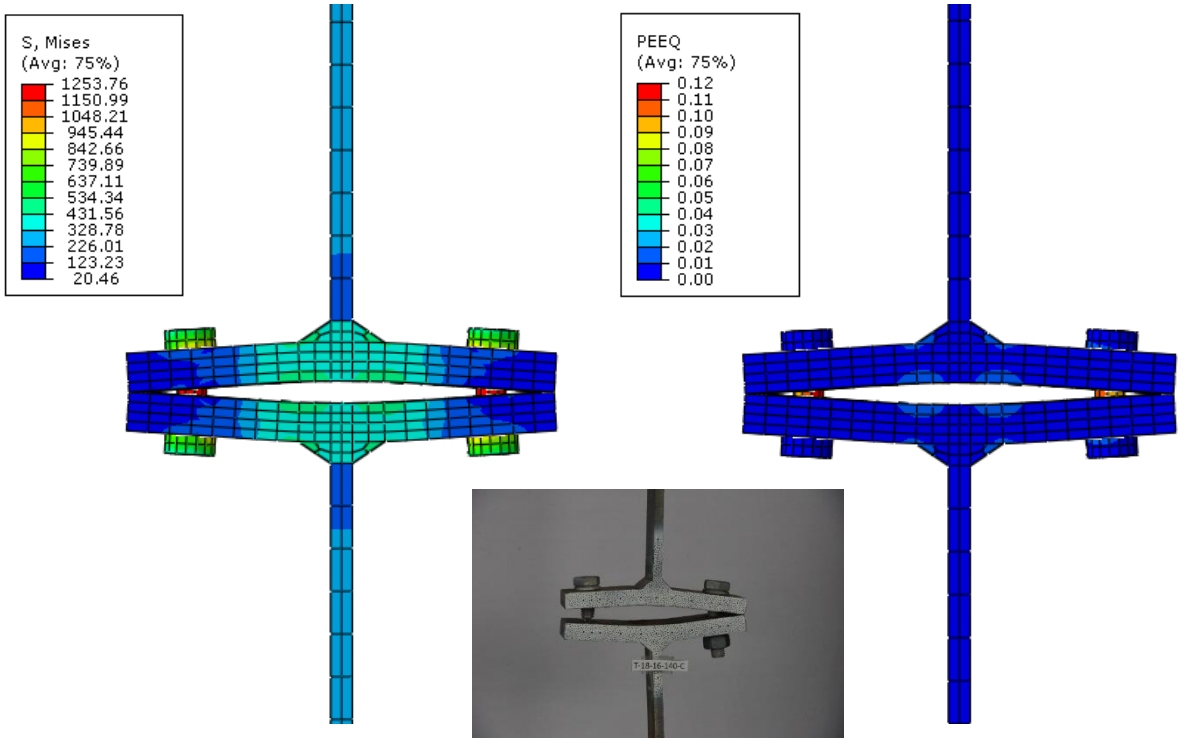
S, Mises
(Avg: 75%)
1253.76
1150.99
1048.21
945.44
842.66
739.89
637.11
534.34
431.56
328.78
226.01
123.23
20.46
PEEQ
(Avg: 75%)
0.12
0.11
0.10
0.09
0.08
0.07
0.06
0.05
0.04
0.03
0.02
0.01
0.00

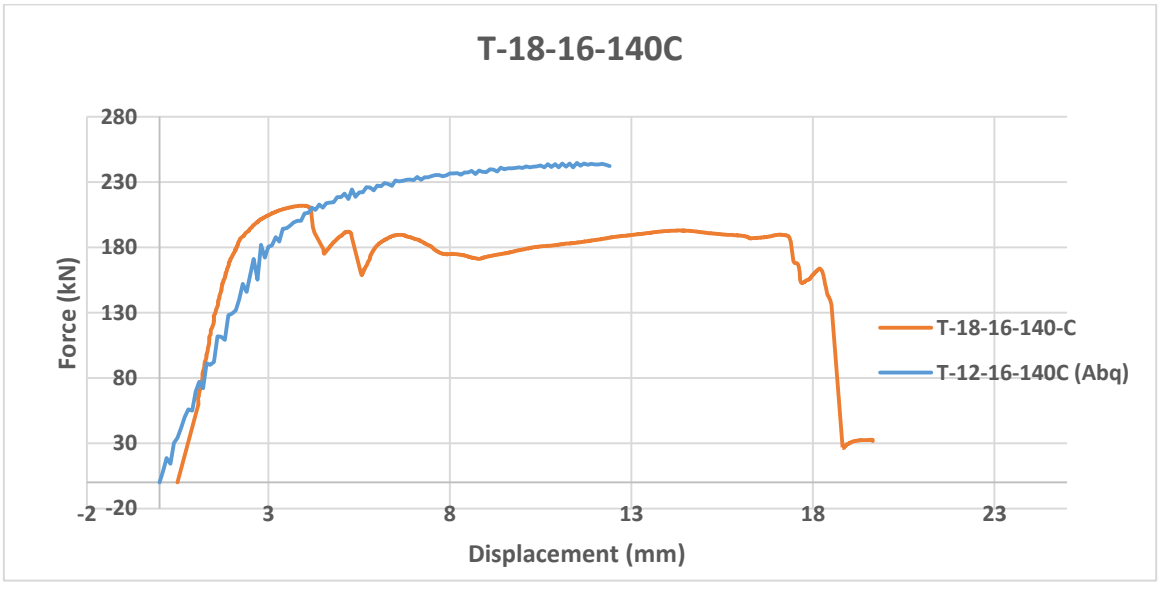
T-18-16-140C
280
230
180
130
80
30
-20
-2
3
8
13
18
23
Force (kN)
Displacement (mm)
T-18-16-140-C
T-12-16-140C (Abq)

6.3. Parametric study

6.3.1. Introduction

Experimental program under Codec presented in chapter 5 has T-stubs with varying material properties at different end plate thicknesses. In order to study relationships between different end plate thicknesses, material properties of the calibrated numerical models were made same. All the parameters were kept same including mass scaling, meshing properties, Step type etc. to study behavior of the T-stub because of the geometrical differences i.e. end plate thickness and distance between the bolts.

All the T-stubs were made to fail in mode 1 or mode 2 to study the reserve capacity and ductility in T-stubs. Following is the list of T-stubs used for the parametric study.

Table 15.T-Stub specimens used for the parametric study

T-Stub	Thickness of the End Plate	Diameter of the bolt	Distance between the bolts
	mm	mm	mm
T-10-16-90 C	10	16	90
T-10-16-100 C	10	16	100
T-10-16-120 C	10	16	120
T-10-16-140 C	10	16	140
T-12-16-90 C	12	16	90
T-12-16-100 C	12	16	100
T-12-16-120 C	12	16	120
T-12-16-140 C	12	16	140
T-15-16-90 C	15	16	90
T-15-16-100 C	15	16	100
T-15-16-120 C	15	16	120
T-15-16-140 C	15	16	140
T-18-16-90 C	18	16	90
T-18-16-100 C	18	16	100
T-18-16-120 C	18	16	120
T-18-16-140 C	18	16	140

6.3.2. Modeling description

Same material properties for all the T-stubs were used. Following table shows elastic material properties along with the damage evaluation criterions used in different parts of the T-Stub macro-component. T-stub weld part was modeled using S355, end-plate using S235 and bolts of 10.9.

Table 16. Elastic properties used for all T-stub specimens in parametric study

Elastic Property	**Value**	**Unit**
Young's Modulus	210000	N/mm^2
Poisson's Ratio	0.3	-
Density	$7.85x10^{-9}$	$Tons/mm^3$

Table 17.Fracture criterion for S355 materials in parametric study

Coefficients for S355	**Value**
Fracture Strain	0.8
Stress Triaxiality	0.8
Strain Rate	0.5
Displacement at Failure	0.81

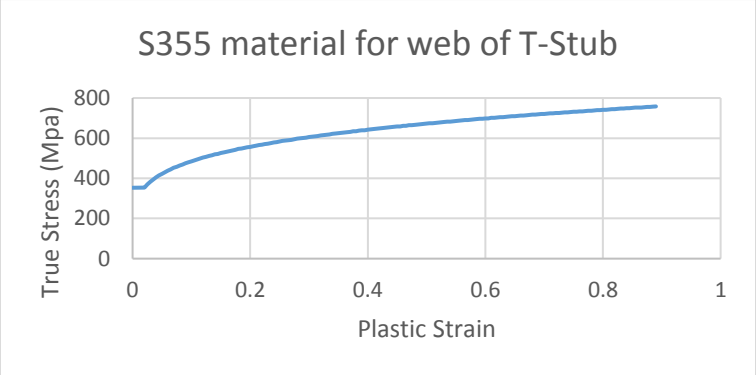

Figure 61.True stress vs plastic strain graph for S355 material

Table 18. Fracture criterion for S235 materials in parametric study

Coefficients for S235	**Value**
Fracture Strain	0.5
Stress Triaxiality	0.8
Strain Rate	0.2
Displacement at Failure	0.52

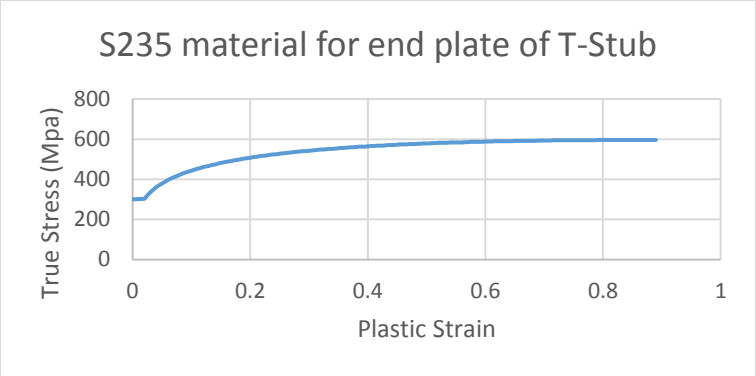

Figure 62. True stress vs plastic strain graph for S235 material

Table 19. Fracture criterion for 10.9 bolt materials in parametric study

Coefficients for 10.9	**Value**
Fracture Strain	0.13
Stress Triaxiality	0.8
Strain Rate	0.5
Displacement at Failure	0.15

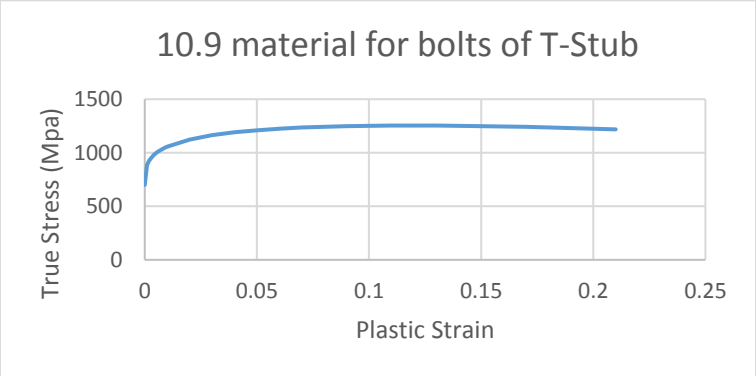

Figure 63. True stress vs plastic strain graph for 10.9 bolt material

Rest of the modeling description is the same as mentioned in this chapter previously.

6.3.3. Numerical model of T-30-16-100 with failure mode 3

Failure mode 3 indicates brittle failure of the T-stub macro-component with bolts failure and no yielding in the end plate of the T-stub. End plate thickness was increased to 30mm to have a mode 3 failure.

Following figure shows the force-displacement behavior of the T-stub macro component with failure mode 3. T-stub with end plate thickness of 30mm was used with 16mm diameter bolts and center to center distance of the bolts was 100mm to achieve failure mode 3.

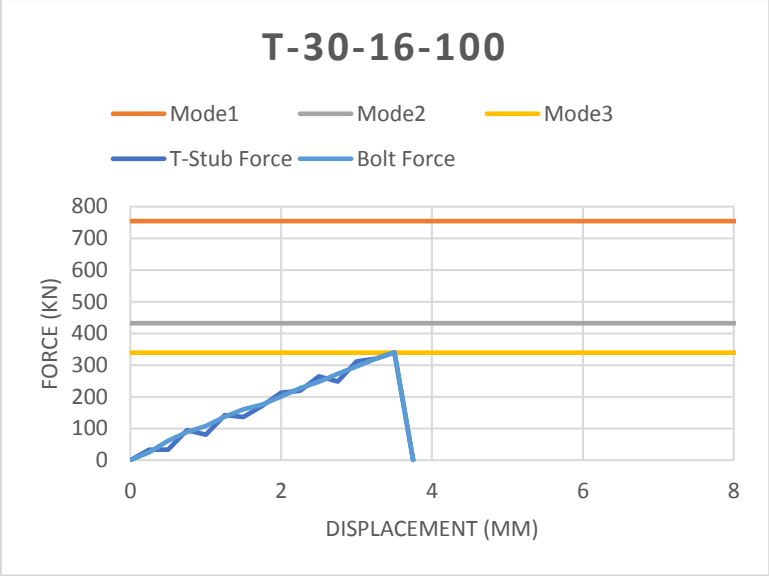

Figure 64. Force-displacement behavior of T-stub in failure mode 3

Eurocode 1993-1-8 [20] was used to calculate all three modes which are shown in (Figure 64). The governing failure mode is mode 3 indicating brittle failure of the bolts. Eurocodes predict the failure of the T-stub macro-component by bolt fracture at the applied force of 339 kN after removing the safety factors in calculations. Numerical model shows exactly the same behavior. The force in the T-stub keeps on increasing till it reaches the 330 kN where the T-stub fails because of bolt fracture. The graph shows no reserve capacity in case of failure mode 3. Brittle failure occurs at the calculated force from Eurocodes which is not desirable failure mode.

6.3.4. Numerical model of T-10-16-100 with failure mode 1

Failure mode 1 indicates ductile failure of the T-stub macro-component with yielding in the end plate of the T-stub. A numerical model T-10-16-100 C is used to explain the behavior of T-stub macro-component with a failure mode 1.

Eurocode 1993-1-8 was used to calculate all three modes for T-stub T-10-16-100 C shown in (Table 20). Safety factors were removed to have exact forces where failure is occurring.

Table 20. Failure modes of T-10-16-100 calculated from EN-1993-1-8

Modes	**Force at failure (kN)**
Mode 1	84
Mode 2	114
Mode 3	339

Failure mode 1 is governing which indicates the failure of the T-stub through yielding of the end plate at force of 84 kN. Following graph shows all three failure modes with the force displacement behavior from numerical modeling of the T-Stub.

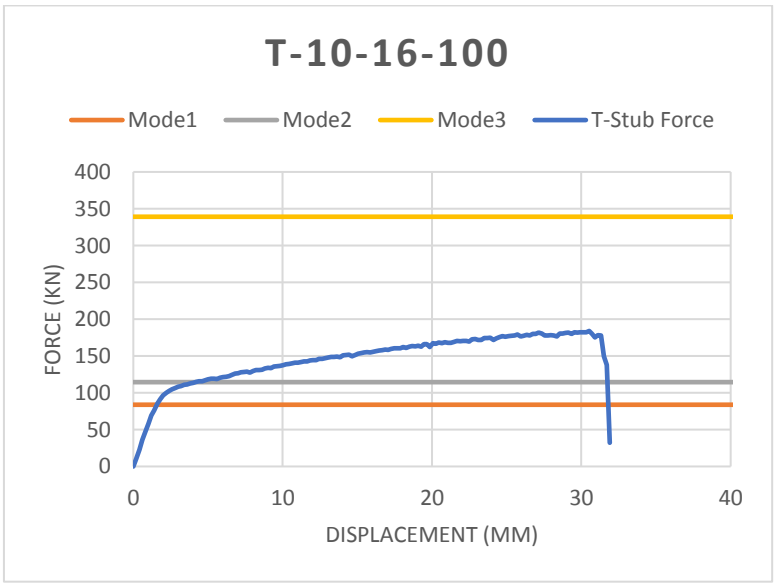

Figure 65. Force-displacement behavior of T-stub in failure mode 1

The force-displacement curve of the T-stub macro-component T-10-16-100 shows elastic and plastic behavior of the T-stub until ultimate failure. Initially elastic with some stiffness till the yield point. The graph shows yielding of the end plate at around 80 kN which is according to Eurocodes analytical formulas. Unlike mode 3 type failure, mode 1 and mode 2 shows large reserve capacities beyond the failure criterion of the Eurocodes. The T-stub failing in mode 1

can take much more load after the yielding point has reached. Experimental investigations and numerical modeling suggest that even for failure mode 1 and failure mode 2 the ultimate failure of the T-stub occurs because of the failure of the bolts. For this particular T-Stub yielding starts at approximately 80 kN, same as Eurocodes prediction. The yielding occurs around the welds i.e. the connection between the endplates and web of the T-stub. Some of the yielding is also observed around the bolt holes. (Figure 66) shows yielding of the endplate prior to ultimate failure of the T-stubs.

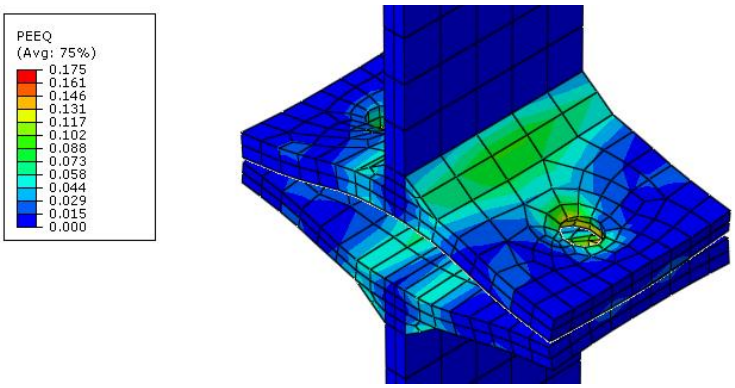

Figure 66. PEEQ strains in T-10-16-100C at ultimate failure

Plastic strains continue to develop after the yielding because of plasticity and strain hardening of the material. The T-stub ultimately fails at a load of 184 kN because of the failure of the bolts. At failure mode 1 where yielding starts the observed displacement of the T-Stub is 1.6mm while at ultimate failure the displacement is 31.5mm indicating high ductility in case of failure mode 1 and failure mode 2. Failure mode 1 and 2 indicates high reserve ultimate capacity and ductility which is vital in robust designing of a structure. For all the T-stubs numerically modeled from end plate thickness of 10mm to 18mm and center to center bolt distance of 100mm to 140 mm, the ultimate failure of the T-stub occurs because of the failure of the bolts no matter the failure mode.

According to the Eurocodes the ultimate capacity of the bolt is 339 kN and ultimate failure of the T-stub is because of the failure of the bolt indicating the failure should occur at a force of 339 kN. But the bolt fails at the applied T-stub force of 184 kN for mode 1 type failure of T-stub T-10-16-100C see (Figure 67) indicating the force in the bolts is much higher than the applied force.

Forces in the bolts were calculated using the same numerical model. (Figure 67) shows the force-displacement relationship of the T-stub and the forces in the bolts.

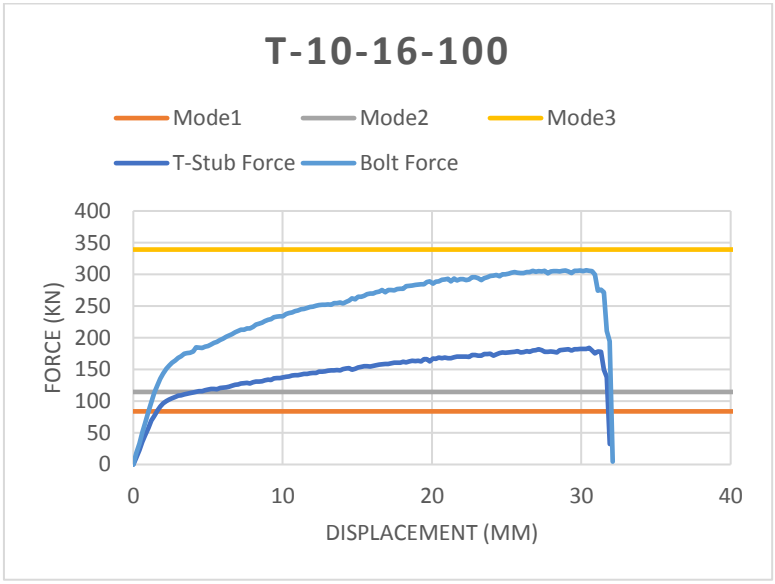

Figure 67. Force-displacement behavior of T-stub force and force in bolts

This graph shows the axial forces in the bolts are much higher than the applied force because of the prying action in the T-Stub. The ultimate failure of the T-stub occurs when the force in the bolts reaches 306 kN. The failure of the bolts still occurs before its ultimate axial capacity is reached i.e. 339 kN. This is because in addition to the prying forces, bending in the bolts reduces the ultimate axial capacity of the bolts. (Figure 68) shows the positive and negative stresses and bending of the bolts clearly indicating bending moments in the bolts in addition to the axial forces.

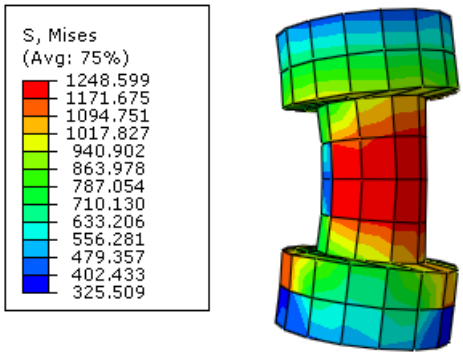

Figure 68. Mises stresses and bending in the bolts prior to failure

(Figure 69) shows the bending moment in the bolts determined using numerical model.

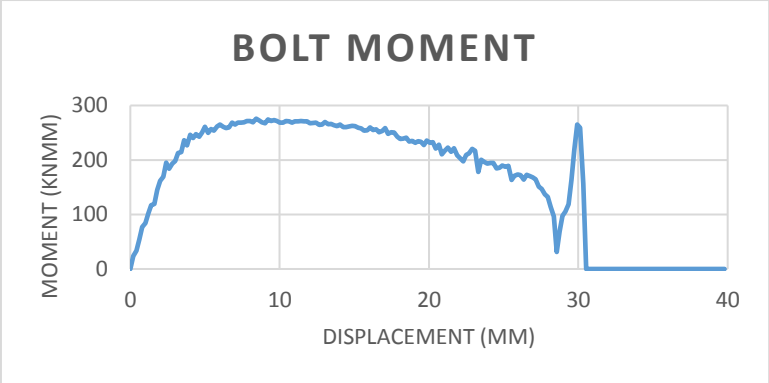

Figure 69. Moment-displacement behavior of bolt in T-10-16-100

With increasing axial force in the T-stub, the bending moment in the bolts increases and then gradually starts decreasing till the fracture of the bolts. Because of the axial force and bending interaction the bolts can't reach their ultimate axial capacity of 338 kN as predicted by Eurocodes analytical models.

Hence ultimate capacity of the T-stub for mode1 and mode 2 can be calculated by taking into account the bending of the bolts and prying forces. It is concluded that fracture of the bolts occur at nearly the axial ultimate capacity of the bolt but because of the prying forces the T-stub macro-component fails at much lower axial force which can be calculated considering prying forces and bending of the bolts. Results for all T-stubs used in this parametric study are presented in Annex-III. Eurocode calculations for different failure modes is presented in Annex-IV

6.3.5. Influence of geometric properties on T-Stubs

This section explains the variation of different T-stub properties by varying end plate thickness and distance between the bolts. (Figure 70) explains the variation of the different failure modes for a T-stub with end plate thickness of 10mm on varying center to center distance between the bolts.

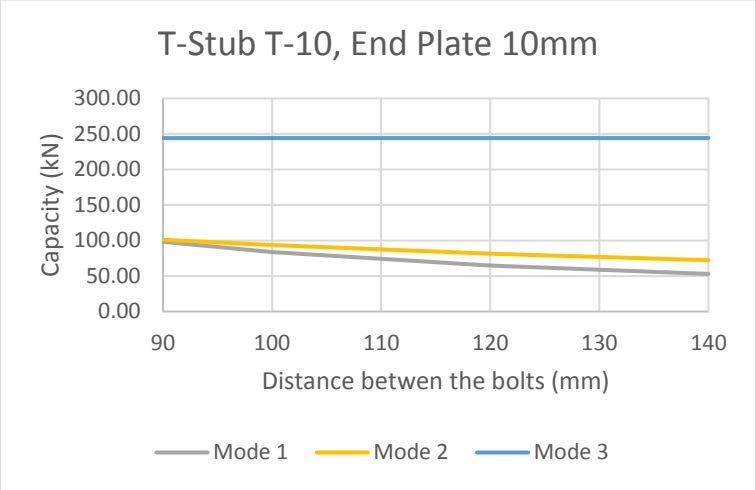

Figure 70. Failure mode variation on distance between the bolts

The figure shows the effect of varying distance between the bolts on different failure modes. Mode 3 has no effect on increasing the distance between the bolts while the mode 1 and mode 2 shows a reduction in the overall capacity by increasing the distance between the bolts. Increasing the bolt distance increases the ductility but has negative effect on the yield strengths of the T-stub. Increasing distance between the bolts require more material yet it has negative effect on the yield strength of the T-stub. It is also important to note that the effect on the Mode 1 is much more than the effect on the mode 2 by varying the distance between the bolts. Results for remaining T-stubs is presented in Annex-V.

(Figure 71) explains the effect of end plates thicknesses on different failure modes. The center to center distance between the bolts is 120mm, rest of the dimensions are kept same and behavior is studied by varying end plate thickness of the T-Stub.

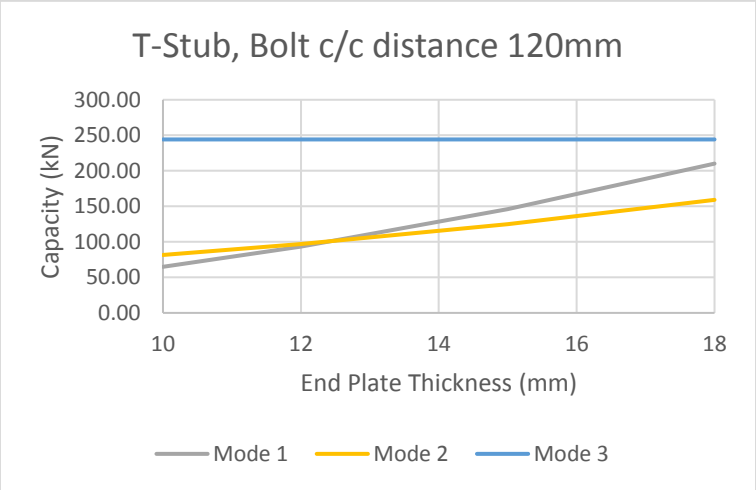

Figure 71.Failure mode variation on end plate thickness

Increasing end-plate thickness has no effect on mode 3 while for mode 1 and mode 2 yeild capacities increases with increasing end-plate thickness. Hence the failure mode changes from mode 1 to ultimately mode 3 by keep on increasing the end plate thickness. For end plate thickness of 10mm failure mode 1 is governing and there is a transition from failure mode 1 to failure mode 2 between end plate thickness of 12mm and 13mm. the overall increase in axial capacities is observed by increasing the end plate thickness. Results for remaining end plate thicknesses is presented in Annex-VI

Ultimate capacity of T-stub, factors effecting the ultimate capacity and how to calculate the maximum ultimate capacity a T-stub prior to fracture for mode 1 and mode 2 are very important parameters from robustness point of view. (Figure 72) explains the variation of ultimate force, bolt force, praying force and bending moment in the bolt for varying distance between the bolts for an end plate thickness of 10mm

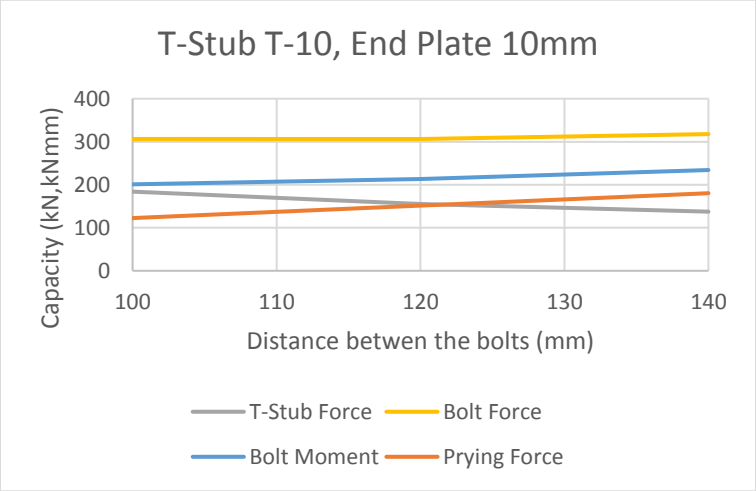

Figure 72.Variation of T-stub force and Bolt behavior on distance between the bolts

Increasing the distance between the bolts results in decrease in the ultimate capacity of the T-stub while no significant difference is observed in the bolt force prior to failure. The reason of the reduction in the ultimate capacity of the T-stub can be explained from bending moment in the bolts. With the increase in the distance between the bolts the bending of the bolts increases resulting in axial force and bending moment interaction of the bolts causing reduction of the ultimate T-stub capacity. The increase in prying forces is also observed with the increase in the distance between the bolts. This increase in the prying forces is because of the increased bending of the endplates due to enhanced ductility of the T-stubs.

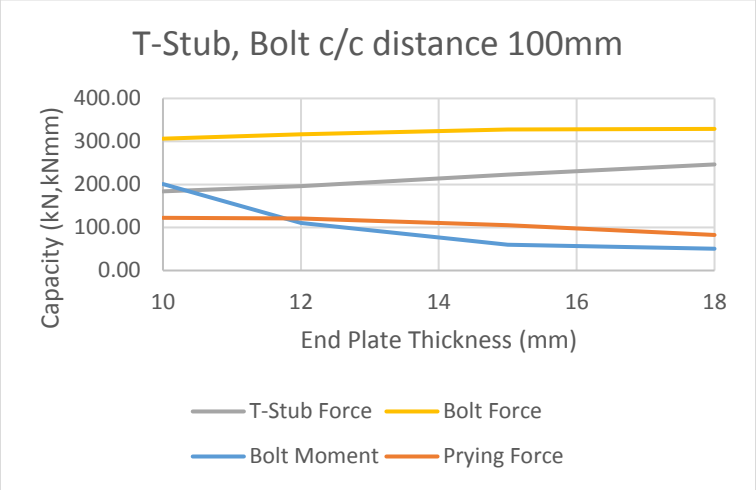

Figure 73. Variation of T-stub force and Bolt behavior on end plate thickness

(Figure 73) shows increase in axial capacities of T-stub by increasing the end plate thicknesses while the force in the bolts remain the same no matter what the endplate thickness is. Increase in axial capacities is because of the reduction in bending of the bolts. By increasing endplate thickness, reduction in bending moment of the bolts is observed which results in increased axial capacities because of the fact that overall axial bending interaction results in high axial bolt strength. The decrease in the prying force is also observed due to reduced bending of the endplate which is in turn because of the reduced ductility of the T-Stub.

Other important parameters are strength, stiffness and ductility of T-stub. A good connection should have high ductility, stiffness and large axial strength to prevent progressive collapse. (Figure 74) explains the behavior of these properties on varying distances between the bolts.

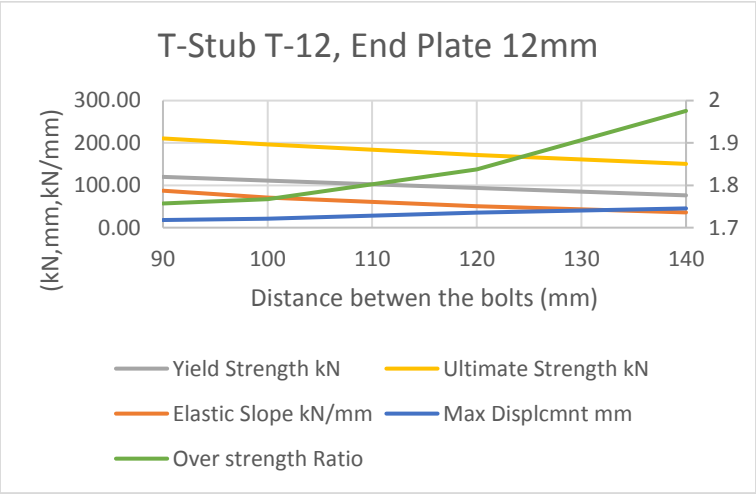

Figure 74. Variation of T-stub parameters on distance between the bolts

This graph shows all the important parameters that have influence on changing the distance between the bolts. This graph explains the strength, stuffiness and ductility in terms of ultimate strength, elastic slope and maximum displacement between the end plates before failure. By increasing the distance between the bolts the yield strength decreases. The reduction in ultimate capacity is also observed by increasing the distance between the bolts which is because of the large bending moments and slight increase in the axial forces in the bolts prior to failure. The reduction in the elastic slope is observed which, an indicator of stiffness. Hence increasing distance between the bolts would result in decrease in the initial stiffness and increase in the ductility as increasing distance between the bolts results in increase in the maximum displacement of the T-stub before failure. The over strength ratio is an important parameter showing the additional reserve capacity T-stub macro-component has beyond its yield point. The vertical secondary scale on the right of the graph shows the over strength ratio values. The graph shows increase in the reserve capacity by increasing the distance between the bolts.

(Figure 75) explains the same parameters by varying the end plate thicknesses of the T-stub and keeping the distance between the bolts constant.

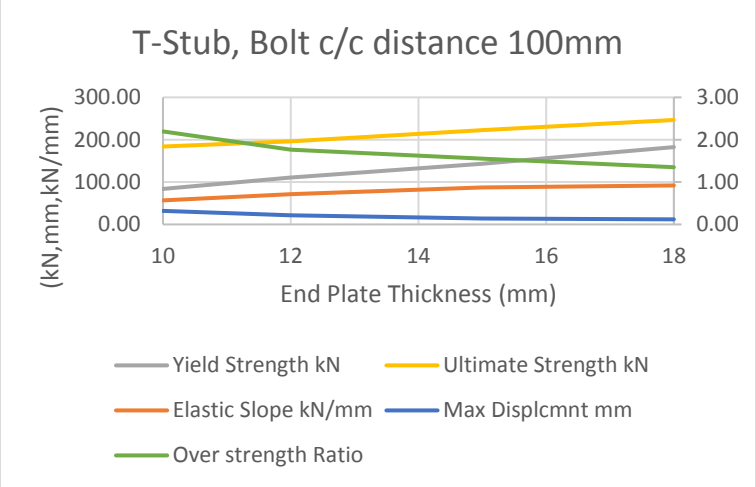

Figure 75. Variation of T-stub force and Bolt behavior on end plate thickness

The figure shows increase in the yield strength and ultimate strength of the T-stub macro-component by increasing the end plate thickness. The increase in the elastic slope is also observed which indicates high elastic initial stiffness. A decrease in the trend of maximum displacement prior to failure is observed indicating decreased ductility. Over strength ratio which is an indicator of the reserve capacity of the T-stub macro-component also shows a decrease trend by increasing end plate thickness of the T-Stub. Results for the rest of the T-stubs are presented in Annex-VII

7. CONCLUSIONS AND RECOMMENDATIONS

7.1. Conclusions

Within the research framework of CODEC project (Structural conception and collapse control performance based design of multistory structures under accidental actions), the aim of the thesis was to investigate the behavior of T-stub macro-components. For this purpose, extensive experimental testing and advanced numerical finite element investigations were carried out.

- Experimental program to study the behavior of T-stub macro-component under different loading conditions.
- Calibration of material model based on tensile data.
- Calibration of the T-stub macro-components with End plate thickness ranging from 10mm to 18mm and distance between the bolts ranging from 90mm to 140mm.
- Parametric study for the investigation of several parameters (end plate thickness, distance between the bolts) to study the influence on strength, stiffness and ductility.

The experimental program gives detailed insight about the post yield behavior of the T-stub micro-component with different endplate thickness and distance between the bolts. The experimental tests revealed reserve capacities in terms of ductility and ultimate capacity for ductile failure modes. The experimental tests also showed reduction in ultimate capacity and significant increase in ductility by increasing the distance between the bolts. Similar behavior was observed for different end plate thicknesses. The reduction in yield strength capacity and elastic stiffness was also observed with increasing distance between the bolts.

Material models were calibrated to be used in T-stub macro-components calibration. Calibration of material models was based on tensile test data performed in the coupons extracted from T-stub profiles. Three coupon tests were performed for each T-stub of different end plate thickness and were calibrated using finite element analysis software Abaqus. The finite element material models provide with good accuracy the actual response of the tested material samples. Following observations were made

- Material models replicate exact behavior of experiment.
- Finite element analysis results are reasonably close to experimental results showing accuracy of FEM numerical models
- The PEEQ and maximum stresses before failure were found same from that of experimental data.

T-stub macro-component numerical calibration was performed using calibrated material models and actual geometric measurements of the T-stubs. The models provide response of the T-stub with reasonably good accuracy. The calibration of T-stub macro-components with varying distance between the bolts for each end plate thickness leads to better understanding of the behavior. The numerical models were able to explain the reasons behind the reduction in yield strengths and ultimate capacities with increasing distance between the bolts. The numerical models also helped in understanding the bolt force relation with ultimate capacities, the influence of the prying force, bending of the bolts and its influence on defining the ultimate capacities of T-stubs failing in mode 1 and mode 2. Following main observations were made from the T-stub macro-component calibration in relation to increasing distance between the bolts for each endplate thickness of T-stub.

- The decrease in yield strength was observed with increasing distance between the bolts in accordance with the EN-1993-1-8 [20] formulas.
- The decrease in ultimate capacity was also observed with increasing distance between the bolts. The detailed numerical study revealed this decrease in ultimate capacity is because of the increase in bending moment of the bolts.
- For a ductile T-stub failure, Eurocodes overestimate the ultimate capacity of T-stubs ignoring the prying action and bending of the bolts. Hence for a ductile T-stub failure i.e. Mode 1 and Mode 2, a new set of formulas are required to predict the ultimate capacity of the T-stub in order to account for the reserve capacity and ductility for a robust design of structures.

Experimental program was designed with different material properties for T-stubs with different endplate thicknesses which can't be compared with each other. Parametric study was carried out in order to study the behavior of T-stubs with different endplate thicknesses. Calibrated T-stubs were used for parametric study with same material properties for all the T-stubs with different endplate thicknesses and distances between the bolts. The main outcomes from the parametric study are as following.

- For a T-stub with each endplate thickness the yield capacity for mode 1 and mode 2 decreases with the increase in the distance between the bolts and the behavior of mode 1 is more significant than mode 2 while mode 3 exhibit no change with changing the distance between the bolts of the T-stub. By keep on increasing the distance between the bolts the behavior tends to go from mode 3 to mode 1.

- For T-stub with constant distance between the bolts, increasing endplate thickness results in increase yield capacities of mode 1 and mode 2 while mode 3 capacity is independent of the endplate thickness. The behavior of T-stub moves from mode 1 to mode 3 by keep on increasing the endplate thickness while keeping other dimensions constant.
- T-stubs with endplate thickness of 10mm to 18mm and distance between the bolts ranging from 90mm to 140mm which are usually used in the steel building construction industry comes under ductile failure mode category for S235 and S355 materials and 10.9 bolt category with 16mm i.e. failure mode is either mode 1 or mode 2. Although the failure mode is ductile, the ultimate failure still results because of the fracture of the bolts. In order to improve the ultimate failure properties, numerical model suggest improving the capacity of the bolts.
- Increasing the distance between the bolts decreases the ultimate axial capacity of the T-stubs while the force in the bolts at failure almost remains the same. This decrease in the axial capacity accounts for the increase in bending of the bolts and axial-bending moment interaction causes bolts to fail prior reaching their ultimate axial capacity.
- Increasing the endplate thickness reduces the bending of the bolts which results in achieving higher axial strength of the bolts before failure, hence overall improving the ultimate capacity of the T-stub.
- Increasing the endplate thickness results in reduction of prying force while increasing the distance between the bolts results in the increase of the prying force. Prying force also has a relationship with ductility, higher the ductility of the T-Stub micro-component, larger would be the prying force resulting in reduced ultimate capacity. Hence it is important to note that ductility and ultimate capacity of the T-stub has inverse relationship with each other.
- Since all the T-stubs defined in parametric study were ultimately failing because of the fracture of the bolts, hence improving the bolts would result in improving the overall behavior of the T-stub.
- Parametric study revealed that by increasing the distance between the bolts yield strength and ultimate strength of the T-stub decreases but ductility increases similarly increasing the end plate thickness of the T-stub results in increase in the yield strength and ultimate axial strength but decreases the ductility.

- Parametric study also revealed decrease in initial stiffness and overall increase in the over strength ratio by increasing the distance between the bolts showing increased reserve capacity and ductility with increasing distance between the bolts
- Similarly increasing the endplate thickness of the T-stub macro component would increase the initial stiffness but decrease the reserve capacity and overall ductility.

7.2. Recommendations

- Increasing the distance between the bolts results in lower yield strength and lower ultimate strengths of the T-stub macro component although more material, hence overall cost is required to achieve increased distance between the bolts. Therefore increasing the distance between the bolts might not be a good choice in regions where there is no such ductility requirement e.g. non-seismic regions.
- In seismic regions or buildings prone to catastrophic events, ductility of a structure and reserve ultimate capacities before a structural member collapse is of paramount importance. Increasing distance between the bolts results increase in ductility and reserve capacity of a structural member which can be used in case of earthquakes or accidental loadings situations.
- Increasing distance between the bolts also results in the decrease of initial stiffness of T-stub macro-component which can be a positive aspect in seismic regions as decreasing the stiffness of a structure would attract less earthquake forces but would induce large drift and total displacement of the structure, so tradeoff has to be made and these studies help us to understand the behavior of joint beyond yield point, hence helping in making a wise decision.
- The behavior of the joint can be different from the T-stub macro-component as different bolts carry different share of the forces and prying forces also differ in different bolt rows for a particular joint connection. A similar study of joints is recommended to understand influence of distance between the bolts and end plate thicknesses on strength, stiffness and ductility of the joint.

REFERENCES

[1] Wikipedia, “Progressive collapse,” 2016. [Online]. Available: https://en.wikipedia.org/wiki/Progressive_collapse.

[2] BBC, “Ronan point.” [Online]. Available: news.bbc.co.uk/onthisday/hi/dates/stories/may/16/newsid_2514000/2514277.stm.

[3] Wikipedia, “Skyline Tower collapse,” 2016. [Online]. Available: https://en.wikipedia.org/wiki/Skyline_Towers_collapse.

[4] Wikipedia, “Collapse of Hotel New World,” 2016.

[5] Wikipedia, “Alfred P. Murrah Federal Building.” [Online]. Available: https://en.wikipedia.org/wiki/Alfred_P._Murrah_Federal_Building.

[6] Wikipedia, “Sampoong Department Store collapse,” 2016. [Online]. Available: https://en.wikipedia.org/wiki/Sampoong_Department_Store_collapse.

[7] FEMA, “FEMA 403 ‘World Trade Center Building Performance Study,’” 2002.

[8] F. Dinu, “Structural conception and collapse control performance based design of multistory structures under accidental actions.” [Online]. Available: www.ct.upt.ro/centre/cemsig/codec.htm.

[9] Z. Dreveny, “Behaviour of beam-to-column joints under large vertical displacements following the loss of a column,” 2014.

[10] B. Standard, “Eurocode 1 — Actions on structures —Part 1-7: General actions — Accidental actions,” vol. 3, no. February 2010, 2011.

[11] U.S. General Services Administration (GSA), “Alternate Path Analysis & Design Guidelines for Progressive Collapse Resistance,” *U.S. Gen. Serv. Adm.*, 2013.

[12] (Department of Defense) DoD, “Design of Buildings To Resist Progressive Collapse,” *Unified Facil. Criteria 4-023-03*, no. June, p. 245, 2009.

[13] ASCE 41-06, *Seismic rehabilitation of existing buildings*. 2007.

[14] a G. J. Way, *P391 Structural robustnes of Steel framed buildings*. 2011.

[15] A. A. T, “ASCE Standard 7-05 Minimum Design Loads for Buildings and Other

Structures.," 2010.

[16] B. R. Ellingwood, R. Smilowitz, D. O. Dusenberry, D. Duthinh, H. S. Lew, and N. J. Carino, "Best practices for reducing the potential for progressive collapse in buildings," *U.S. Natl. Inst. Stand. Technol. (NIST).*, p. 216, 2007.

[17] D. B. Moore, "The UK and European Regulations for Accidental Actions," in *National Workshop on Prevention of Progressive Collapse in Rosemont, III, Multihazard Mitigation Council of the National Institute of Building Sciences, Washington, DC. 2002.*, 2002.

[18] CEN, "Eurocode - Basis of structural design," *En*, vol. 3, no. December 2008, p. 89, 2002.

[19] F. Dinu, D. Dubina, I. Marginean, C. Neagu, and I. Petran, "Axial strength and deformation demands for T-stub connection components at catenary stage in the beams," in *8th International Conference on Behavior of Steel Structures in Seismic Areas*, 2015.

[20] CEN, "EN 1993-1-8 Eurocode 3: Design of steel structures - Part 1-8: Design of joints," vol. 3, 2005.

[21] J. Kim and T. Kim, "Assessment of progressive collapse-resisting capacity of steel moment frames," *J. Constr. Steel Res.*, vol. 65, no. 1, pp. 169–179, 2009.

[22] B. Yang and K. H. Tan, "Numerical analyses of steel beam-column joints subjected to catenary action," *J. Constr. Steel Res.*, vol. 70, no. January, pp. 1–11, 2012.

[23] B. Yang and K. H. Tan, "Experimental tests of different types of bolted steel beam-column joints under a central-column-removal scenario," *Eng. Struct.*, vol. 54, no. September, pp. 112–130, 2013.

[24] Y. Gong, "Ultimate tensile deformation and strength capacities of bolted-angle connections (a) End view (b) Front view," *JCSR*, vol. 100, pp. 50–59, 2014.

[25] Y. Gong, "Analysis and design for the resilience of shear connections," *Can J Civ Eng*, vol. 37, no. 12, pp. 1581–9, 2010.

[26] B. Yang and K. Hai, "Robustness of bolted-angle connections against progressive collapse : Mechanical modelling of bolted-angle connections under tension," *Eng.*

Struct., vol. 57, pp. 153–168, 2013.

[27] N. Baldassino, M. Bernardi, and R. Zandonini, "STRAIN RATE INFLUENCE ON T-STUB RESPONSE," no. mode 1, 2016.

[28] A. Abidelah, A. Bouchaïr, and D. Elddine, "Influence of the flexural rigidity of the bolt on the behavior of the T-stub steel connection," *Eng. Struct.*, vol. 81, pp. 181–194, 2014.

[29] P. Barata, J. Ribeiro, C. Rigueiro, A. Santiago, and J. Paulo, "Assessment of the T-stub joint component at ambient and elevated temperatures," *Fire Saf. J.*, vol. 70, pp. 1–13, 2014.

[30] G. Hu and M. D. Engelhardt, "Experimental investigation of steel single plate beam end connections at elevated temperatures," *Eng. Struct.*, vol. 58, pp. 141–151, 2014.

[31] Simulia, "Getting Started with Abaqus: Interactive Edition," *Get. Started with Abaqus Interact. Ed.*, p. 4.50-4.54, 2012.

[32] INSTRON, "INstron 8805." [Online]. Available: http://www.instron.us/en-us/products/testing-systems/dynamic-and-fatigue-systems/servohydraulic-fatigue/8805.

[33] NovoTechnic, "Linear Rod Type." [Online]. Available: http://www.novotechnik.com/Linear-Rod-Type/linear-rod-type.html.

[34] correlated solutions, "Digital Image Correlation with Vic-3D Quick Reference Guide," 2012.

[35] correlated solutions, "Vic 3D." [Online]. Available: http://correlatedsolutions.com/vic-3d/.

[36] INSTRON, "INSTRON." [Online]. Available: http://www.instron.com/en.

ANNEX-I

P-19 Coupon

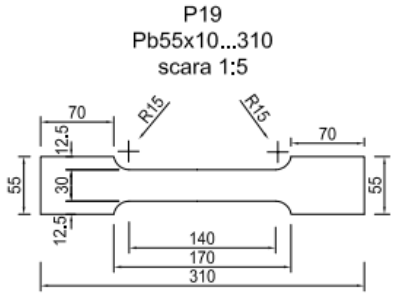

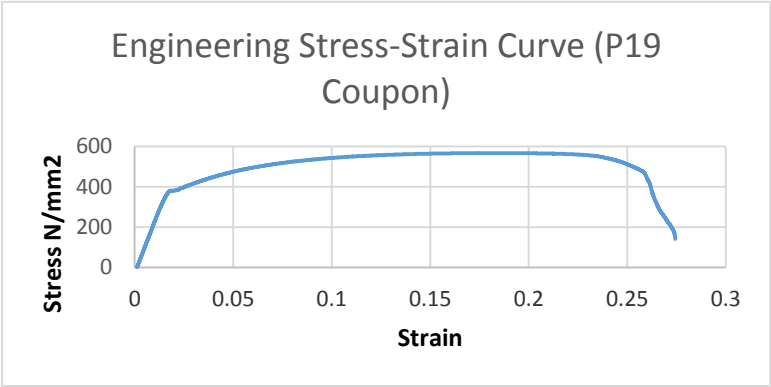

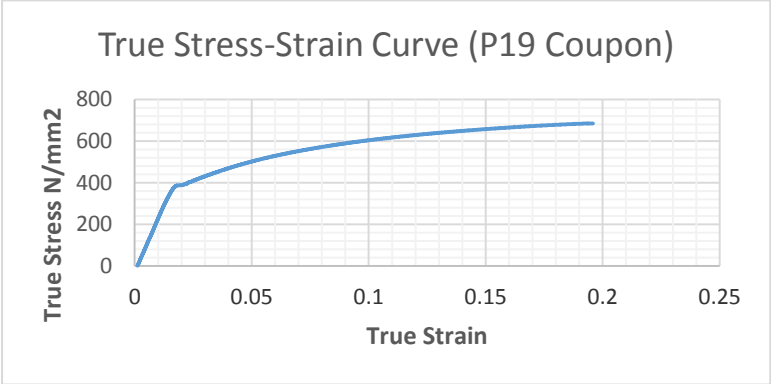

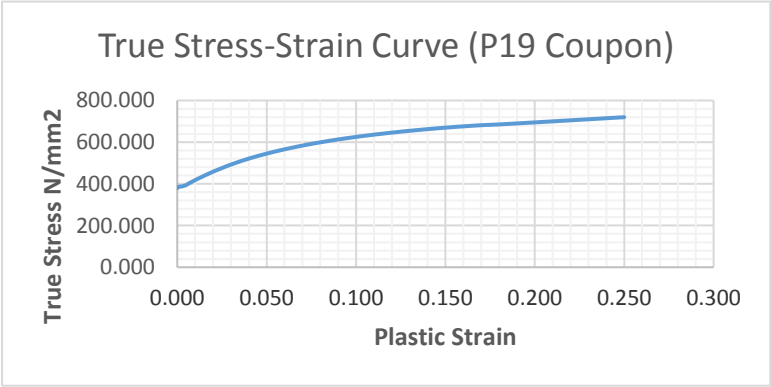

Plastic Strain	Plastic Stress
	N/mm2
0.000	379.335
0.001	386.124
0.002	387.235
0.003	387.989
0.004	391.353
0.005	393.966
0.008	407.748
0.015	439.652
0.024	471.864
0.032	499.655
0.041	523.240
0.049	543.328
0.057	560.882
0.066	576.360
0.074	590.138
0.082	602.368
0.090	613.271
0.098	623.087
0.106	632.033
0.115	640.775
0.123	648.840
0.130	654.841
0.138	660.919
0.146	667.172
0.154	672.210
0.162	677.217
0.171	681.911
0.179	684.709
0.200	695.000
0.250	720.000
0.300	750.000
0.400	790.000
0.500	830.000
0.600	860.000

P-19 Coupon

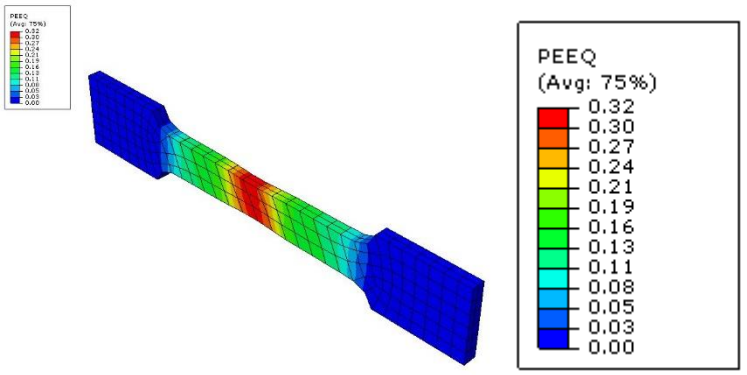
PEEQ
(Avg: 75%)
0.32
0.30
0.27
0.24
0.21
0.19
0.16
0.13
0.11
0.08
0.05
0.03
0.00

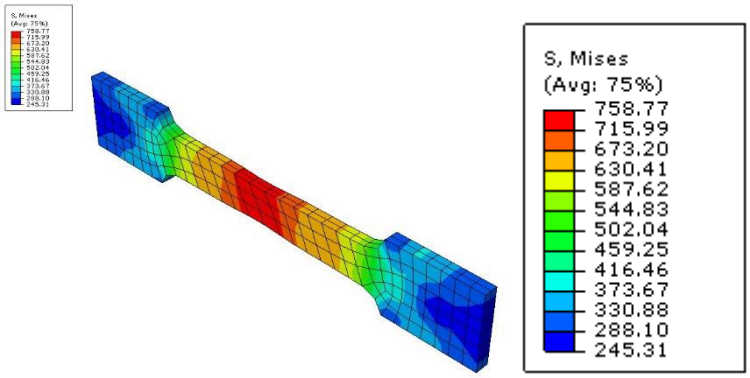
S, Mises
(Avg: 75%)
758.77
715.99
673.20
630.41
587.62
544.83
502.04
459.25
416.46
373.67
330.88
288.10
245.31

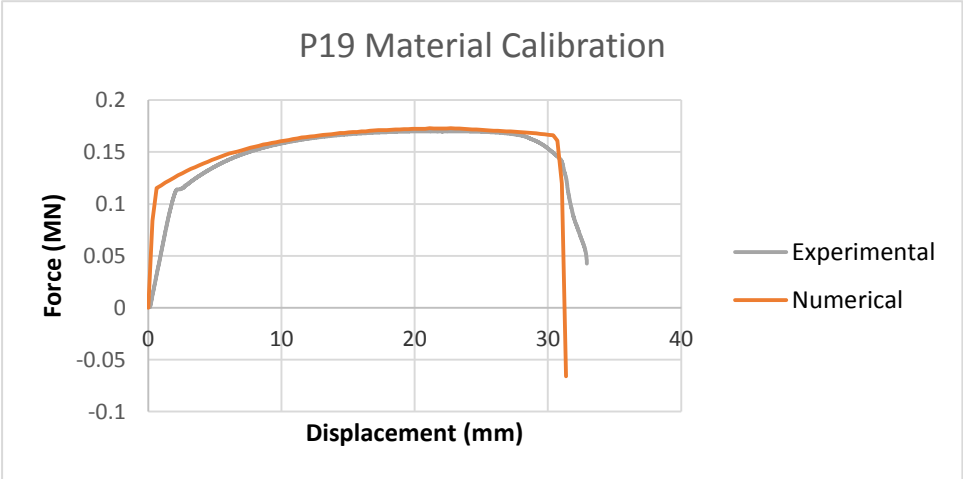
P19 Material Calibration
Force (MN)
0.2
0.15
0.1
0.05
0
-0.05
-0.1
0
10
20
30
40
Displacement (mm)
Experimental
Numerical

P-20 Coupon

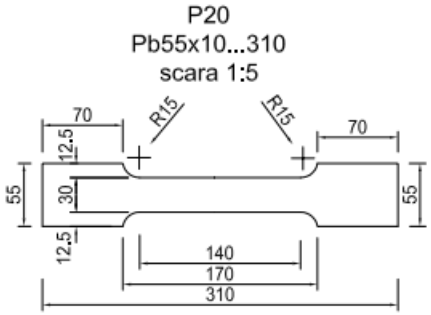

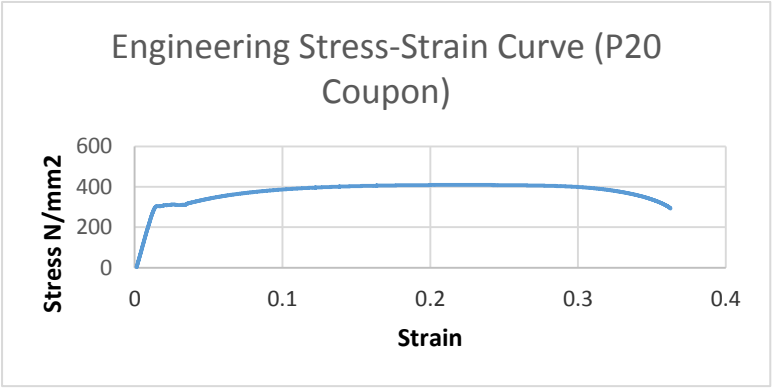

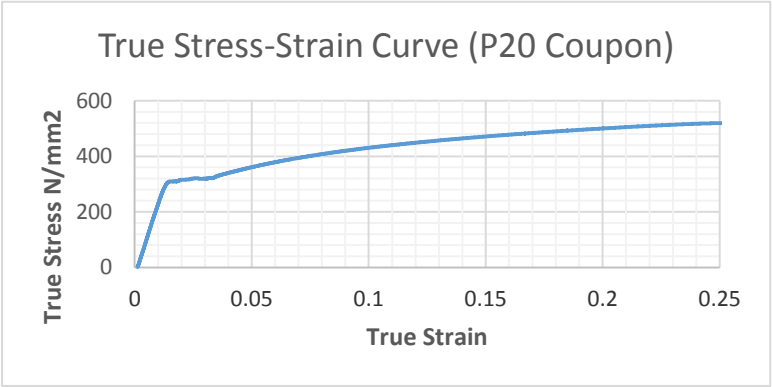

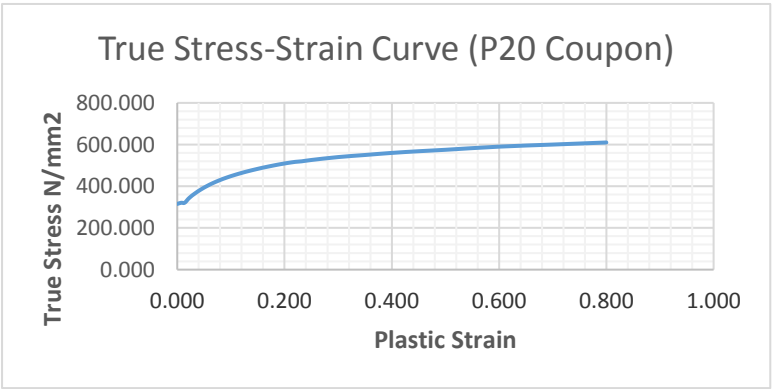

Plastic Strain	Plastic Stress
	N/mm2
0.000	315.274
0.007	320.749
0.014	321.098
0.022	343.954
0.033	365.961
0.044	385.051
0.055	401.187
0.065	413.795
0.078	428.410
0.092	441.912
0.107	454.537
0.122	465.152
0.134	473.555
0.147	481.936
0.158	488.142
0.172	496.016
0.185	502.494
0.194	506.548
0.197	507.912
0.202	510.352
0.208	512.728
0.220	516.914
0.232	519.708
0.250	526.000
0.300	540.000
0.350	550.000
0.400	560.000
0.450	568.000
0.500	575.000
0.600	590.000
0.700	600.000
0.800	610.000

P-20 Coupon

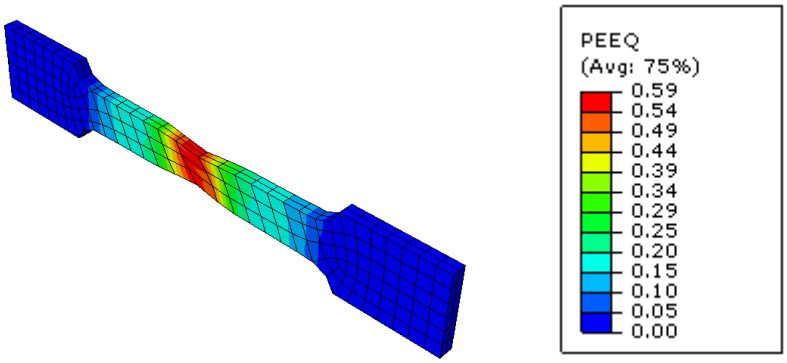
PEEQ
(Avg: 75%)
0.59
0.54
0.49
0.44
0.39
0.34
0.29
0.25
0.20
0.15
0.10
0.05
0.00

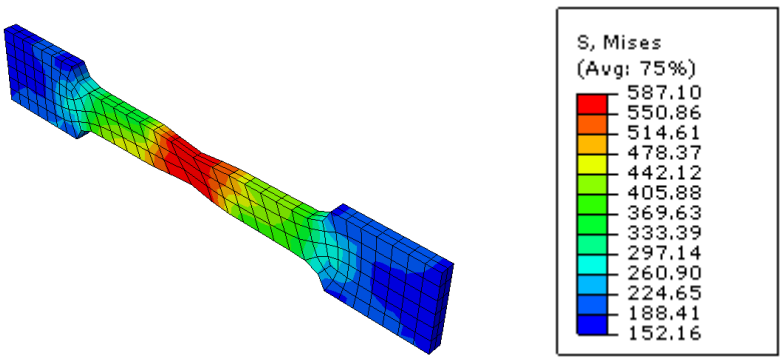
S, Mises
(Avg: 75%)
587.10
550.86
514.61
478.37
442.12
405.88
369.63
333.39
297.14
260.90
224.65
188.41
152.16

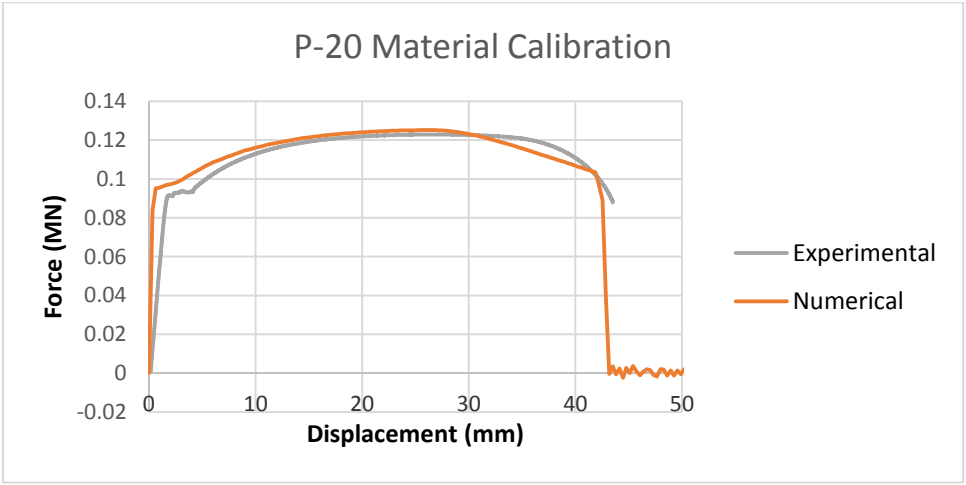
P-20 Material Calibration
0.14
0.12
0.1
0.08
0.06
0.04
0.02
0
-0.02
Force (MN)
0
10
20
30
40
50
Displacement (mm)
Experimental
Numerical

P-21 Coupon

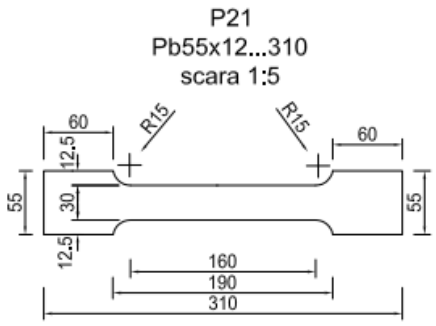

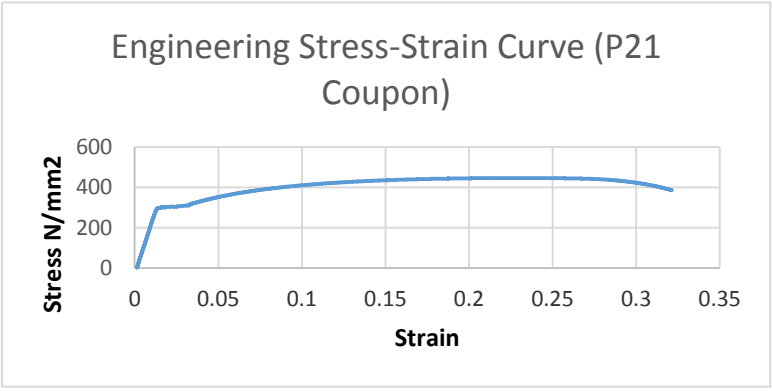

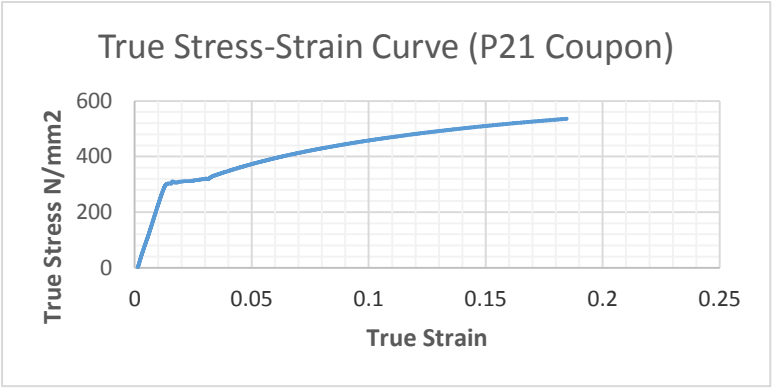

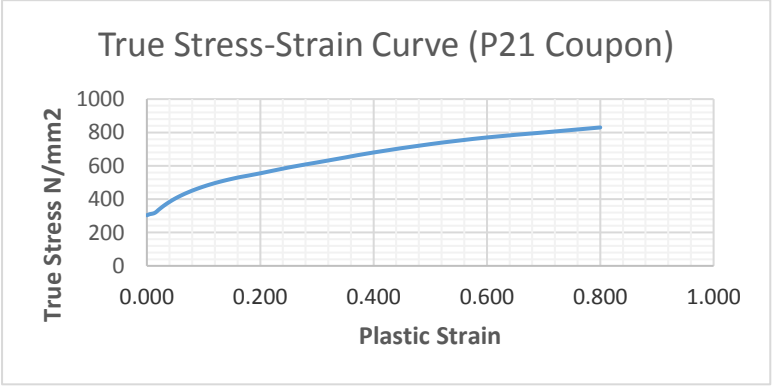

Plastic Strain	Plastic Stress
	N/mm2
0.000	303.3862
0.005	310.0053
0.010	313.1091
0.015	319.8377
0.020	334.1687
0.025	347.9684
0.030	360.8924
0.055	413.0037
0.060	421.4558
0.065	429.5102
0.070	437.1119
0.075	444.2837
0.080	451.1493
0.085	457.6637
0.090	463.9778
0.095	469.9539
0.130	505.6035
0.135	509.8467
0.140	514.0258
0.145	518.0216
0.150	521.948
0.155	525.7231
0.160	529.2906
0.165	532.8653
0.2	555
0.25	590
0.3	620
0.35	650
0.4	680
0.5	730
0.6	770
0.7	800
0.8	830

P-21 Coupon

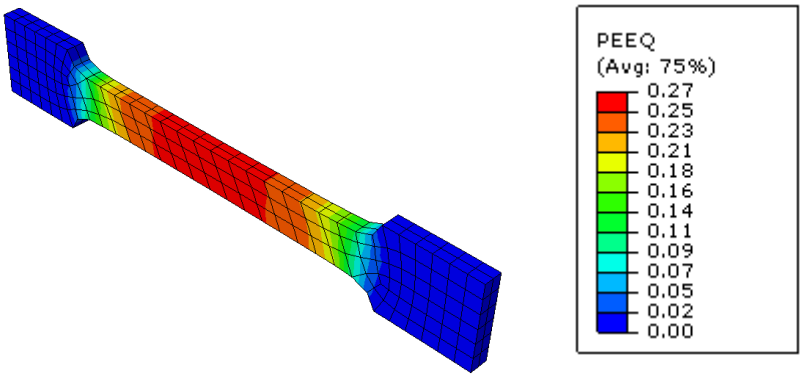
PEEQ
(Avg: 75%)
0.27
0.25
0.23
0.21
0.18
0.16
0.14
0.11
0.09
0.07
0.05
0.02
0.00

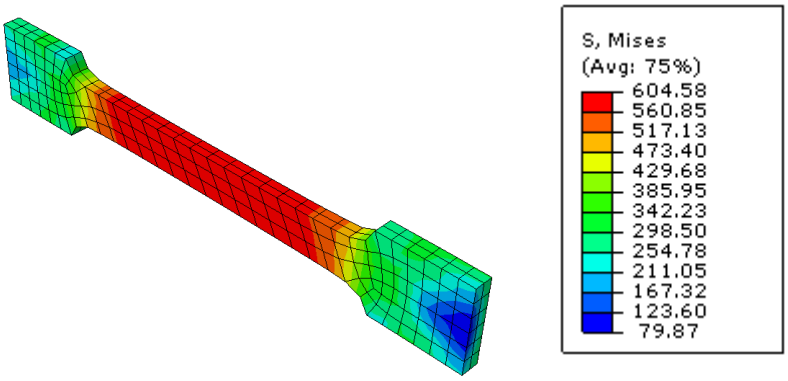
S, Mises
(Avg: 75%)
604.58
560.85
517.13
473.40
429.68
385.95
342.23
298.50
254.78
211.05
167.32
123.60
79.87

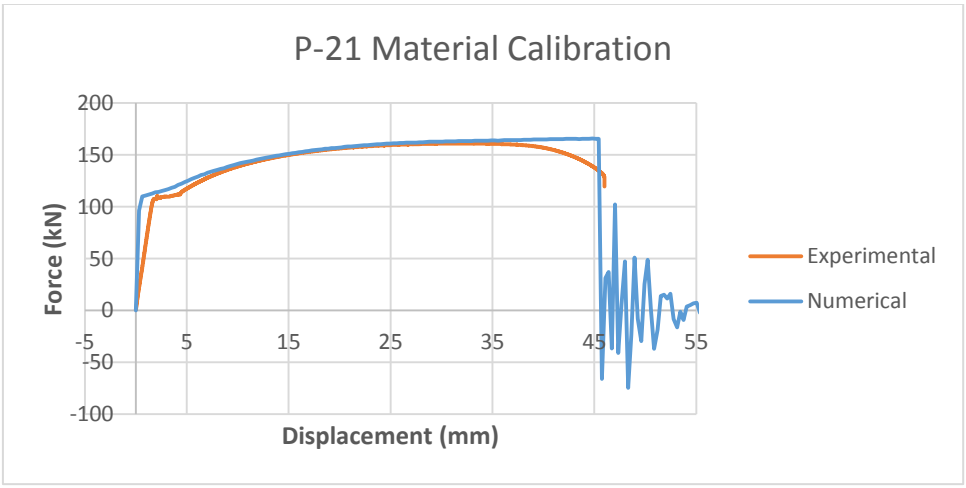
P-21 Material Calibration
200
150
100
50
0
-50
-100
-5
5
15
25
35
45
55
Force (kN)
Displacement (mm)
Experimental
Numerical

P-22 Coupon

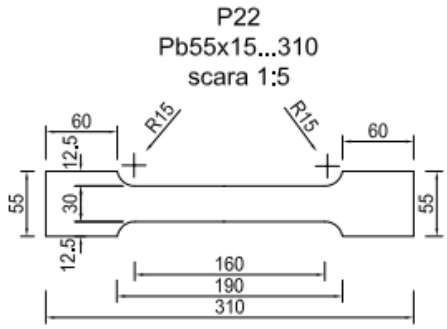

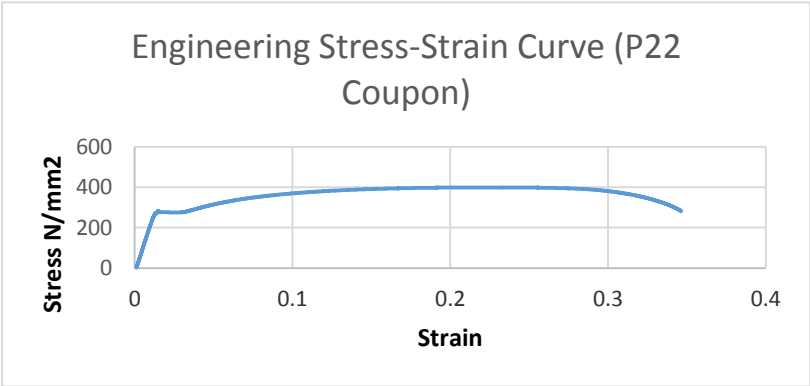

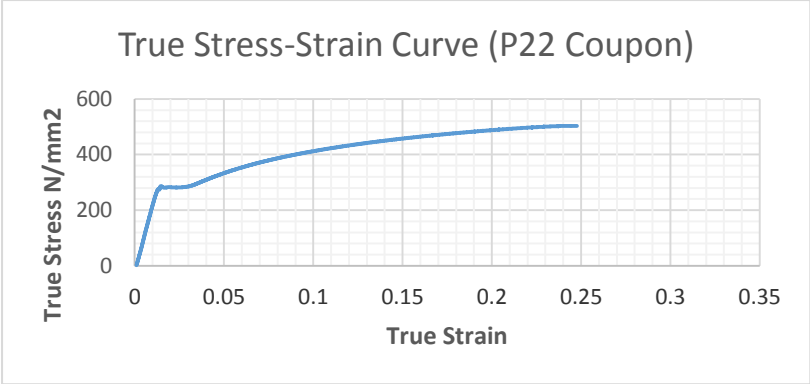

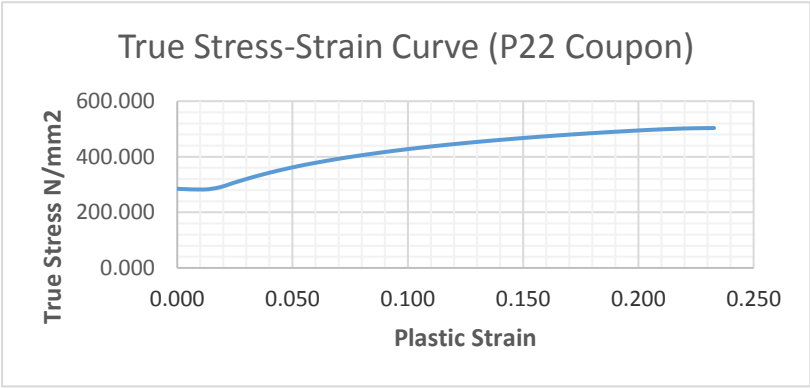

Plastic Strain	Plastic Stress
	N/mm
0.000	284.787
0.011	282.122
0.018	289.886
0.023	303.200
0.030	320.994
0.037	336.816
0.044	350.981
0.052	364.894
0.059	376.077
0.069	391.781
0.078	403.053
0.087	413.251
0.094	421.856
0.105	432.191
0.115	441.479
0.124	448.838
0.134	456.085
0.144	463.595
0.155	470.477
0.166	477.526
0.178	483.861
0.189	489.625
0.200	494.797
0.212	499.187
0.222	502.184
0.233	503.345
0.300	530.000
0.350	550.000
0.400	570.000
0.500	600.000
0.600	630.000
0.700	660.000
0.800	690.000

P-22 Coupon

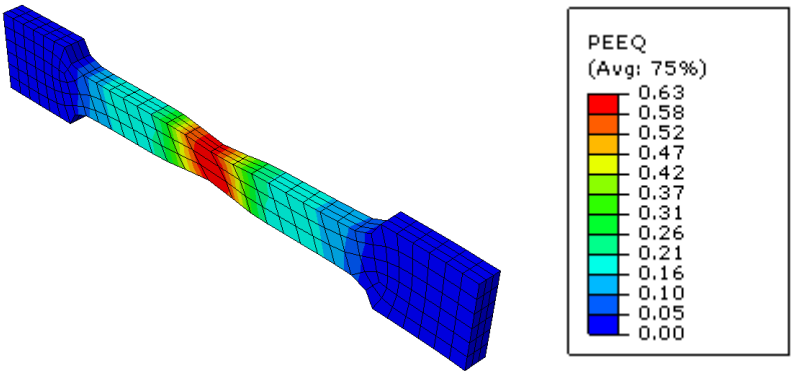
PEEQ
(Avg: 75%)
0.63
0.58
0.52
0.47
0.42
0.37
0.31
0.26
0.21
0.16
0.10
0.05
0.00

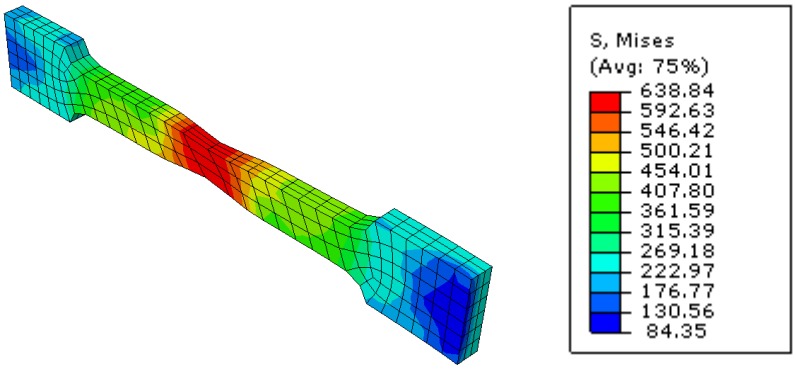
S, Mises
(Avg: 75%)
638.84
592.63
546.42
500.21
454.01
407.80
361.59
315.39
269.18
222.97
176.77
130.56
84.35

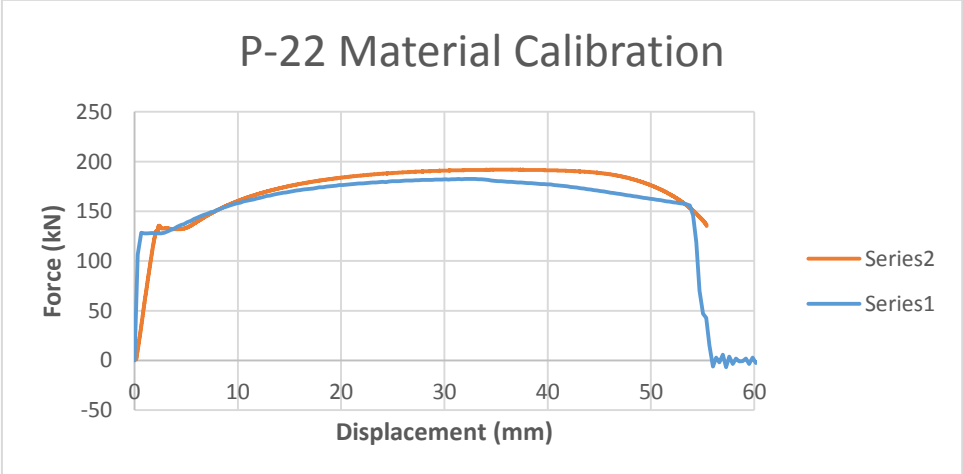
P-22 Material Calibration
250
200
150
100
50
0
-50
Force (kN)
0
10
20
30
40
50
60
Displacement (mm)
Series2
Series1

P-23 Coupon

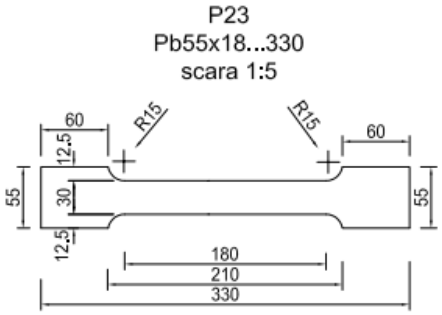

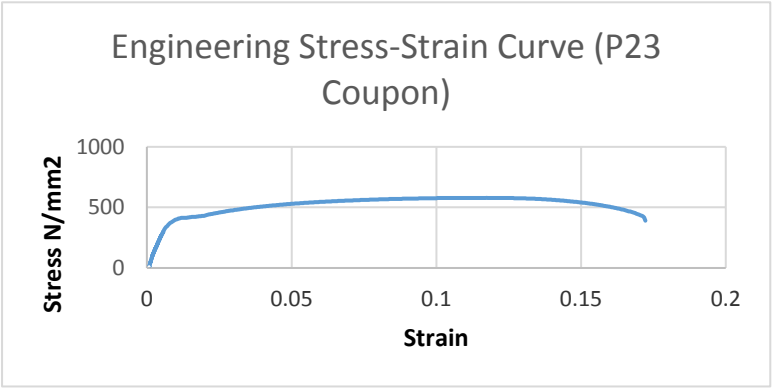

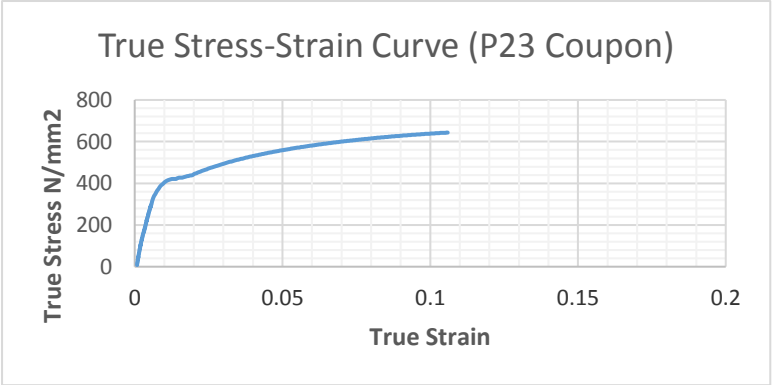

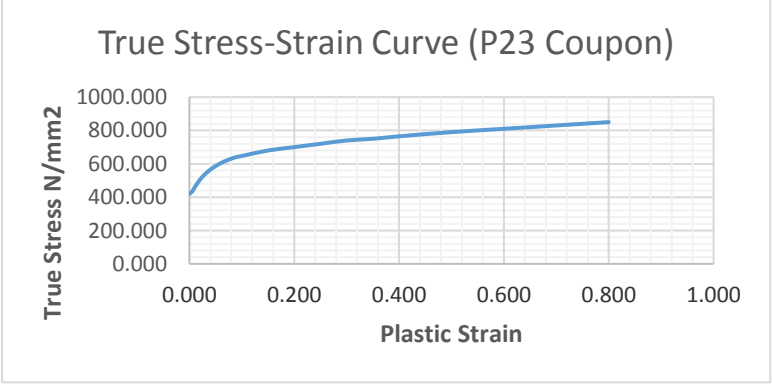

Plastic Strain	Plastic stress
	N/mm2
0.000	420.451
0.001	421.666
0.002	426.570
0.004	430.325
0.006	437.955
0.009	451.341
0.012	469.550
0.019	500.357
0.026	525.494
0.033	546.393
0.039	563.874
0.046	578.696
0.059	603.282
0.072	622.146
0.085	636.441
0.092	642.000
0.100	647.000
0.150	680.000
0.200	700.000
0.250	720.000
0.300	740.000
0.350	750.000
0.400	765.000
0.500	790.000
0.600	810.000
0.700	830.000
0.800	850.000

P-23 Coupon

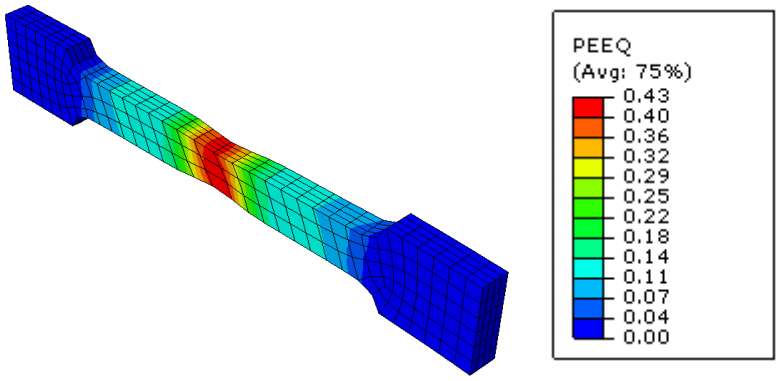
PEEQ
(Avg: 75%)
0.43
0.40
0.36
0.32
0.29
0.25
0.22
0.18
0.14
0.11
0.07
0.04
0.00

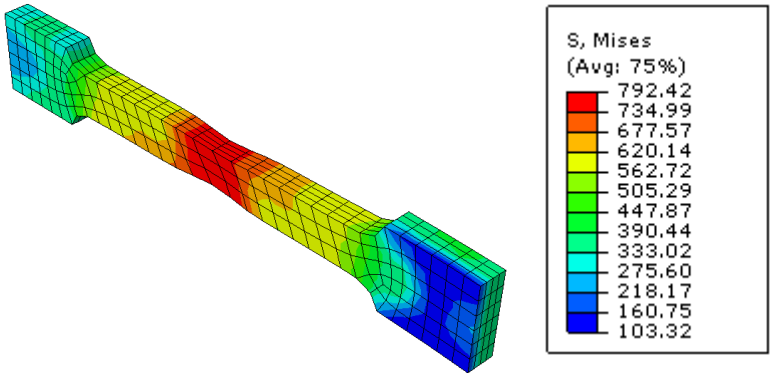
S, Mises
(Avg: 75%)
792.42
734.99
677.57
620.14
562.72
505.29
447.87
390.44
333.02
275.60
218.17
160.75
103.32

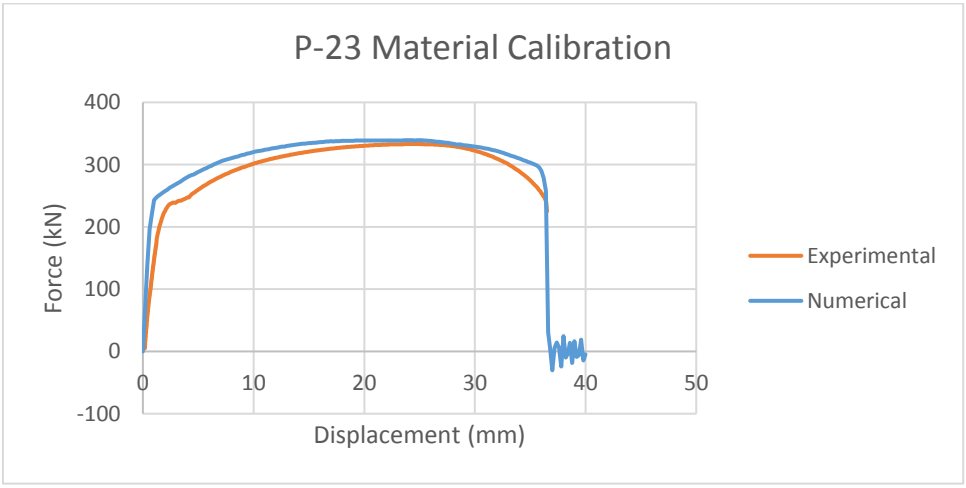
P-23 Material Calibration
400
300
200
100
0
-100
Force (kN)
0
10
20
30
40
50
Displacement (mm)
Experimental
Numerical

ANNEX-II

Following table explains the testing scheme under CODEC program. Experimental test data results of T-stubs of 10mm and 12 mm end plate thickness were already available before starting this dissertation work while T-stubs of 15mm and 18mm endplate thickness were tested as a part of this dissertation under CODEC program.

Varianta S235		2	3	4	5	7	8	9	10	12	13	14
t	10	X	X	X	X	X	X	X	X			
	12									X	X	X
	15											
	18											
c	70											
	90	X				X				X		
	100		X				X				X	
	120			X				X				X
	140				X				X			
M.16	8.8	X	X	X	X					X	X	X
	10.9					X	X	X	X			
M20	8.8											
	10.9											
Mode 1		101	87	67	55	101	87	67	55	144	123	95
Mode 2		87	81	71	63	102	95	83	73	106	98	85
Mode 3		181	181	181	181	244	244	244	244	181	181	181

Varianta S235		15	17	18	19	20	22	23	24	25	27	28	29	30	34	35	39	40
t	10																	
	12	X	X	X	X	X												
	15						X	X	X	X	X	X	X	X				
	18														X	X	X	X
c	70																	
	90		X				X				X							
	100			X				X				X						
	120				X				X				X		X		X	
	140	X				X				X				X		X		X
M.16	8.8	X					X	X	X	X					X	X		
	10.9		X	X	X	X					X	X	X	X			X	X
M20	8.8																	
	10.9																	
Mode 1		77	144	123	95	77	202	173	134	109	202	173	134	109	294	240	294	240
Mode 2		76	121	112	98	87	131	122	106	94	147	136	118	105	192	170	204	181
Mode 3		181	244	244	244	244	181	181	181	181	244	244	244	244	181	181	244	244

ANNEX-III

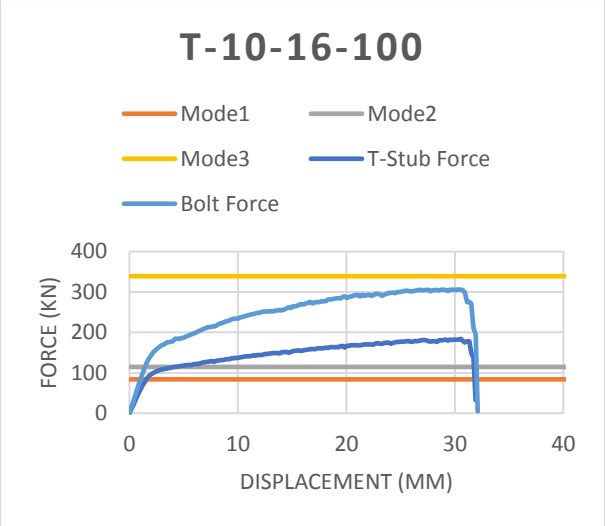
T-10-16-100
Mode1
Mode2
Mode3
T-Stub Force
Bolt Force
FORCE (KN)
400
300
200
100
0
0
10
20
30
40
DISPLACEMENT (MM)

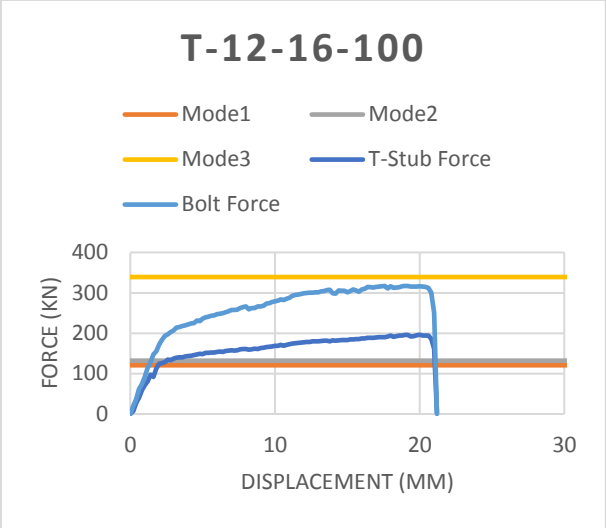
T-12-16-100
Mode1
Mode2
Mode3
T-Stub Force
Bolt Force
FORCE (KN)
400
300
200
100
0
0
10
20
30
DISPLACEMENT (MM)

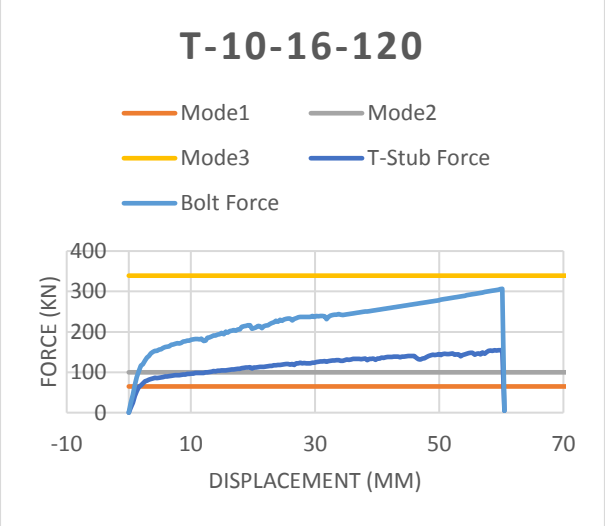
T-10-16-120
Mode1
Mode2
Mode3
T-Stub Force
Bolt Force
FORCE (KN)
400
300
200
100
0
-10
10
30
50
70
DISPLACEMENT (MM)

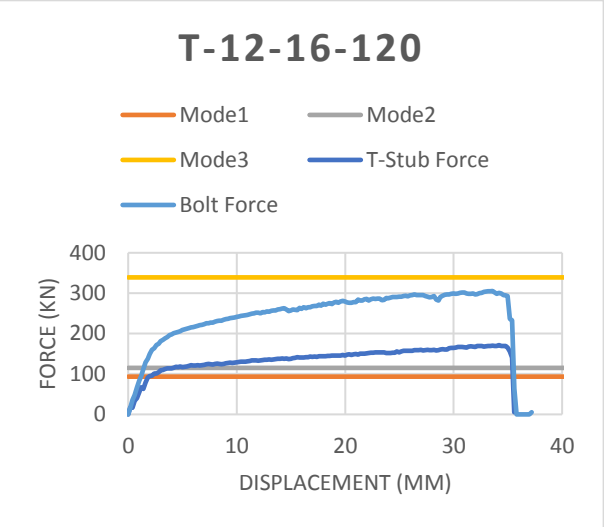
T-12-16-120
Mode1
Mode2
Mode3
T-Stub Force
Bolt Force
FORCE (KN)
400
300
200
100
0
0
10
20
30
40
DISPLACEMENT (MM)

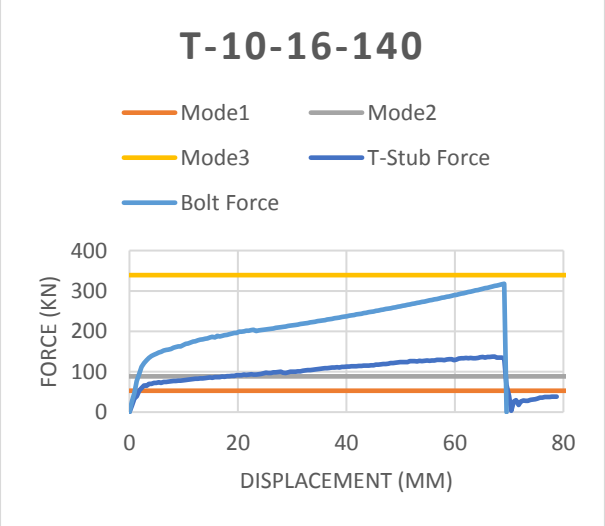
T-10-16-140
Mode1
Mode2
Mode3
T-Stub Force
Bolt Force
FORCE (KN)
400
300
200
100
0
0
20
40
60
80
DISPLACEMENT (MM)

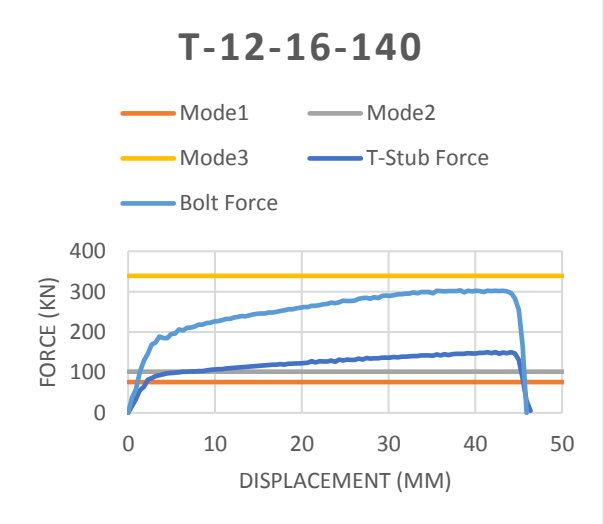
T-12-16-140
Mode1
Mode2
Mode3
T-Stub Force
Bolt Force
FORCE (KN)
400
300
200
100
0
0
10
20
30
40
50
DISPLACEMENT (MM)

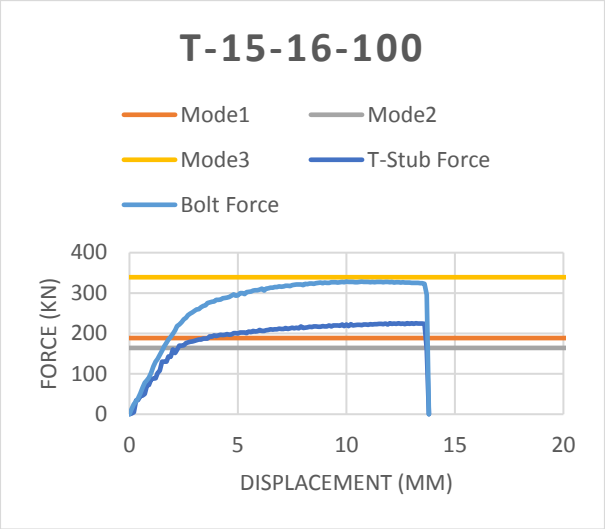
T-15-16-100
Mode1
Mode2
Mode3
T-Stub Force
Bolt Force
FORCE (KN)
400
300
200
100
0
0
5
10
15
20
DISPLACEMENT (MM)

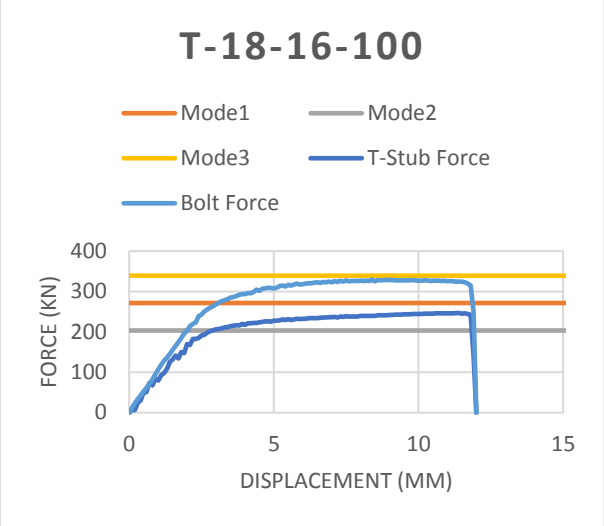
T-18-16-100
Mode1
Mode2
Mode3
T-Stub Force
Bolt Force
FORCE (KN)
400
300
200
100
0
0
5
10
15
DISPLACEMENT (MM)

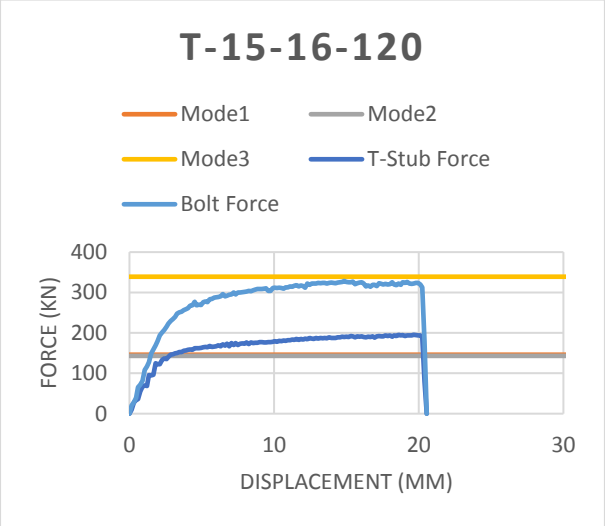
T-15-16-120
Mode1
Mode2
Mode3
T-Stub Force
Bolt Force
FORCE (KN)
400
300
200
100
0
0
10
20
30
DISPLACEMENT (MM)

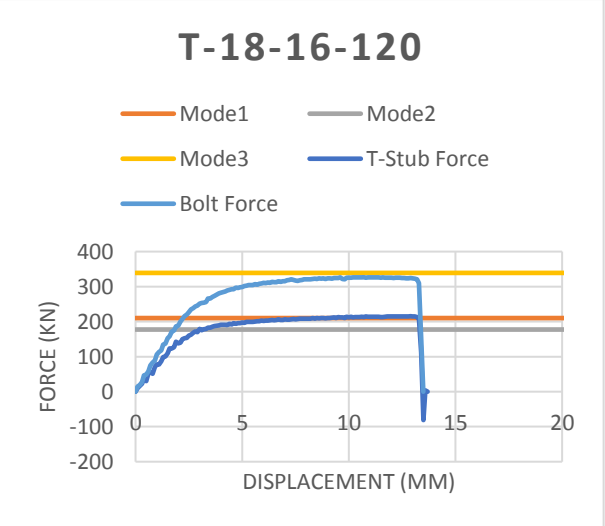
T-18-16-120
Mode1
Mode2
Mode3
T-Stub Force
Bolt Force
FORCE (KN)
400
300
200
100
0
-100
-200
0
5
10
15
20
DISPLACEMENT (MM)

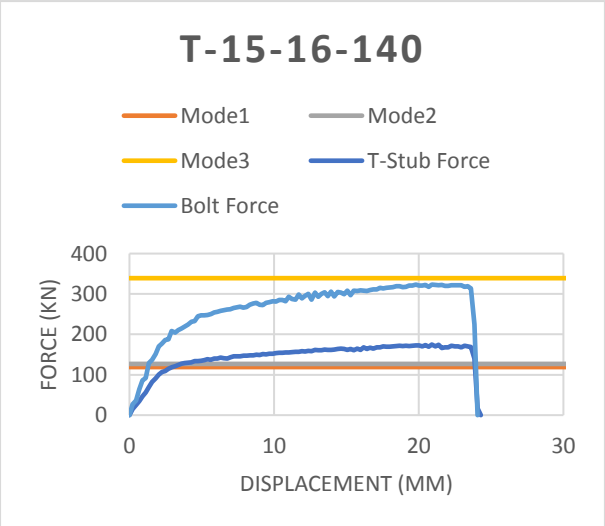
T-15-16-140
Mode1
Mode2
Mode3
T-Stub Force
Bolt Force
FORCE (KN)
400
300
200
100
0
0
10
20
30
DISPLACEMENT (MM)

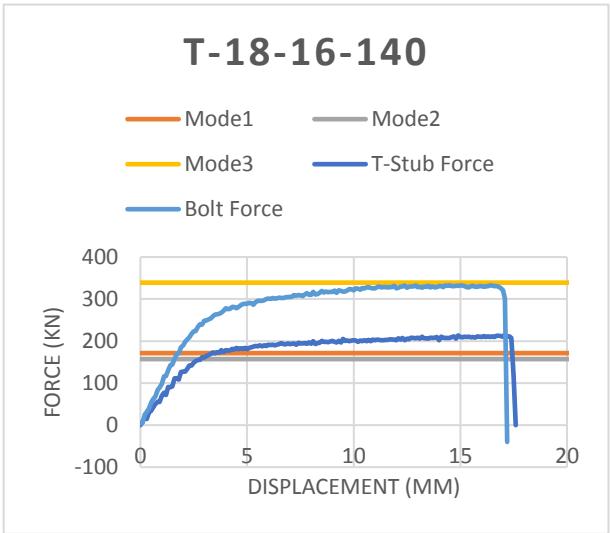
T-18-16-140
Mode1
Mode2
Mode3
T-Stub Force
Bolt Force
FORCE (KN)
400
300
200
100
0
-100
0
5
10
15
20
DISPLACEMENT (MM)

ANNEX-IV

Bolt 8.8																							
T-Stub				Leff1	Leff2	tf	fyf	m	n	fub	#no.	As	dw	ɣm0	ɣm2	Mpl1Rd	Mpl2Rd	Ft.Rd	mode1	mode2	mode3		
				mm	mm	mm	Mpa	mm	mm	Mpa						kNm	kNm	kN	kN	kN	kN		
T	10	16	90	90	90	10	300	33	30	800	2	157	26.75	1	1.25	0.675	0.675	90.432	98.14	85.92	180.86	Mode2	85.92
T	10	16	100	90	90	10	300	38	30	800	2	157	26.75	1	1.25	0.675	0.675	90.432	83.81	79.60	180.86	Mode2	79.60
T	10	16	120	90	90	10	300	48	30	800	2	157	26.75	1	1.25	0.675	0.675	90.432	64.86	69.40	180.86	Mode1	64.86
T	10	16	140	90	90	10	300	58	30	800	2	157	26.75	1	1.25	0.675	0.675	90.432	52.90	61.51	180.86	Mode1	52.90
T	12	16	90	90	90	12	300	33	30	800	2	157	26.75	1	1.25	0.972	0.972	90.432	141.32	104.78	180.86	Mode2	104.78
T	12	16	100	90	90	12	300	38	30	800	2	157	26.75	1	1.25	0.972	0.972	90.432	120.68	97.07	180.86	Mode2	97.07
T	12	16	120	90	90	12	300	48	30	800	2	157	26.75	1	1.25	0.972	0.972	90.432	93.40	84.63	180.86	Mode2	84.63
T	12	16	140	90	90	12	300	58	30	800	2	157	26.75	1	1.25	0.972	0.972	90.432	76.18	75.01	180.86	Mode2	75.01
T	15	16	90	90	90	15	300	33	30	800	2	157	26.75	1	1.25	1.519	1.519	90.432	220.82	139.49	180.86	Mode2	139.49
T	15	16	100	90	90	15	300	38	30	800	2	157	26.75	1	1.25	1.519	1.519	90.432	188.57	129.23	180.86	Mode2	129.23
T	15	16	120	90	90	15	300	48	30	800	2	157	26.75	1	1.25	1.519	1.519	90.432	145.94	112.67	180.86	Mode2	112.67
T	15	16	140	90	90	15	300	58	30	800	2	157	26.75	1	1.25	1.519	1.519	90.432	119.03	99.86	180.86	Mode2	99.86
T	18	16	90	90	90	18	300	33	30	800	2	157	26.75	1	1.25	2.187	2.187	90.432	317.98	181.92	180.86	Mode3	180.86
T	18	16	100	90	90	18	300	38	30	800	2	157	26.75	1	1.25	2.187	2.187	90.432	271.54	168.54	180.86	Mode2	168.54
T	18	16	120	90	90	18	300	48	30	800	2	157	26.75	1	1.25	2.187	2.187	90.432	210.16	146.94	180.86	Mode2	146.94
T	18	16	140	90	90	18	300	58	30	800	2	157	26.75	1	1.25	2.187	2.187	90.432	171.41	130.24	180.86	Mode2	130.24

	Bolt 10.9																						
T-Stub				Leff1	Leff2	tf	fyf	m	n	fub	#no.	As	dw	γm0	γm2	Mpl1Rd	Mpl2Rd	Ft.Rd	mode1	mode2	mode3		
				mm	mm	mm	Mpa	mm	mm	Mpa						kNm	kNm	kN	kN	kN	kN		
T	10	16	90	90	90	10	300	33	30	1080	2	157	26.75	1	1.25	0.675	0.675	122.0832	98.14	100.99	244.17	Mode1	98.14
T	10	16	100	90	90	10	300	38	30	1080	2	157	26.75	1	1.25	0.675	0.675	122.0832	83.81	93.57	244.17	Mode1	83.81
T	10	16	120	90	90	10	300	48	30	1080	2	157	26.75	1	1.25	0.675	0.675	122.0832	64.86	81.57	244.17	Mode1	64.86
T	10	16	140	90	90	10	300	58	30	1080	2	157	26.75	1	1.25	0.675	0.675	122.0832	52.90	72.30	244.17	Mode1	52.90
T	12	16	90	90	90	12	300	33	30	1080	2	157	26.75	1	1.25	0.972	0.972	122.0832	141.32	119.85	244.17	Mode2	119.85
T	12	16	100	90	90	12	300	38	30	1080	2	157	26.75	1	1.25	0.972	0.972	122.0832	120.68	111.04	244.17	Mode2	111.04
T	12	16	120	90	90	12	300	48	30	1080	2	157	26.75	1	1.25	0.972	0.972	122.0832	93.40	96.80	244.17	Mode1	93.40
T	12	16	140	90	90	12	300	58	30	1080	2	157	26.75	1	1.25	0.972	0.972	122.0832	76.18	85.80	244.17	Mode1	76.18
T	15	16	90	90	90	15	300	33	30	1080	2	157	26.75	1	1.25	1.519	1.519	122.0832	220.82	154.56	244.17	Mode2	154.56
T	15	16	100	90	90	15	300	38	30	1080	2	157	26.75	1	1.25	1.519	1.519	122.0832	188.57	143.20	244.17	Mode2	143.20
T	15	16	120	90	90	15	300	48	30	1080	2	157	26.75	1	1.25	1.519	1.519	122.0832	145.94	124.84	244.17	Mode2	124.84
T	15	16	140	90	90	15	300	58	30	1080	2	157	26.75	1	1.25	1.519	1.519	122.0832	119.03	110.65	244.17	Mode2	110.65
T	18	16	90	90	90	18	300	33	30	1080	2	157	26.75	1	1.25	2.187	2.187	122.0832	317.98	196.99	244.17	Mode2	196.99
T	18	16	100	90	90	18	300	38	30	1080	2	157	26.75	1	1.25	2.187	2.187	122.0832	271.54	182.51	244.17	Mode2	182.51
T	18	16	120	90	90	18	300	48	30	1080	2	157	26.75	1	1.25	2.187	2.187	122.0832	210.16	159.11	244.17	Mode2	159.11
T	18	16	140	90	90	18	300	58	30	1080	2	157	26.75	1	1.25	2.187	2.187	122.0832	171.41	141.03	244.17	Mode2	141.03

ANNEX-V

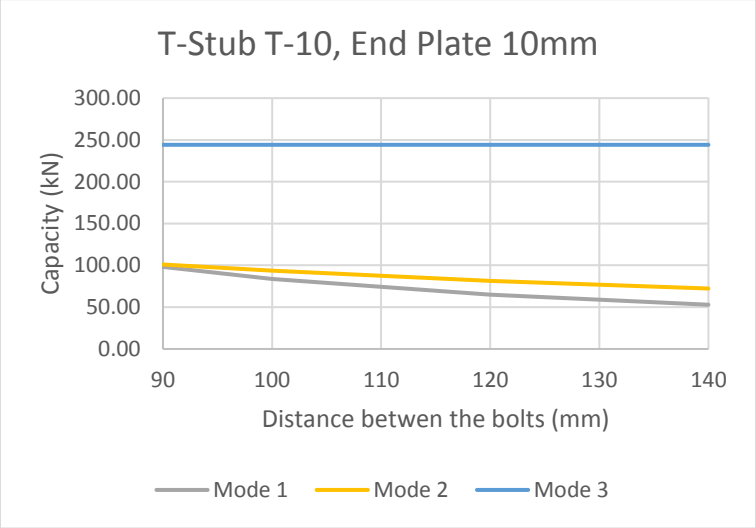
T-Stub T-10, End Plate 10mm
300.00
250.00
200.00
150.00
100.00
50.00
0.00
Capacity (kN)
90
100
110
120
130
140
Distance betwen the bolts (mm)
Mode 1
Mode 2
Mode 3

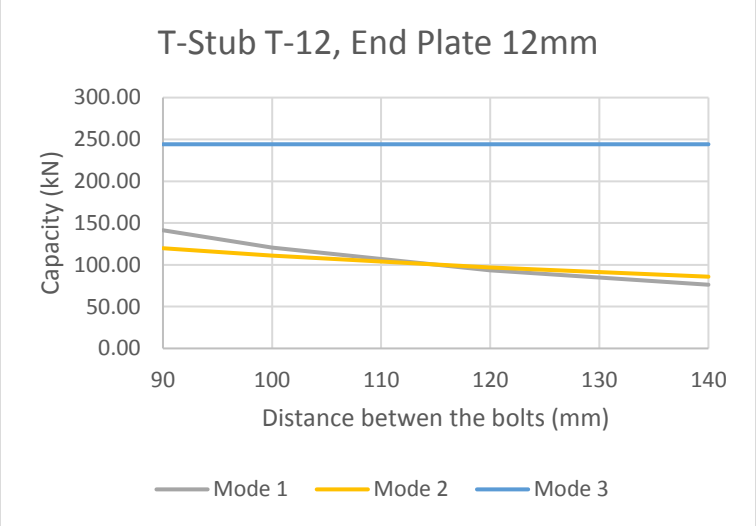
T-Stub T-12, End Plate 12mm
300.00
250.00
200.00
150.00
100.00
50.00
0.00
Capacity (kN)
90
100
110
120
130
140
Distance betwen the bolts (mm)
Mode 1
Mode 2
Mode 3

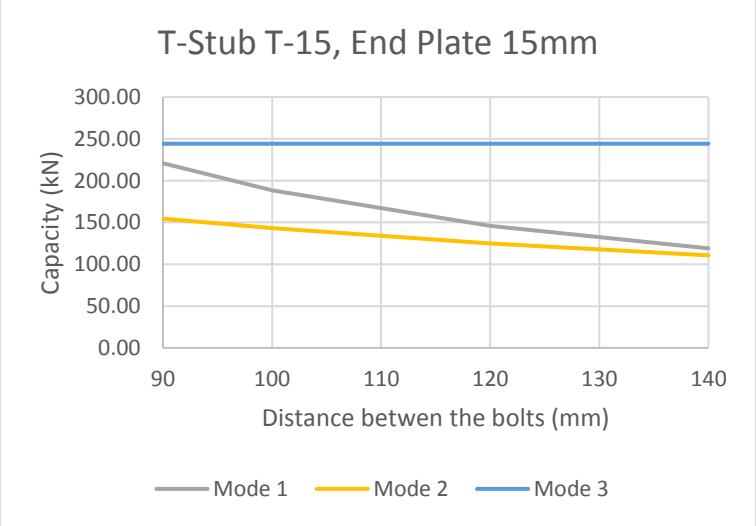
T-Stub T-15, End Plate 15mm
300.00
250.00
200.00
150.00
100.00
50.00
0.00
Capacity (kN)
90
100
110
120
130
140
Distance betwen the bolts (mm)
Mode 1
Mode 2
Mode 3

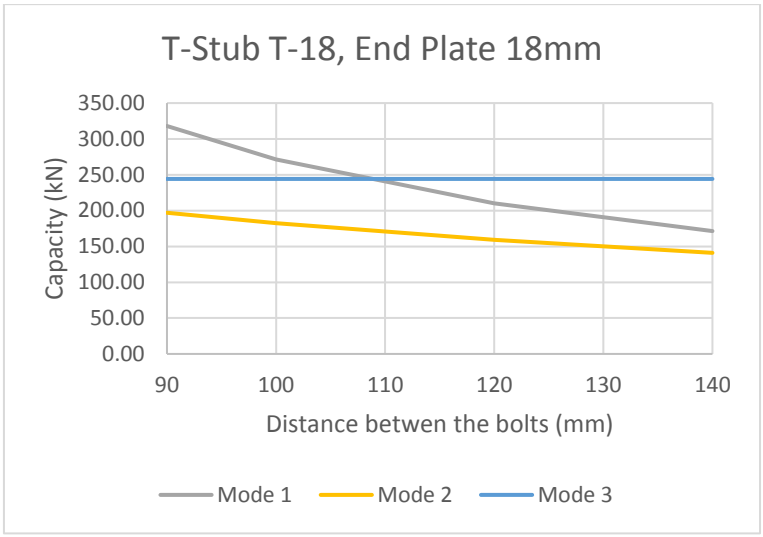
T-Stub T-18, End Plate 18mm
350.00
300.00
250.00
200.00
150.00
100.00
50.00
0.00
Capacity (kN)
90
100
110
120
130
140
Distance betwen the bolts (mm)
Mode 1
Mode 2
Mode 3

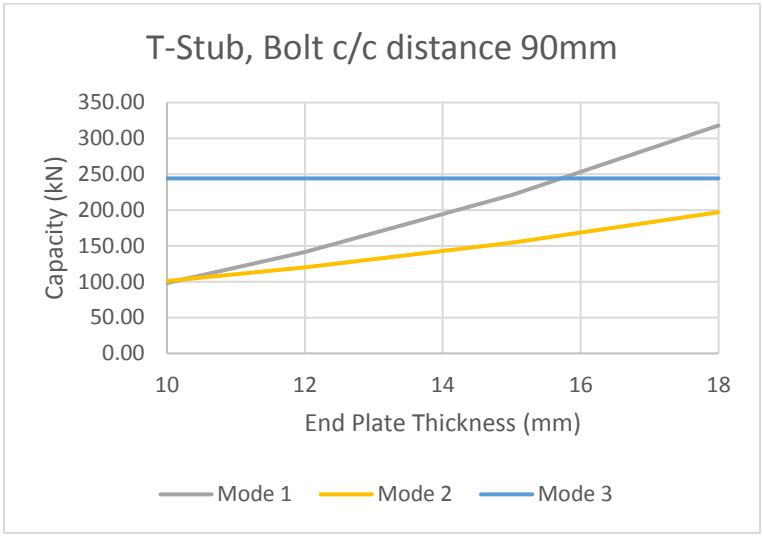
T-Stub, Bolt c/c distance 90mm
350.00
300.00
250.00
200.00
150.00
100.00
50.00
0.00
Capacity (kN)
10
12
14
16
18
End Plate Thickness (mm)
Mode 1
Mode 2
Mode 3

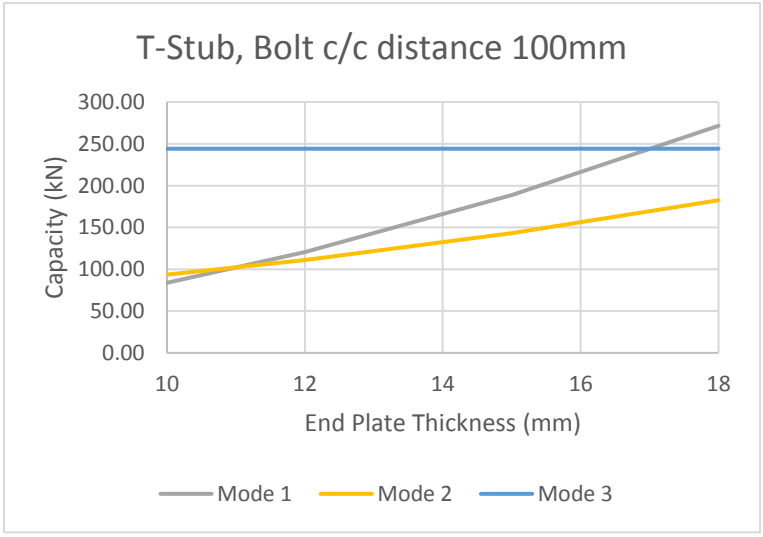
T-Stub, Bolt c/c distance 100mm
300.00
250.00
200.00
150.00
100.00
50.00
0.00
Capacity (kN)
10
12
14
16
18
End Plate Thickness (mm)
Mode 1
Mode 2
Mode 3

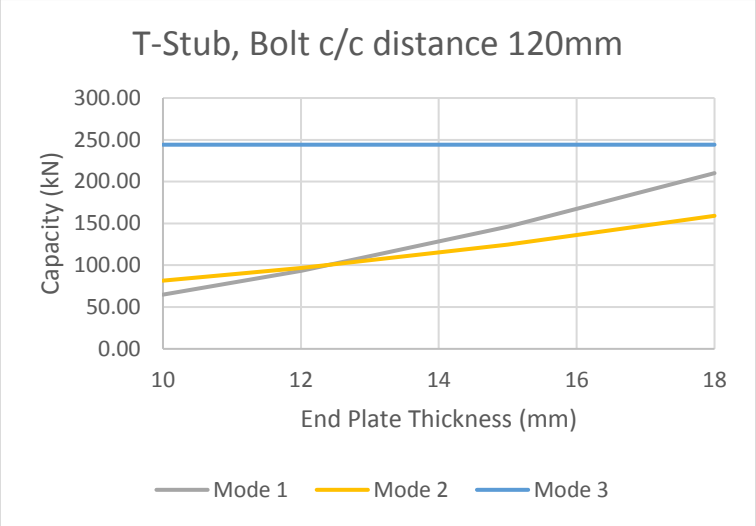
T-Stub, Bolt c/c distance 120mm
300.00
250.00
200.00
150.00
100.00
50.00
0.00
Capacity (kN)
10
12
14
16
18
End Plate Thickness (mm)
Mode 1
Mode 2
Mode 3

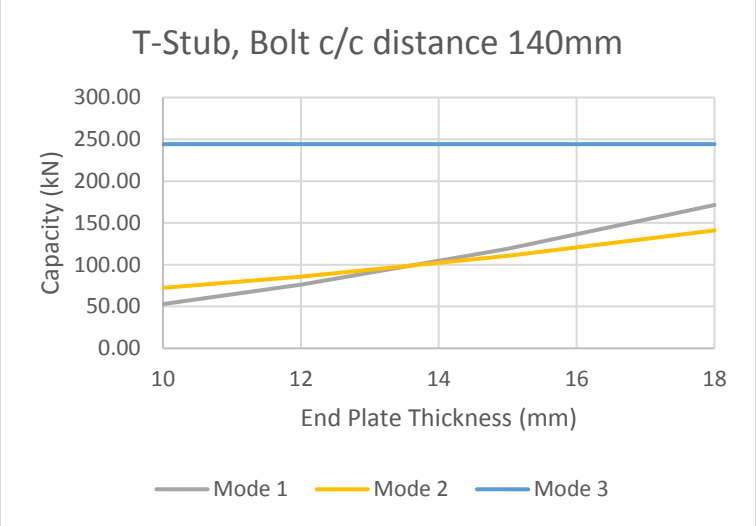
T-Stub, Bolt c/c distance 140mm
300.00
250.00
200.00
150.00
100.00
50.00
0.00
Capacity (kN)
10
12
14
16
18
End Plate Thickness (mm)
Mode 1
Mode 2
Mode 3

ANNEX-VI

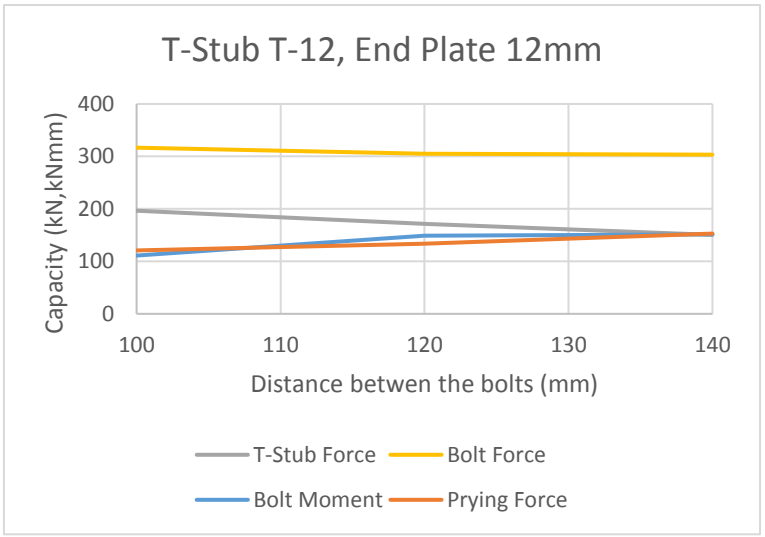
T-Stub T-12, End Plate 12mm
Capacity (kN,kNmm)
400
300
200
100
0
100
110
120
130
140
Distance betwen the bolts (mm)
T-Stub Force
Bolt Force
Bolt Moment
Prying Force

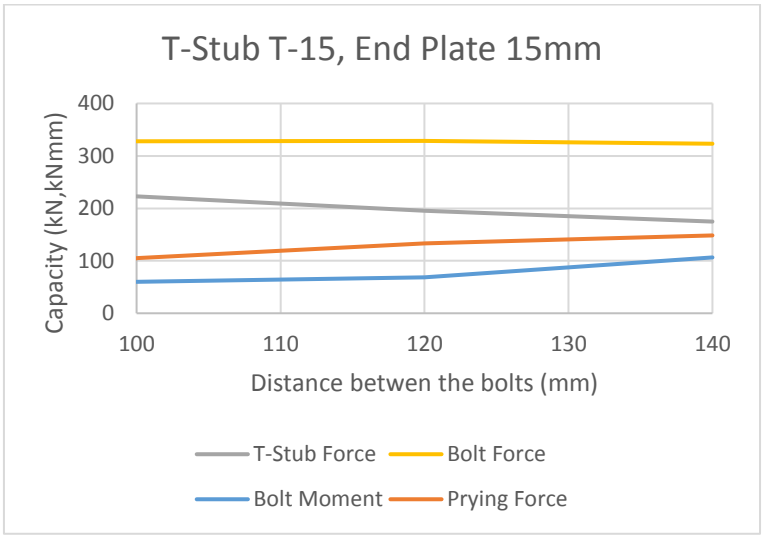
T-Stub T-15, End Plate 15mm
Capacity (kN,kNmm)
400
300
200
100
0
100
110
120
130
140
Distance betwen the bolts (mm)
T-Stub Force
Bolt Force
Bolt Moment
Prying Force

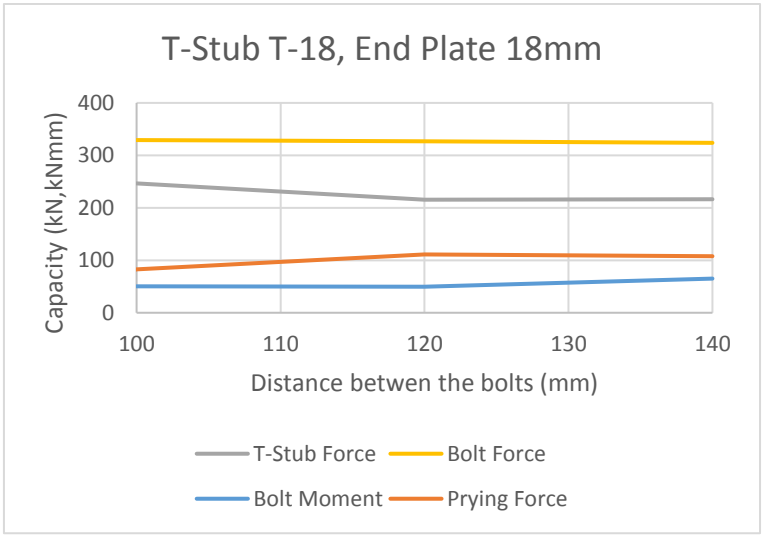
T-Stub T-18, End Plate 18mm
Capacity (kN,kNmm)
400
300
200
100
0
100
110
120
130
140
Distance betwen the bolts (mm)
T-Stub Force
Bolt Force
Bolt Moment
Prying Force

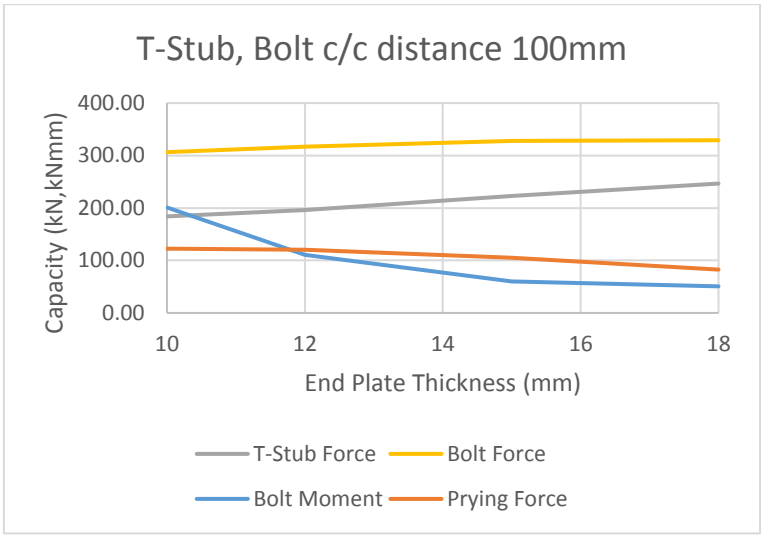
T-Stub, Bolt c/c distance 100mm
Capacity (kN,kNmm)
400.00
300.00
200.00
100.00
0.00
10
12
14
16
18
End Plate Thickness (mm)
T-Stub Force
Bolt Force
Bolt Moment
Prying Force

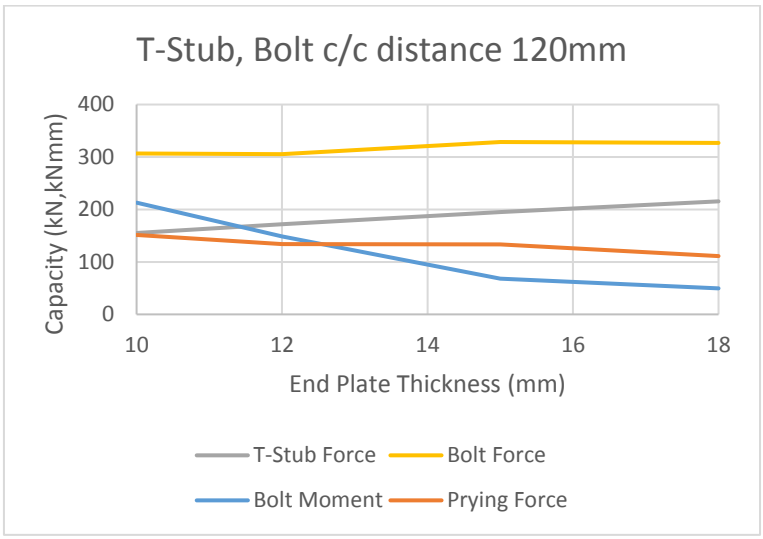
T-Stub, Bolt c/c distance 120mm
Capacity (kN,kNmm)
400
300
200
100
0
10
12
14
16
18
End Plate Thickness (mm)
T-Stub Force
Bolt Force
Bolt Moment
Prying Force

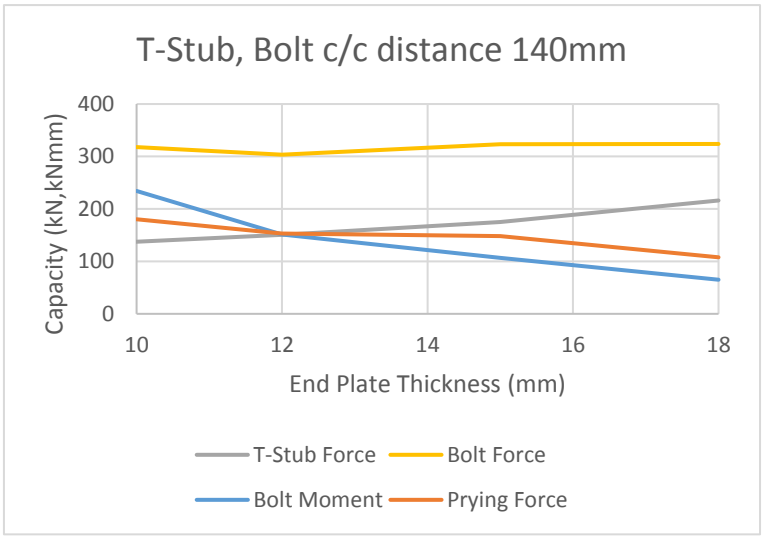
T-Stub, Bolt c/c distance 140mm
Capacity (kN,kNmm)
400
300
200
100
0
10
12
14
16
18
End Plate Thickness (mm)
T-Stub Force
Bolt Force
Bolt Moment
Prying Force

ANNEX-VII

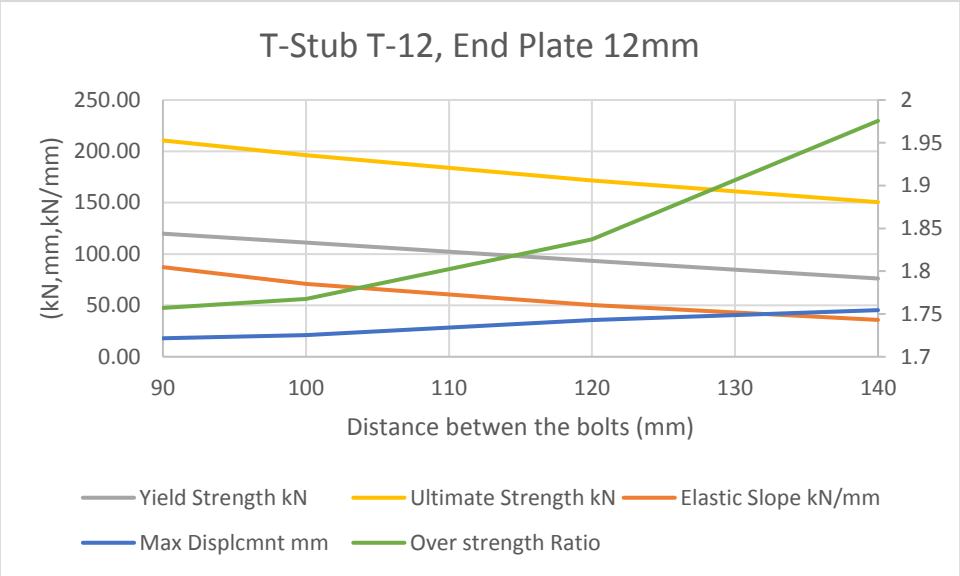
T-Stub T-12, End Plate 12mm
(kN,mm,kN/mm)
250.00
200.00
150.00
100.00
50.00
0.00
2
1.95
1.9
1.85
1.8
1.75
1.7
90
100
110
120
130
140
Distance betwen the bolts (mm)
Yield Strength kN
Ultimate Strength kN
Elastic Slope kN/mm
Max Displcmnt mm
Over strength Ratio

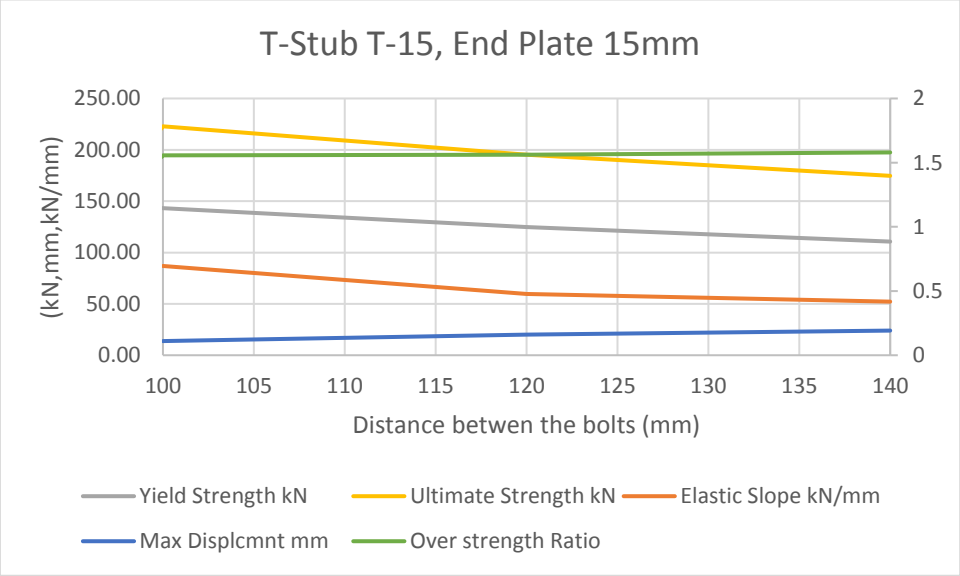
T-Stub T-15, End Plate 15mm
(kN,mm,kN/mm)
250.00
200.00
150.00
100.00
50.00
0.00
2
1.5
1
0.5
0
100
105
110
115
120
125
130
135
140
Distance betwen the bolts (mm)
Yield Strength kN
Ultimate Strength kN
Elastic Slope kN/mm
Max Displcmnt mm
Over strength Ratio

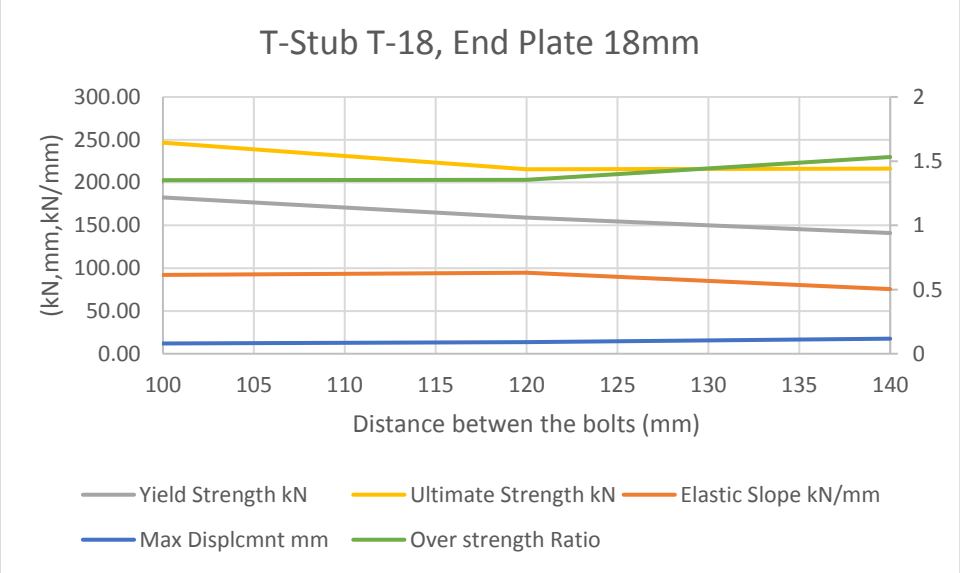
T-Stub T-18, End Plate 18mm
(kN,mm,kN/mm)
300.00
250.00
200.00
150.00
100.00
50.00
0.00
2
1.5
1
0.5
0
100
105
110
115
120
125
130
135
140
Distance betwen the bolts (mm)
Yield Strength kN
Ultimate Strength kN
Elastic Slope kN/mm
Max Displcmnt mm
Over strength Ratio

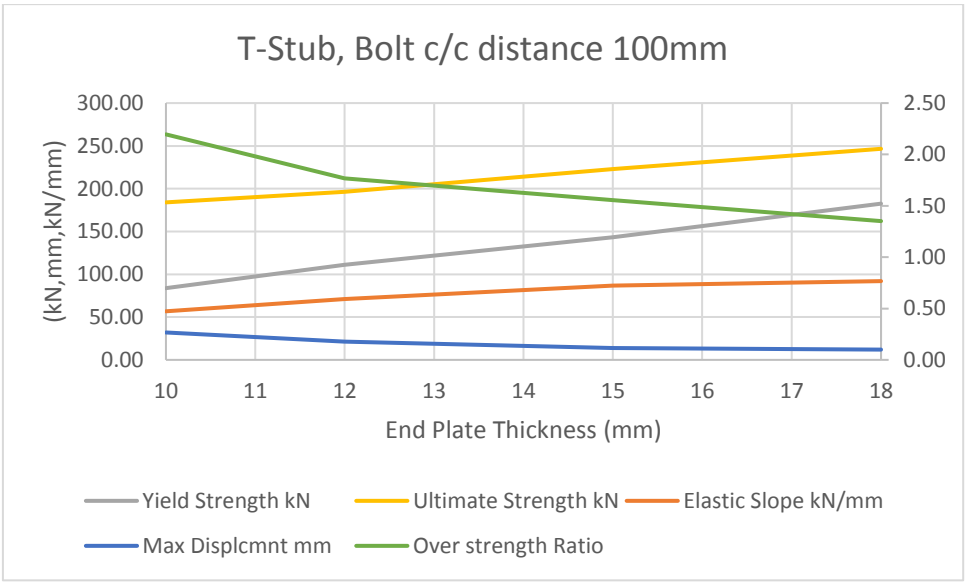
T-Stub, Bolt c/c distance 100mm
(kN,mm,kN/mm)
300.00
250.00
200.00
150.00
100.00
50.00
0.00
2.50
2.00
1.50
1.00
0.50
0.00
10
11
12
13
14
15
16
17
18
End Plate Thickness (mm)
Yield Strength kN
Ultimate Strength kN
Elastic Slope kN/mm
Max Displcmnt mm
Over strength Ratio

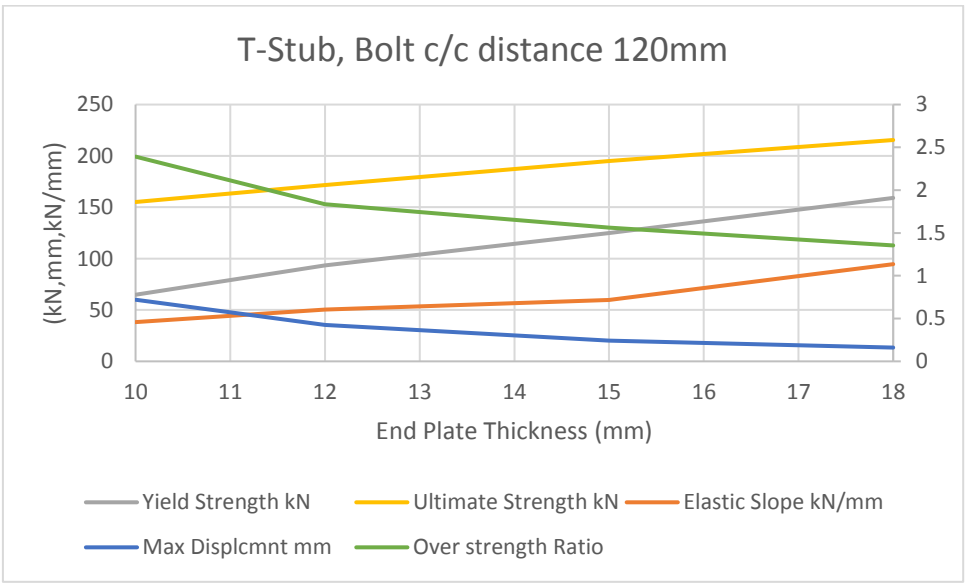
T-Stub, Bolt c/c distance 120mm
(kN,mm,kN/mm)
250
200
150
100
50
0
3
2.5
2
1.5
1
0.5
0
10
11
12
13
14
15
16
17
18
End Plate Thickness (mm)
Yield Strength kN
Ultimate Strength kN
Elastic Slope kN/mm
Max Displcmnt mm
Over strength Ratio

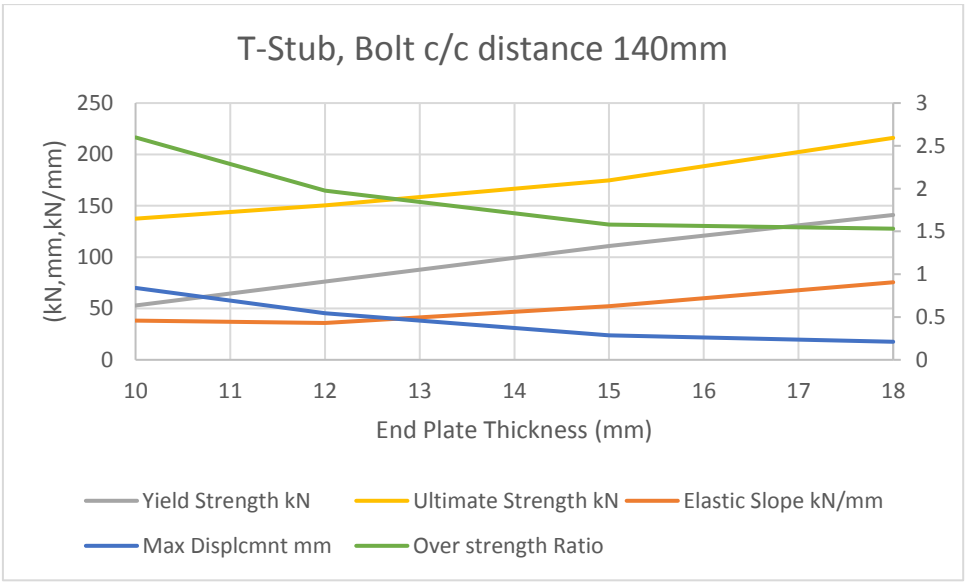
T-Stub, Bolt c/c distance 140mm
(kN,mm,kN/mm)
250
200
150
100
50
0
3
2.5
2
1.5
1
0.5
0
10
11
12
13
14
15
16
17
18
End Plate Thickness (mm)
Yield Strength kN
Ultimate Strength kN
Elastic Slope kN/mm
Max Displcmnt mm
Over strength Ratio